Computer modelling of terrestrial gamma-radiation fields

Kirkegaard, P.; Løvborg, L.

Publication date:
1974

Document Version
Publisher's PDF, also known as Version of record

Risø Report No. 303

Risø Report No. 303

Danish Atomic Energy Commission

Research Establishment Risø

Computer Modelling of Terrestrial Gamma-Radiation Fields

by Peter Kirkegaard and Leif Løvborg

September 1974

Sales distributors: Jul. Gjellerup, 87, Sølvgade, DK-1307 Copenhagen K, Denmark

Available on exchange from: Library, Danish Atomic Energy Commission, Risø, DK-4000 Roskilde, Denmark

INIS Descriptors

EARTH CRUST
G CODES
GAMMA RADIATION
GAMMA TRANSPORT THEORY
GEOLOGIC DEPOSITS
NATURAL RADIOACTIVITY
ONE-DIMENSIONAL CALCULATIONS
PHOTON TRANSPORT
POTASSIUM 40
PI-APPROXIMATION
THORIUM
URANIUM
WATER

UDC 539.122 : 681.3.06

September 1974 Risø Report No. 303

Computer Modelling of Terrestrial Gamma-Radiation Fields

by

Peter Kirkegaard
Computer Installation

and

Leif Løvborg
Electronics Department

Danish Atomic Energy Commission
Research Establishment Risø

Abstract

The plane, one-dimensional photon transport equation is considered in the case of two adjacent media, where one medium contains the γ-ray sources and the other is inactive. Assuming that the sources have a composite line spectrum, and that they are uniformly distributed, an explicit solution is given for the uncollided flux component. The scattered component is evaluated on the basis of the double-P_1 approximation, involving separate treatments of the upstreaming and the downstreaming flux, and a numerical method for solution of the corresponding equations is presented. The computational method permits determination of the differential and angular energy flux throughout the inactive medium. Formulas for obtaining integral field quantities (scalar energy flux, scalar number flux, and absorbed dose rate) are given. The flux calculation method is used in conjunction with a data processing system for evaluation of terrestrial gamma-radiation fields. A detailed description is given of both the data files and the programs of which the system consists. To illustrate the performance of the system, results obtained for the radiation field in water above sand are presented.

ISBN 87550 0299 4

CONTENTS

1. INTRODUCTION

In this report we describe techniques for computational evaluation of terrestrial gamma-radiation fields, i.e. environmental radiation fields produced by the natural gamma-ray emitters (^{40}K and members of the thorium and the uranium decay series) in the crustal materials of the earth. The techniques are currently being used as an aid to the interpretation of radiometric surveys of geologic formations. The methods developed, and the results selected to illustrate their performance, are considered to be a valuable supplement to the similar, though more comprehensive achievements of Beck and co-workers at the USAEC Health and Safety Laboratory[1-5]. Thus we have independently solved a one-dimensional, two-media photon transport problem, and the solution has been used for compilation of data on terrestrial gamma-radiation fields in water.

The basic idealization made in this work is indicated in fig. 1. Two semi-infinite, homogeneous media, I and II, border on each other along a plane interface a-a. Medium I contains spatially uniform gamma-ray emitters having a composite line spectrum in the general case. We shall focus our interest on prediction of the photon flux at selected heights in medium II ($z \geq 0$), although it will be necessary to work out solutions for the radiation field in both media as a whole.

In a previous work[6] the same problem was solved by means of the double-P_ℓ polynomial expansion method for the more simple case in which medium II is a vacuum. The double-P_1 approximation proved to yield an efficient and reasonably accurate flux calculation for semi-infinite, plane-geometry conditions, and the present work is therefore based on a further development of this technique. In the same way as in[6], the formulation and solution of the double-P_1 equations was influenced by Gerstl[7], who considered a finite slab with a source at one end-face.

In the following we shall first (chapter 2) set up the plane, one-dimensional transport equation satisfied by the total flux of photons, uncollided as well as scattered, and give expressions for the uncollided flux. Chapter 3 is devoted to the double-P_1 approximation, where the components of the transport equation for the scattered flux are expanded in half-range Legendre polynomials through the first-order terms; an equation system for the expansion coefficients is established in section 3.1, and in section 3.2 its numerical solution is discussed. Formulas for integral field quantities (e.g. scalar number flux and absorbed dose rate) derived from the calculated angular flux densities are given in chapter 4.

Two computer programs were written to carry out the flux calculations delineated in chapters 2-4. They are part of a data processing system, which in addition covers three editing programs, three files with basic data and one with angular flux results. By means of this system, which is described in chapter 5, radiation field calculations can be accomplished for any combination of medium I and medium II.

Chapter 6 can be read independently. Tables and graphs are presented illustrating the flux distributions in water resulting from the natural radioactivity of the underlying material.

2. THE TRANSPORT EQUATION

Several computational advantages are obtained by formulating the plane one-dimensional photon transport equation in terms of wavelength and energy flux in preference to energy and number flux[6, 7, 8]:

$$\omega \frac{\partial}{\partial z} I(z,\omega,\lambda) + \mu(z,\lambda) I(z,\omega,\lambda) = \int_{\lambda-2}^{\lambda} \int_{4\pi} I(z,\omega',\lambda') k(\lambda',\lambda) \frac{\delta(1+\lambda'-\lambda-\underline{\Omega}\cdot\underline{\Omega}')}{2\pi} d\underline{\Omega}' d\lambda' + \frac{E q(z,\lambda)}{4\pi} \qquad (-\infty < z < \infty) \quad , \tag{1}$$

where

- $I(z, \omega, \lambda)$ = angular energy flux of photons (Mev cm^{-2} s^{-1} Mev^{-1} sterad^{-1})
- z = distance along the z-axis, cf. fig. 1 (cm)
- $\underline{\Omega}$ = unit vector in the direction of photon movement
- ω = $\underline{i} \cdot \underline{\Omega}$, where $\underline{i}$ is the unit vector parallel to the z-axis
- λ = wavelength of the radiation in units of Compton wavelength
- $\mu(z, \lambda)$ = total macroscopic cross section without coherent scattering (cm^{-1})
- E = energy (Mev), and
- $q(z, \lambda)$ = position and wavelength distribution of isotropically radiating source (photons cm^{-3} Mev^{-1}).

Dashed symbols refer to conditions prior to photon scattering. The Klein-Nishina scattering kernel $k(\lambda', \lambda)$ has the expression

$$k(\lambda',\lambda) = \begin{cases} n_e(z)\sigma_0 \frac{3}{8} \frac{\lambda'}{\lambda}\left(\frac{\lambda}{\lambda'} + \frac{\lambda'}{\lambda} - 2(\lambda-\lambda') + (\lambda-\lambda')^2\right), \\ \qquad\qquad \lambda - 2 \le \lambda' \le \lambda; \\ 0, \quad \text{otherwise;} \end{cases} \tag{2}$$

where $n_e(z)$ is the electron density (cm^{-3}), and $\sigma_0 = \frac{8}{3}\pi r_0^2$ is the Thomson cross section; inserting the value $r_0 = 0.281776 \times 10^{-12}$ cm for the classical electron radius, we find $\sigma_0 = 0.66516$ barns/electron.

Specializing to the present two-media problem (fig. 1), the source term may be written

$$q(z,\lambda) = H(-z)\, q(\lambda), \tag{3}$$

where H is Heaviside's step function. Further, the cross section $\mu(z, \lambda)$ becomes a piecewise constant function of z:

$$\mu(z,\lambda) = \begin{cases} \mu_I(\lambda), & z < 0 \\ \mu_{II}(\lambda), & z > 0 \ . \end{cases} \tag{4}$$

The energy flux I may be split into an uncollided part U and a scattered part ψ:

$$I(z,\omega,\lambda) = U(z,\omega,\lambda) + \psi(z,\omega,\lambda). \tag{5}$$

The uncollided component U satisfies the scattering-free transport equation

$$\omega \frac{\partial}{\partial z} U(z,\omega,\lambda) + \mu(z,\lambda) U(z,\omega,\lambda) = \frac{E H(-z) q(\lambda)}{4\pi}, \qquad (-\infty < z < \infty) \tag{6}$$

whereas the equation for the scattered component ψ is characterized by a source term equal to the density of first-collisions:

$$\omega \frac{\partial}{\partial z} \psi(z,\omega,\lambda) + \mu(z,\lambda)\,\psi(z,\omega,\lambda) =$$

$$\int_{\lambda-2}^{\lambda} \int_{4\pi} \left[\psi(z,\omega',\lambda') + U(z,\omega',\lambda')\right] k(\lambda',\lambda) \frac{\delta(1+\lambda'-\lambda-\underline{\Omega}\cdot\underline{\Omega}')}{2\pi}\, d\underline{\Omega}'\, d\lambda' \qquad (7)$$

$$(-\infty < z < \infty).$$

The proper boundary conditions are similar for eqs. (6) and (7):

(a) the flux at the boundary must be continuous with respect to z:

$$\begin{aligned} U(-0,\omega,\lambda) &= U(+0,\omega,\lambda) \\ \psi(-0,\omega,\lambda) &= \psi(+0,\omega,\lambda) \end{aligned} \qquad (8)$$

and

(b) the flux must be finite in both limits:

$$\begin{aligned} U(\pm\infty,\omega,\lambda) &< \infty \\ \psi(\pm\infty,\omega,\lambda) &< \infty \quad . \end{aligned} \qquad (9)$$

The solution for U is easily constructed and is given in the following scheme:

$U(z,\omega,\lambda)$ =

	$\omega > 0$ (upgoing)	$\omega < 0$ (downgoing)
$z < 0$ (I)	$p(\lambda)$	$p(\lambda)\left[1-\exp(-\frac{\mu_I(\lambda)}{\omega} z)\right]$
$z > 0$ (II)	$p(\lambda)\exp(-\frac{\mu_{II}(\lambda)}{\omega} z)$	0

(10)

with

$$p(\lambda) = \frac{E\, q(\lambda)}{4\pi\, \mu_I(\lambda)} \quad . \qquad (11)$$

An approximate solution for ϕ using double-P_1 expansions is developed in the following chapter.

3. DOUBLE-P_1 APPROXIMATION

The basic idea in double-P_ℓ technique is to expand the up-streaming flux ($\omega > 0$) and the down-streaming flux ($\omega < 0$) into separate half-range spherical harmonics. Such a procedure seems natural to apply to the present problem in view of the different expressions for the direct flux U when $\omega > 0$ and when $\omega < 0$ (eq. (10)).

3.1. Derivation of Equations

We define

$$\left.\begin{aligned} \psi^{\pm}(z,\omega,\lambda) &= \psi(z,\omega,\lambda)\, H(\pm\omega) \\ U^{\pm}(z,\omega,\lambda) &= U(z,\omega,\lambda)\, H(\pm\omega) \end{aligned}\right\} \quad . \qquad (12)$$

For any ω we have $\phi = \phi^+ + \phi^-$ and $U = U^+ + U^-$; the expressions for U^+ and U^- follow from (10). Eq. (7) can be written

$$\omega \frac{\partial \psi^{\pm}(z,\omega,\lambda)}{\partial z} + \mu(z,\lambda)\,\psi^{\pm}(z,\omega,\lambda) = \qquad (13)$$

$$\int_{\lambda-2}^{\lambda} \int_{4\pi} (\psi^+ + U^+ + \psi^- + U^-)(z,\omega',\lambda')\, k(\lambda',\lambda) \frac{\delta(1+\lambda'-\lambda-\underline{\Omega}\,\underline{\Omega}')}{2\pi}\, d\underline{\Omega}'\, d\lambda',$$

where the upper sign is taken for $\omega > 0$, the lower for $\omega < 0$. The boundary conditions are

$$\psi^{\pm}(-0,\omega,\lambda) = \psi^{\pm}(+0,\omega,\lambda) \quad , \qquad (14)$$

and

$$\psi^{\pm}(\pm\infty,\omega,\lambda) < \infty \quad . \qquad (15)$$

For $0 < \omega \leq 1$ the general half-range spherical harmonics expansion is

$$\varphi(\omega) = \sum_{\ell=0}^{\infty} (2\ell+1)\, a_\ell\, P_\ell(2\omega-1), \qquad a_\ell = \int_0^1 \varphi(\omega)\, P_\ell(2\omega-1)\, d\omega, \qquad (16)$$

and for $-1 \leq \omega < 0$

$$\varphi(\omega) = \sum_{\ell=0}^{\infty} (2\ell+1) a_\ell P_\ell(2\omega+1), \qquad a_\ell = \int_{-1}^{0} \varphi(\omega) P_\ell(2\omega+1)\, d\omega. \tag{17}$$

Here P_ℓ stands for the usual Legendre polynomial of order ℓ. Making the abbreviations[7]

$$P_\ell^{\pm}(\omega) \equiv P_\ell(2\omega \mp 1) H(\pm\omega), \quad \int^{+} \equiv \int_0^1, \quad \int^{-} \equiv \int_{-1}^0,$$

we expand the different components of eq. (13) according to (16) and (17):

$$\left.\begin{aligned} \psi^{\pm}(z,\omega,\lambda) &= \sum_{\ell=0}^{\infty} (2\ell+1)\, \psi_\ell^{\pm}(z,\lambda)\, P_\ell^{\pm}(\omega) \\ \text{with} \quad \psi_\ell^{\pm}(z,\lambda) &= \int^{\pm} \psi(z,\omega,\lambda) P_\ell^{\pm}(\omega)\, d\omega \end{aligned}\right\}, \tag{18}$$

and

$$\left.\begin{aligned} U^{\pm}(z,\omega,\lambda) &= \sum_{\ell=0}^{\infty} (2\ell+1)\, U_\ell^{\pm}(z,\lambda)\, P_\ell^{\pm}(\omega) \\ \text{with} \quad U_\ell^{\pm}(z,\lambda) &= \int^{\pm} U(z,\omega,\lambda) P_\ell^{\pm}(\omega)\, d\omega \end{aligned}\right\}. \tag{19}$$

Orthogonality and recursion relations for the half-range spherical harmonics $P_\ell^{\pm}(\omega)$ are given in Appendix I. If the expansions above are substituted in (13), and Compton's angular scattering kernel $\delta(1+\lambda'-\lambda-\underline{\Omega}\cdot\underline{\Omega}')/2\pi$ is expanded in full-range spherical harmonics in $\underline{\Omega}\cdot\underline{\Omega}'$, it is possible after some reductions[6,7] to obtain an infinite set of interlinked integro-differential equations satisfied by the expansion coefficients $\psi_\ell^{\pm}(z,\lambda)$ for the scattered flux ψ:

$$\begin{aligned} &\frac{\ell}{2(2\ell+1)} \frac{\partial \psi_{\ell-1}^{\pm}}{\partial z} \pm \frac{\partial \psi_\ell^{\pm}}{\partial z} + \frac{\ell+1}{2(2\ell+1)} \frac{\partial \psi_{\ell+1}^{\pm}}{\partial z} + \mu(z,\lambda)\, \psi_\ell^{\pm} = \\ &\sum_{n=\ell}^{\infty} \frac{2n+1}{2} c_{n\ell}^{\pm} \int_{\lambda-2}^{\lambda} k(\lambda',\lambda) P_n(1+\lambda'-\lambda) \sum_{\ell'=0}^{n} (2\ell'+1) \left[(\psi_{\ell'}^{+} + U_{\ell'}^{+})(z,\lambda') c_{n\ell'}^{+} \right. \\ &\left. + (\psi_{\ell'}^{-} + U_{\ell'}^{-})(z,\lambda') c_{n\ell'}^{-} \right] d\lambda' \quad ; \end{aligned} \tag{20}$$

(the coefficients $c_{n\ell}^{\pm} = \int^{\pm} P_n(\omega) P_\ell^{\pm}(\omega)\, d\omega$ are discussed in Appendix II). From this point it becomes necessary to distinguish between the cases $z < 0$ and $z > 0$. We put $\mu'_I \equiv \mu_I(\lambda')$, $\mu'_{II} \equiv \mu_{II}(\lambda')$, introduce the auxiliary quantities $V_\ell(y) = \int_0^{+} P_\ell^{+}(\omega) \exp(-y/\omega)\, d\omega$ (see Appendix III) and find

I) $z < 0$:

$$\begin{aligned} U_{\ell'}^{-} &= p(\lambda') \int^{-} P_{\ell'}^{-}(\omega) \left[1 - \exp(-\mu'_I z/\omega) \right] d\omega \\ &= p(\lambda') \left[\delta_{\ell'0} - (-1)^{\ell'} V_{\ell'}(\mu'_I |z|) \right], \end{aligned} \tag{21}$$

$$U_{\ell'}^{+} = p(\lambda') \int^{+} P_{\ell'}^{+}(\omega)\, d\omega = p(\lambda')\, \delta_{\ell'0}, \tag{22}$$

the right side of (20) =

$$\begin{aligned} &\delta_{\ell 0} \int_{\lambda-2}^{\lambda} k(\lambda',\lambda) p(\lambda')\, d\lambda' + \sum_{n=\ell}^{\infty} \frac{2n+1}{2} c_{n\ell}^{\pm} \int_{\lambda-2}^{\lambda} k(\lambda',\lambda) P_n(1+\lambda'-\lambda) \cdot \\ &\sum_{\ell'=0}^{n} (2\ell'+1) \left[\psi_{\ell'}^{+}(z,\lambda') c_{n\ell'}^{+} + (\psi_{\ell'}^{-}(z,\lambda') - (-1)^{\ell'} p(\lambda') V_{\ell'}(\mu'_I|z|)) c_{n\ell'}^{-} \right] d\lambda' ; \end{aligned} \tag{23}$$

and

II) $z > 0$:

$$U_{\ell'}^{-} = 0, \tag{24}$$

$$\begin{aligned} U_{\ell'}^{+} &= p(\lambda') \int^{+} P_{\ell'}^{+}(\omega) \exp(-\mu'_{II} z/\omega)\, d\omega \\ &= p(\lambda')\, V_{\ell'}(\mu'_{II} z), \end{aligned} \tag{25}$$

the right side of (20) =

$$\sum_{n=\ell}^{\infty} \frac{2n+1}{2} c_{n\ell}^{\pm} \int_{\lambda-2}^{\lambda} k(\lambda',\lambda)\, P_n(1+\lambda'-\lambda) \cdot \tag{26}$$

$$\sum_{\ell'=0}^{n} (2\ell'+1)\left[\left(\psi_{\ell'}^{+}(z,\lambda') + p(\lambda')\, V_{\ell'}(\mu_{II}'\, z)\right) c_{n\ell'}^{+} + \psi_{\ell'}^{-}(z,\lambda')\, c_{n\ell'}^{-}\right] d\lambda' .$$

Henceforward we shall be concerned with the consistent double-P_1 approximation, i.e. we postulate $\forall \ell > 1$: $\phi_\ell^{\pm} = V_\ell = 0$. Then the equation valid for $z < 0$ ((20), (23)) and that valid for $z > 0$ ((20), (26)) each reduces to a set of four coupled differential equations:

$$D_0^{\pm}(z,\lambda) + \mu_I(\lambda)\, \psi_0^{\pm}(z,\lambda) = \int_{\lambda-2}^{\lambda} k(\lambda',\lambda)\, p(\lambda')\, d\lambda' +$$

$$\sum_{n=0}^{\infty} \frac{2n+1}{2} c_{n0}^{\pm} \int_{\lambda-2}^{\lambda} P_n(1+\lambda'-\lambda)\, k(\lambda',\lambda) \sum_{\ell=0}^{1} (2\ell+1)\left[c_{n\ell}^{+}\, \psi_\ell^{+}(z,\lambda') + \right. \tag{27}$$

$$\left. c_{n\ell}^{-}\left(\psi_\ell^{-}(z,\lambda') - (-1)^\ell p(\lambda')\, V_\ell(\mu_I'|z|)\right)\right] d\lambda' ,$$

$$D_1^{\pm}(z,\lambda) + \mu_I(\lambda)\, \psi_1^{\pm}(z,\lambda) =$$

$$\sum_{n=1}^{\infty} \frac{2n+1}{2} c_{n1}^{\pm} \int_{\lambda-2}^{\lambda} P_n(1+\lambda'-\lambda)\, k(\lambda',\lambda) \sum_{\ell=0}^{1} (2\ell+1)\left[c_{n\ell}^{+}\, \psi_\ell^{+}(z,\lambda') + \right. \tag{28}$$

$$\left. c_{n\ell}^{-}\left(\psi_\ell^{-}(z,\lambda') - (-1)^\ell p(\lambda')\, V_\ell(\mu_I'|z|)\right)\right] d\lambda' ,$$

both valid for $z < 0$, and

$$D_0^{\pm}(z,\lambda) + \mu_{II}(\lambda)\, \psi_0^{\pm}(z,\lambda) =$$

$$\sum_{n=0}^{\infty} \frac{2n+1}{2} c_{n0}^{\pm} \int_{\lambda-2}^{\lambda} P_n(1+\lambda'-\lambda)\, k(\lambda',\lambda) \sum_{\ell=0}^{1} (2\ell+1)\left[c_{n\ell}^{+}\left(\psi_\ell^{+}(z,\lambda') + \right.\right. \tag{29}$$

$$\left.\left. p(\lambda')\, V_\ell(\mu_{II}'\, z)\right) + c_{n\ell}^{-}\, \psi_\ell^{-}(z,\lambda')\right] d\lambda' ,$$

$$D_1^{\pm}(z,\lambda) + \mu_{II}(\lambda)\, \psi_1^{\pm}(z,\lambda) =$$

$$\sum_{n=1}^{\infty} \frac{2n+1}{2} c_{n1}^{\pm} \int_{\lambda-2}^{\lambda} P_n(1+\lambda'-\lambda)\, k(\lambda',\lambda) \sum_{\ell=0}^{1} (2\ell+1)\left[c_{n\ell}^{+}\left(\psi_\ell^{+}(z,\lambda') + \right.\right. \tag{30}$$

$$\left.\left. p(\lambda')\, V_\ell(\mu_{II}'\, z)\right) + c_{n\ell}^{-}\, \psi_\ell^{-}(z,\lambda')\right] d\lambda' ,$$

both valid for $z > 0$. In these expressions we have used the abbreviations

$$\frac{1}{2} \frac{\partial}{\partial z}\left(\pm\, \psi_0^{\pm}(z,\lambda) + \psi_1^{\pm}(z,\lambda)\right) \equiv D_0^{\pm}(z,\lambda) \tag{31}$$

and

$$\frac{1}{6} \frac{\partial}{\partial z}\left(\psi_0^{\pm}(z,\lambda) \pm 3\,\psi_1^{\pm}(z,\lambda)\right) \equiv D_1^{\pm}(z,\lambda) . \tag{32}$$

(In the ℓ-summuation in (27) and (29) we have let the upper limit be 1 even for $n = 0$, because $c_{01}^{\pm} = 0$, cf. (A5) in Appendix II).

We shall now assume that the source is a spectrum containing P lines:

$$q(\lambda) = \sum_{p=1}^{P} Q_p\, \delta(E - E_p) \quad ; \tag{33}$$

Q_p is the intensity (photons $cm^{-3}\ s^{-1}$) of line no. p with the energy E_p and the wavelength $\lambda^{(p)} = f_o/E_p$ ($f_o = 0.5110058$). According to (11), for an arbitrary function $G(\lambda', \lambda)$ we have

$$\int_{\lambda-2}^{\lambda} G(\lambda',\lambda)\, p(\lambda',\lambda)\, d\lambda' = \sum_{p} \frac{Q_p\, \lambda^{(p)}}{4\pi\, \mu_I^{(p)}}\, G(\lambda^{(p)},\lambda) , \tag{34}$$

where $\mu_I^{(p)} = \mu_I(\lambda^{(p)})$. The summation is extended over all lines in the integration interval from $\lambda - 2$ to λ.

The equations (27) - (30) can be summarized as

$$\begin{bmatrix} \frac{1}{2} & \frac{1}{2} & 0 & 0 \\ \frac{1}{6} & \frac{1}{2} & 0 & 0 \\ 0 & 0 & -\frac{1}{2} & \frac{1}{2} \\ 0 & 0 & \frac{1}{6} & -\frac{1}{2} \end{bmatrix} \frac{\partial}{\partial z} \begin{bmatrix} \phi_0^+(z,\lambda) \\ \phi_1^+(z,\lambda) \\ \phi_0^-(z,\lambda) \\ \phi_1^-(z,\lambda) \end{bmatrix} + \mu(z,\lambda) \begin{bmatrix} \phi_0^+(z,\lambda) \\ \phi_1^+(z,\lambda) \\ \phi_0^-(z,\lambda) \\ \phi_1^-(z,\lambda) \end{bmatrix} =$$

$$\int_{\lambda-2}^{\lambda} k(\lambda',\lambda) \begin{bmatrix} A & 3C & B & 3D \\ C & 3E & -D & 3F \\ B & -3D & A & -3C \\ D & 3F & -C & 3E \end{bmatrix}_{\lambda-\lambda'} \begin{bmatrix} \phi_0^+(z,\lambda') \\ \phi_1^+(z,\lambda') \\ \phi_0^-(z,\lambda') \\ \phi_1^-(z,\lambda') \end{bmatrix} d\lambda' +$$

$$\sum_p Q_p\, a(\lambda^{(p)},\lambda)\ \underline{\sigma}(z,\lambda^{(p)},\lambda) \qquad (35)$$

$$(-\infty < z < \infty) \quad ,$$

where $\mu(z,\lambda)$ is given by (4), the abbreviation

$$a(\lambda^{(p)},\lambda) \equiv \frac{\lambda^{(p)} k(\lambda^{(p)},\lambda)}{4\pi \mu_I^{(p)}} \qquad (36)$$

has been used, and the vector $\underline{\sigma}(z,\lambda^{(p)},\lambda)$ has the expression

$$\underline{\sigma} = \begin{cases} \begin{bmatrix} 1 \\ 0 \\ 1 \\ 0 \end{bmatrix} + \begin{bmatrix} -B & 3D \\ D & 3F \\ -A & -3C \\ C & 3E \end{bmatrix}_{\lambda-\lambda^{(p)}} \cdot \begin{bmatrix} V_0(\mu_I^{(p)} \mid z\mid) \\ \\ V_1(\mu_I^{(p)} \mid z\mid) \end{bmatrix} & z < 0 \\ \\ \begin{bmatrix} A & 3C \\ C & 3E \\ B & -3D \\ D & 3F \end{bmatrix}_{\lambda-\lambda^{(p)}} \cdot \begin{bmatrix} V_0(\mu_{II}^{(p)} \mid z\mid) \\ \\ V_1(\mu_{II}^{(p)} \mid z\mid) \end{bmatrix} & z > 0 \end{cases},$$

$$\mu_{II}^{(p)} \equiv \mu_{II}(\lambda^{(p)}). \qquad (37)$$

The coefficients A, B, C, D, E, F, which depend on $\lambda-\lambda'$ (or $\lambda-\lambda^{(p)}$), are equal to sums of the type $s(\alpha_n, \beta_n) = \sum_{n=o}^{\infty} \frac{2n+1}{2} P_n(1+\lambda'-\lambda)\alpha_n\beta_n$; in fact we have

$$A = s(c_{no}^+, c_{no}^+), \quad B = s(c_{no}^+, c_{no}^-), \quad C = s(c_{no}^+, c_{n1}^+),$$

$$D = s(c_{no}^+, c_{n1}^-), \quad E = s(c_{n1}^+, c_{n1}^+), \quad F = s(c_{n1}^+, c_{n1}^-).$$

They are further discussed in Appendix IV and in section 5.2. If (35) is premultiplied by the matrix $-\underline{M}$, where

$$\underline{M} \equiv \begin{bmatrix} -3 & 3 & 0 & 0 \\ 1 & -3 & 0 & 0 \\ 0 & 0 & 3 & 3 \\ 0 & 0 & 1 & 3 \end{bmatrix}, \qquad (38)$$

the result is

$$\frac{\partial}{\partial z}\begin{bmatrix}\phi_0^+(z,\lambda)\\ \phi_1^+(z,\lambda)\\ \phi_0^-(z,\lambda)\\ \phi_1^-(z,\lambda)\end{bmatrix} = \mu(z,\lambda)\begin{bmatrix}-3 & 3 & 0 & 0\\ 1 & -3 & 0 & 0\\ 0 & 0 & 3 & 3\\ 0 & 0 & 1 & 3\end{bmatrix}\begin{bmatrix}\phi_0^+(z,\lambda)\\ \phi_1^+(z,\lambda)\\ \phi_0^-(z,\lambda)\\ \phi_1^-(z,\lambda)\end{bmatrix} +$$

$$\int_{\lambda-2}^{\lambda} k(\lambda',\lambda)\begin{bmatrix}a & b & c & d\\ e & f & g & h\\ -c & d & -a & b\\ g & -h & e & -f\end{bmatrix}_{\lambda-\lambda'}\begin{bmatrix}\phi_0^+(z,\lambda')\\ \phi_1^+(z,\lambda')\\ \phi_0^-(z,\lambda')\\ \phi_1^-(z,\lambda')\end{bmatrix} d\lambda' +$$

$$\sum_p Q_p\, a(\lambda^{(p)},\lambda)\, \underline{s}(z,\lambda^{(p)},\lambda)\ , \qquad (39)$$

where the vector $\underline{s} = -\underline{\underline{M}}\,\underline{\sigma}$ is equal to

$$\underline{s} = \begin{cases}\begin{bmatrix}3\\ -1\\ -3\\ -1\end{bmatrix} + \begin{bmatrix}-c & d\\ -g & h\\ a & b\\ -e & -f\end{bmatrix}_{\lambda-\lambda^{(p)}} \cdot \begin{bmatrix}V_0(\mu_I^{(p)}|z|)\\ V_1(\mu_I^{(p)}|z|)\end{bmatrix}, & z<0\\ \begin{bmatrix}a & b\\ e & f\\ -c & d\\ g & -h\end{bmatrix}_{\lambda-\lambda^{(p)}} \cdot \begin{bmatrix}V_0(\mu_{II}^{(p)} z)\\ V_1(\mu_{II}^{(p)} z)\end{bmatrix}, & z>0\end{cases} \qquad (40)$$

and where $a = 3A - 3C$, $b = 9C - 9E$, $c = 3B + 3D$, $d = 9D - 9F$, $e = -A + 3C$, $f = -3C + 9E$, $g = -B - 3D$, and $h = -3D + 9F$. Defining

$$\underline{\phi}(z,\lambda) \equiv \begin{bmatrix}\phi_0^+(z,\lambda)\\ \phi_1^+(z,\lambda)\\ \phi_0^-(z,\lambda)\\ \phi_1^-(z,\lambda)\end{bmatrix} \qquad (41)$$

and

$$\underline{\underline{P}}(\lambda-\lambda') \equiv \begin{bmatrix}a & b & c & d\\ e & f & g & h\\ -c & d & -a & b\\ g & -h & e & -f\end{bmatrix}_{\lambda-\lambda'} \qquad (42)$$

(39) may be written in the condensed form:

$$\frac{\partial}{\partial z}\underline{\Psi}(z,\lambda) = \mu(z,\lambda)\,\underline{\underline{M}}\cdot\underline{\Psi}(z,\lambda) + \int_{\lambda-2}^{\lambda} k(\lambda',\lambda)\,\underline{\underline{P}}(\lambda-\lambda')\,\underline{\Psi}(z,\lambda')\,d\lambda' + \sum_p Q_p\, a(\lambda^{(p)},\lambda)\,\underline{s}(z,\lambda^{(p)},\lambda)\,. \qquad (43)$$

3.2. Numerical Solution

In this section we shall consider the numerical solution of (39) or (43). The two variables in the problem, λ and z, are treated differently: the wavelength is discretized and integration over λ is approximated by summation, whereas the integration of the equations with respect to z is carried out by a combination of an analytical and a least-squares method.

Let E_{max} be the highest energy in the source spectrum, and let the energy range of interest go down to some cut-off value E_{cut}. A wavelength mesh is constructed by taking $\lambda_{min} = f_o/E_{max}$ ($f_o = 0.5110058$) and selecting a steplength $\Delta\lambda$ such that $1/\Delta\lambda = m$ is integral (fig. 2). λ_{max} and the number of intervals, N, are chosen such that $\lambda_{max} = \lambda_{min} + N\Delta\lambda$ is approximately equal to f_o/E_{cut}.

Solving the transport problem in terms of wavelength with a constant steplength $\Delta\lambda = 1/m$ simplifies the calculations considerably, because the coefficients a, b, c, d, e, f, g and h in (39) can be calculated in advance for $\lambda-\lambda' = 0,\ 1/m,\ 2/m,\ \ldots,\ 2-1/m,\ 2$, before the λ-integration starts; this advantage would be lost if E were used instead of λ. When the energy range is wide, however, neither E nor λ as integration variable yields a good economy of computation. Out interest is concentrated on the interval 0.1 - 2.6 Mev. If we choose $\Delta\lambda = 1/64$, say, and calculate ΔE according to the formula

$$dE = -f_0/\lambda^2 d\lambda = -E^2/f_0\alpha\lambda\ , \tag{44}$$

we find $|\Delta E| \approx 0.2$ Mev at $E = 2.6$ Mev and $|\Delta E| \approx 0.0003$ Mev at $E = 0.1$ Mev. Hence, a constant steplength $\Delta\lambda$ implies perhaps too large energy steps near the upper energy limit and unneccessarily small steps near the lower limit. The coarse energy-mesh width at 2.6 Mev seems tolerable because the scattered energy flux varies only slightly in this range (apart from the jumps from the source lines); but the very fine energy-mesh near 0.1 Mev involves indeed much computing time spent at low energies. For instance, a calculation from 2.6 Mev down to 0.1 Mev is approximately twice as expensive as the same calculation carried down to 0.2 Mev. An efficient strategy would be to divide the total range into subintervals and double the wavelength step from one subinterval to that next to it with lower energy. However, the price of this is a complication of the calculation scheme when describing transition of photons from one subinterval to another, and in view of the rather few calculations planned, we did not find it worthwhile.

In solving (43) a complication arises because the scattered flux, and hence the vector $\underline{\psi}(z,\lambda)$ of expansion coefficients, has discontinuities induced by the source lines: line no. p causes one jump at $\lambda = \lambda^{(p)}$ and another at $\lambda = \lambda^{(p)} + 2$ (fig. 2). Altogether 2P jumps may occur; at these jumps we shall calculate the magnitude of the jump

$$\Delta\underline{\psi}(z,\lambda) \equiv \underline{\psi}(z,\lambda+0) - \underline{\psi}(z,\lambda-0), \tag{45}$$

as well as the limit from the left, $\underline{\psi}(z,\lambda-0)$. It is readily seen that the jump magnitude for $\lambda = \lambda^{(p)}$ satisfies the equation

$$\frac{\partial}{\partial z}\Delta\underline{\psi}(z,\lambda^{(p)}) = \mu(z,\lambda^{(p)})\,\underline{\underline{M}}\cdot\Delta\underline{\psi}(z,\lambda^{(p)}) + Q_p\,\alpha(\lambda^{(p)},\lambda^{(p)})\,\underline{s}(z,\lambda^{(p)},\lambda^{(p)})\ , \tag{46}$$

and for $\lambda = \lambda^{(p)} + 2$ satisfies

$$\frac{\partial}{\partial z}\Delta\underline{\psi}(z,\lambda^{(p)}+2) = \mu(z,\lambda^{(p)}+2)\,\underline{\underline{M}}\cdot\Delta\underline{\psi}(z,\lambda^{(p)}+2) - Q_p\,\alpha(\lambda^{(p)},\lambda^{(p)}+2)\,\underline{s}(z,\lambda^{(p)},\lambda^{(p)}+2). \tag{47}$$

The usual boundary conditions with respect to z apply to (46) and (47), i.e. $\Delta\underline{\psi}$ must be continuous at $z = 0$ and finite in both limits $z = \pm\infty$. Numerically, (46) and (47) are treated in complete analogy with (43).

Returning now to equation (43), its discrete counterpart with respect to wavelength is

$$\frac{d}{dz}\underline{\psi}_i(z) = \mu_i(z)\,\underline{\underline{M}}\cdot\underline{\psi}_i(z) + \sum_{j=i-2m}^{i}\xi_{ij}\,k_{ji}\,\underline{\underline{P}}(i-j)\cdot\underline{\psi}_j(z)\,\Delta\lambda + \sum_p Q_p\,\alpha(\lambda_{j_p},\lambda_i)\,\underline{s}(z,\lambda_{j_p},\lambda_i). \tag{48}$$

Index i refers to the wavelength

$$\lambda_i = \lambda_{min} + (i-1)\,\Delta\lambda \qquad (1 \le i \le N+1). \tag{49}$$

For brevity we have written $\underline{\psi}_i(z)$ for $\underline{\psi}(z,\lambda_i)$, $\mu_i(z)$ for $\mu(z,\lambda_i)$, and k_{ji} for $k(\lambda_j,\lambda_i)$. The source term is obtained by moving each source wavelength $\lambda^{(p)}$ to its nearest wavelength mesh point $i = j_p$ (several lines may fall in the same mesh point). The ξ_{ij} are suitably chosen quadrature weights (see Appendix V).

Appendix IV shows that for $\lambda-\lambda' = 0$ $(i-j = 0)$ we have $A = 1$, $E = \frac{1}{3}$, $B = C = D = F = 0$, hence $a = 3$, $b = -3$, $e = -1$, $f = 3$, $c = d = g = h = 0$, and $\underline{\underline{P}} = -\underline{\underline{M}}$. This means that (48) is a system of the following type:

$$\frac{d}{dz}\underline{\psi}(z) = \mu(z)\,\underline{\underline{M}}\cdot\underline{\psi}(z) + \underline{\varphi}(z) \tag{50}$$

with $\mu(z) = \mu_i(z) - \Delta\lambda\,\xi_{ii}\,k_{ii}$ (index i in $\underline{\psi}$ and $\underline{\varphi}$ is suppressed). The "source" $\underline{\varphi}(z)$ is the sum of a term due to real sources at $\lambda = \lambda_i$ and slowing-down contributions from shorter wavelengths. $\mu(z)$ can be regarded as an effective cross section, corrected for self-scattering in group i. Such a system exists for all the N+1 wavelength points in the range. It is now essential that we first solve (50) for the shortest wavelength (i = 1) and then for i = 2, i = 3, ..., i = N+1, in that order. In this way $\underline{\varphi}(z)$ will always be a known function. The structure of $\underline{\underline{M}}$ (cf. (38)) permits a partitioning of the vector equation (50) into one system for the up-going flux (the "plus component") and one for the down-going (the "minus component"):

$$\frac{d}{dz}\begin{bmatrix}\underline{\psi}^{+}(z)\\ \underline{\psi}^{-}(z)\end{bmatrix} = \mu(z)\begin{bmatrix}\underline{\underline{T}}^{+} & \underline{\underline{Q}}\\ \underline{\underline{Q}} & \underline{\underline{T}}^{-}\end{bmatrix}\begin{bmatrix}\underline{\psi}^{+}(z)\\ \underline{\psi}^{-}(z)\end{bmatrix} + \begin{bmatrix}\underline{\varphi}^{+}(z)\\ \underline{\varphi}^{-}(z)\end{bmatrix}, \tag{51}$$

$$\text{i.e.}\quad \frac{d}{dz}\underline{\psi}^{\pm}(z) = \mu(z)\,\underline{\underline{T}}^{\pm}\cdot\underline{\psi}^{\pm}(z) + \underline{\varphi}^{\pm}(z), \tag{52}$$

where

$$\underline{\underline{T}}^{+}_{-} = \begin{bmatrix}\mp 3 & 3\\ 1 & \mp 3\end{bmatrix} \tag{53}$$

and

$$\underline{\phi}^{+}_{-}(z) = \begin{bmatrix}\phi^{+}_{-0}(z)\\ \phi^{+}_{-1}(z)\end{bmatrix} \tag{54}$$

(cf. (41); $\underline{\varphi}^{+}_{-}(z)$ has an expression analogous to (54)). We have now separated the plus and minus components of $\underline{\psi}$ and they can be calculated by solving the two eqs. (52), which are of the common form

$$\frac{d}{dz}\underline{f}(z) = \mu(z)\,\underline{\underline{T}}\cdot\underline{f}(z) + \underline{g}(z). \tag{55}$$

This vector equation represents two coupled linear differential equations. The standard way of solution is to apply a functional transformation

$$\underline{f} = \underline{\underline{A}}\,\underline{\chi} \tag{56}$$

to (55), such that the matrix of the new system becomes diagonal. Let A_1 and A_2 be the eigenvalues of $\underline{\underline{T}}$. Then $\underline{\underline{A}}$ is selected as the matrix of eigenvectors of $\underline{\underline{T}}$, i.e.

$$\underline{\underline{T}}\,\underline{\underline{A}} = \underline{\underline{A}}\,\underline{\underline{D}}, \tag{57}$$

where

$$\underline{\underline{D}} = \begin{bmatrix}A_1 & 0\\ 0 & A_2\end{bmatrix}. \tag{58}$$

For $\underline{\underline{T}} = \underline{\underline{T}}^{+}_{-}$ we find

$$\left.\begin{aligned} A^{+}_{1-} &= \mp(3+\sqrt{3})\\ A^{+}_{2-} &= \mp(3-\sqrt{3})\end{aligned}\right\}, \tag{59}$$

and notice that

$$A^{+}_{m} < 0, \qquad A^{-}_{m} > 0\ ; \tag{60}$$

the corresponding eigenvector matrices are

$$\underline{\underline{A}} = \underline{\underline{A}}^{+}_{-} = \begin{bmatrix}\sqrt{3} & \sqrt{3}\\ \mp 1 & \pm 1\end{bmatrix}. \tag{61}$$

The result of applying (56) to (55) is the system

$$\frac{d}{dz}\underline{\chi} = \mu(z)\,\underline{\underline{D}}\cdot\underline{\chi} + \underline{h}(z) \tag{62}$$

with

$$\underline{h} = \underline{\underline{A}}^{-1} \cdot \underline{g} \tag{63}$$

and

$$\underline{\underline{A}}^{-1} = (\underline{\underline{A}}^{+})^{-1} = \begin{bmatrix} \frac{1}{2\sqrt{3}} & \mp \frac{1}{2} \\ \frac{1}{2\sqrt{3}} & \pm \frac{1}{2} \end{bmatrix} . \tag{64}$$

(62) splits into the two uncoupled scalar equations

$$\frac{d}{dz} \chi_m(z) = \mu(z) \Lambda_m \chi_m(z) + h_m(z) . \qquad (m = 1, 2) \tag{65}$$

In the actual case $\mu(z)$ was a piece-wise constant function:

$$\mu(z) = \begin{cases} \mu_I & \text{for } z < 0 \\ \mu_{II} & \text{for } z > 0 \end{cases} , \tag{66}$$

and we can immediately write down the complete solution of (65):

$$\chi_m(z) = \exp(\mu(z)\Lambda_m z) \left\{ \left\{ \exp(-\mu(z)\Lambda_m z)\, h_m(z)\, dz + C_m \right\} . \qquad (m = 1, 2) \right. \tag{67}$$

We get a pair of equations like (67) for all four combinations of media and flux directions, i. e. (I, +), (I, -), (II, +) and (II, -):

$$\chi_m^{I\pm}(z) = \exp(\mu_I \Lambda_m^{\pm} z) \left\{ \left\{ \exp(-\mu_I \Lambda_m^{\pm} z)\, h_m^{I\pm}(z)\, dz + C_m^{I\pm} \right\} , \qquad (m = 1, 2 ;\ z \le 0) \right. \tag{68}$$

$$\chi_m^{II\pm}(z) = \exp(\mu_{II} \Lambda_m^{\pm} z) \left\{ \left\{ \exp(-\mu_{II} \Lambda_m^{\pm} z)\, h_m^{II\pm}(z)\, dz + C_m^{II\pm} \right\} . \qquad (m = 1, 2 ;\ z \ge 0) \right. \tag{69}$$

The exact analytical representations of $\chi_m(z)$ in (68) and (69) are complicated because the source term in our problem induces exponential integrals (cf. Appendix III), and the complexity increases rapidly as the wavelength integration proceeds. We choose instead an approximative method. The physical nature of the problem indicates that each of the four $h_m(z)$ can be adequately represented by a constant plus an exponential multiplied by a polynomial of degree k-1 in z:

$$h_m^{I\pm}(z) = h_{m0}^{I\pm} + \exp(\alpha_m^{I\pm} z) \sum_{j=1}^{k} h_{mj}^{I\pm} z^{j-1} \qquad (z < 0) \tag{70}$$

and

$$h_m^{II\pm}(z) = h_{m0}^{II\pm} + \exp(\alpha_m^{II\pm} z) \sum_{j=1}^{k} h_{mj}^{II\pm} z^{j-1} . \qquad (z > 0) \tag{71}$$

Here, $\alpha_m^{I\pm} > 0$ and $\alpha_m^{II\pm} < 0$. $h_{mo}^{I\pm}$ and $h_{mo}^{II\pm}$ must equal the limits $h_m^{I\pm}(-\infty)$ and $h_m^{II\pm}(\infty)$, which in turn are calculated from the vector $\underline{g}$ (cf. (55) and (63); as medium II is source-free, $h_{mo}^{II\pm} = 0$). The other parameters in (70) and (71) are determined in the least-squares sense: operating with fixed sets $\{z_i\}$ of z-values in both media, we first calculate the actual $h_m(z_i)$ from shorter wavelength solution-values at $z = z_i$ and then execute the least-squares fitting procedure described in Appendix VI. Insertion of (70) and (71) in (68) and (69) yields

$$\chi_m^{I\pm}(z) = -\frac{h_{mo}^{I\pm}}{\mu_I \Lambda_m^{\pm}} + C_m^{I\pm} \exp(\mu_I \Lambda_m^{\pm} z) + \exp(\alpha_m^{I\pm} z) \sum_{j=1}^{k} \varkappa_{mj}^{I\pm} z^{j-1} \qquad (z < 0) \tag{72}$$

and

$$\chi_m^{II\pm}(z) = C_m^{II\pm} \exp(\mu_{II} \Lambda_m^{\pm} z) + \exp(\alpha_m^{II\pm} z) \sum_{j=1}^{k} \varkappa_{mj}^{II\pm} z^{j-1} , \qquad (z > 0) \tag{73}$$

where

$$\left.\begin{aligned} \varkappa_{mk}^{I\pm} &= \frac{h_{mk}^{I\pm}}{\alpha_m^{I\pm} - \mu_I \Lambda_m^{\pm}} , \\ \varkappa_{mj}^{I\pm} &= \frac{h_{mj}^{I\pm} - j\, \varkappa_{m,j+1}^{I\pm}}{\alpha_m^{I\pm} - \mu_I \Lambda_m^{\pm}} \qquad (j = k-1, \ldots, 1) \end{aligned}\right\} \tag{74}$$

with an analogous definition of the $\varkappa_{mj}^{II\pm}$. It is supposed that the denominators in (74) are $\neq 0$. The case where one of them happens to be zero, or approximately zero, is handled as described in Appendix VII.

The integration constants $C_m^{I\pm}$ and $C_m^{II\pm}$ are determined from the boundary conditions

$$|\chi_m^{I+}(-\infty)| < \infty \quad , \tag{75}$$

$$\chi_m^{I\pm}(0) = \chi_m^{II\pm}(0) \quad , \tag{76}$$

$$|\chi_m^{II-}(\infty)| < \infty \quad . \tag{77}$$

Remembering the signs of $A_m^{\pm}$ (see (60)) we derive from (75) that

$$C_m^{I+} = 0 \tag{78}$$

and from (77) that

$$C_m^{II-} = 0 \quad , \tag{79}$$

whereafter (76) yields

$$C_m^{II+} = \chi_{m1}^{I+} - \chi_{m1}^{II+} - \frac{h_{m0}^{I+}}{\mu_I \Lambda_m^+} \tag{80}$$

and

$$C_m^{I-} = \chi_{m1}^{II-} - \chi_{m1}^{I-} + \frac{h_{m0}^{I-}}{\mu_I \Lambda_m^-} \quad . \tag{81}$$

Now the transformed flux χ at the actual wavelength point can be calculated in our grid points $\{z_i\}$ as well as in prescribed calculation heights $\{h_n\}$ in medium II. The transformation back to ϕ is easily established (see (54) - (56) and (61)). The fluxes in $\{z_i\}$ are used for the subsequent flux calcula. ons at longer wavelengths.

If medium II is a vacuum, the computational model outlined above requires certain modifications; these are described in Appendix VIII.

4. INTEGRAL FIELD QUANTITIES

In chapters 2 and 3 we discussed the calculation of the differential and angular energy flux $I(z, \mu, \lambda)$, which was the solution of the transport problem sketched in fig. 1. In this chapter we shall derive certain integral quantities of physical importance. We consider reference points in the source-free medium II, i.e. we assume $z \geq 0$.

When $I(z, \mu, \lambda)$ is integrated over μ we obtain the differential energy flux

$$\Phi(z, E) = \int_{4\pi} I(z, \mu, \lambda)\, d\underline{\Omega} = 2\pi \int_{-1}^{1} I(z, \mu, \lambda)\, d\mu \tag{82}$$

($E = f_o/\lambda$, $f_o = 0.5110058$), and from Φ we derive three integral field quantities by another integration from $E = E_1$ to $E = E_2$ (or from $\lambda = \lambda_2 = f_o/E_2$ to $\lambda = \lambda_1 = f_o/E_1$):

(i) The number flux (photons $cm^{-2}\, s^{-1}$)

$$N(z; E_1, E_2) = \int_{E_1}^{E_2} \Phi(z, E)/E\, dE = \int_{\lambda_2}^{\lambda_1} \Phi(z, E)/\lambda\, d\lambda \quad . \tag{83}$$

(ii) The energy flux (Mev $cm^{-2}\, s^{-1}$)

$$N_e(z; E_1, E_2) = \int_{E_1}^{E_2} \Phi(z, E)\, dE = f_o \int_{\lambda_2}^{\lambda_1} \Phi(z, E)/\lambda^2\, d\lambda \quad . \tag{84}$$

(iii) The absorbed dose rate (Mev $g^{-1}\, s^{-1}$)

$$D(z; E_1, E_2) = \int_{E_1}^{E_2} \Phi(z, E)\mu_{ea}^{II}(E)\, dE = f_o \int_{\lambda_2}^{\lambda_1} \Phi(z, E)\mu_{ea}^{II}(E)/\lambda^2 d\lambda; \tag{85}$$

μ_{ea}^{II} is the energy-absorption coefficient ($cm^2\, g^{-1}$) for medium II.

When specializing eqs. (82) - (85) to the present problem, we partition all the quantities into uncollided and scattered components (as was the case for $I(z, \mu, \lambda)$ in eq. (5))

$$\Phi = \Phi^{(u)} + \Phi^{(s)} \quad , \tag{86}$$

$$N = N^{(u)} + N^{(s)} \quad , \tag{87}$$

$$N_e = N_e^{(u)} + N_e^{(s)} , \tag{88}$$

$$D = D^{(u)} + D^{(s)} , \tag{89}$$

and start to calculate the uncollided terms. We have

$$\Phi^{(u)} = 2\pi \int_{-1}^{1} U(z, \omega, \lambda)\, d\omega \ ; \tag{90}$$

if the expression (10) for U when $z > 0$ is inserted, the result is

$$\Phi^{(u)} = 2\pi \int_0^1 p(\lambda) \exp\left(-\frac{\mu_x(\lambda)}{\omega} z\right) d\omega = 2\pi\, p(\lambda)\, E_2(\mu_x(\lambda) z) , \tag{91}$$

where E_2 is the second-order exponential integral defined in Appendix III. By (11) this can also be written

$$\Phi^{(u)} = \frac{E\, q(\lambda)}{2\,\mu_I(\lambda)} E_2(\mu_x(\lambda) z) , \tag{92}$$

a well-known formula in radiation shielding.

When the line spectrum (33) is substituted for $q(\lambda)$ we easily arrive at the following formulas:

$$\Phi^{(u)} = \sum_{p=1}^{P} \frac{E_p Q_p}{2\mu_I^{(p)}} \delta(E - E_p)\, E_2(\mu_x^{(p)} z) , \tag{93}$$

$$N^{(u)} = \sum_p \frac{Q_p}{2\mu_I^{(p)}} E_2(\mu_x^{(p)} z) , \tag{94}$$

$$N_e^{(u)} = \sum_p \frac{Q_p E_p}{2\mu_I^{(p)}} E_2(\mu_x^{(p)} z) , \tag{95}$$

$$D^{(u)} = \sum_p \frac{Q_p E_p}{2\mu_I^{(p)}} \mu_{ea}^{II}(E_p)\, E_2(\mu_x^{(p)} z) , \tag{96}$$

where the summations in (94) - (96) extend over the lines in the integration interval for E.

Next we calculate the scattered components of (86) - (89). The scattered

differential energy flux can be written (cf. (5), (12), (82)):

$$\Phi^{(s)} = 2\pi \int_{-1}^{1} \psi(z, \omega, \lambda)\, d\omega$$

$$= 2\pi \left[\int_{-1}^{0} \psi^-(z, \omega, \lambda)\, d\omega + \int_0^1 \psi^+(z, \omega, \lambda)\, d\omega \right] . \tag{97}$$

The "minus" and "plus" components ψ^- and ψ^+ are replaced by their double-P_1 approximations (cf. (18))

$$\psi^{\pm}(z, \omega, \lambda) \approx \psi_0^{\pm}(z, \lambda) + 3\,\psi_1^{\pm}(z, \lambda)(2\omega \mp 1) . \tag{98}$$

Only the zero'th harmonics contribute to (97) (cf. the orthogonality properties of $P_\ell^{\pm}(\omega)$, Appendix I), and we find

$$\Phi^{(s)} = 2\pi \left(\psi_0^+(z, \lambda) + \psi_0^-(z, \lambda)\right) , \tag{99}$$

and from this follows immediately

$$N^{(s)} = 2\pi \int_{\lambda_1}^{\lambda_2} \left(\psi_0^+(z, \lambda) + \psi_0^-(z, \lambda)\right)/\lambda \, d\lambda , \tag{100}$$

$$N_e^{(s)} = 2\pi f_0 \int_{\lambda_1}^{\lambda_2} \left(\psi_0^+(z, \lambda) + \psi_0^-(z, \lambda)\right)/\lambda^2 \, d\lambda , \tag{101}$$

and

$$D^{(s)} = 2\pi f_0 \int_{\lambda_1}^{\lambda_2} \left(\psi_0^+(z, \lambda) + \psi_0^-(z, \lambda)\right) \mu_{ea}^{II}(\epsilon)/\lambda^2 \, d\lambda . \tag{102}$$

5. DATA PROCESSING SYSTEM

A self-contained system of data files and computer programs related to the subjects treated in chapters 2-4 was established for operation on the B6700 at the Computer Installation at Risø. As the programs are written in FORTRAN and the data files contain card images, this data-processing system could be implemented on other machines without great effort.

The four data files are collected on a single multi-file magnetic tape GAMMABANK and are described in detail in section 5.1.

The programs GAMP1 and GFX calculate double-P_1 angular flux co-

efficients and integral field quantities, respectively. Both use the GAMMABANK as data source, and GAMP1 may in addition pass calculation results to it. These programs are discussed in sections 5.1. and 5.2. In section 5.3. three editing programs GBUPDATE, GBCROS, and GBPRINT are discussed.

The operation of the complete data-processing system appears from the flow diagram in fig. 3.

5.1. Data File System: GAMMABANK

The multi-file tape GAMMABANK contains three files of basic data and one file of results and may be considered as the heart of the complete data--processing system, see fig. 3. This figure also shows the various possibilities for updating GAMMABANK: the program GBUPDATE (sec. 5.4.) may update FILE1 and FILE2, whereas GAMP1 (sec. 5.2.) may update FILE4. Any updating of GAMMABANK proceeds in the "ping-pong" mode with two magnetic tapes and with the disk of the computer as intermediate storage; at the next updating the two tapes are interchanged, and so on.

All the four files are composed of card images, i.e. the records are EBCDIC character strings of maximum length 80 char. In the following a short description is given of the contents of the files and the format of the records.

FILE1: Photon Emission Data

The photon source in our problem is the line spectrum from Th, U, or K. The evaluation of emission data for these radionuclides (number of photons per 100 disintegrations for each line) is discussed in Appendix XI. Here we shall only consider the representation of the data on FILE1. The structure appears from Appendix XII which contains a print-out per 1. Sep. 1974 of FILE1. The first record on the file is an identification no. for the whole tape (identifier NOTAPE, format I10). Each time GAMMABANK is updated, NOTAPE is increased by 1. All remaining records in FILE1 have the form

ENERGY, YIELD, ILINE, NLINE, IEMIT

and the format F7.4, F7.2, 2I4, I6. The emitter code IEMIT is a four-digit number (pos. 25-28). The code for tr. first digit is:

1: Thorium
2: Uranium
3: Potassium.

The last three digits form an isotope code, such that IEMIT altogether may assume the following four values:

1232 for ^{232}Th
2238 for ^{238}U
2235 for ^{235}U
3040 for ^{40}K.

All records with one emitter code are placed consecutively on the file. NLINE is the number of emission lines for the actual IEMIT. ILINE denotes the sequence no. of the actual line for the actual IEMIT, and ENERGY its energy. Increasing line nos. correspond to decreasing energies. YIELD denotes the intensity of the actual line, in photons per 100 disintegrations. The program GBUPDATE is used to perform updatings of FILE1, see section 5.4.

FILE2: Material Composition Data

A print-out of FILE2 as of 1st September 1974 is given in Appendix XII; it comprises the materials studied in chapter 6. A record has the form

IZ, WPCT, ICONST, NCONST, RHO, MIX

and the format I4, F9.4, 2I4, F12.6, I4. The composition code MIX lies in the interval $1 \leq MIX \leq 99$ and characterizes the material. Records for one material are placed consecutively on the file. Their number is NCONST = number of elements in the material. RHO is the density of the material (g cm^{-3}). NCONST, RHO and MIX do not change for records belonging to one material; the first of these has ICONST = 1, the next ICONST = 2 and so on, until ICONST = NCONST. IZ is the atomic number; these values must be ranged in increasing order. WPCT is the weight percent of the actual elements in the material. The weight percents for one material must total $100.00 \pm 0.01\%$ to be accepted by the system. The program GBUPDATE is used to perform updatings of FILE2, see section 5.4.

FILE3: Cross Section Data

This file contains cross-section data in ENDF/B-format for the following 19 elements:

Z	SYMBOL
1	H
6	C
7	N
8	O
11	Na
12	Mg
13	Al
14	Si
15	P
16	S
17	Cl
19	K
20	Ca
22	Ti
25	Mn
26	Fe
53	I
56	Ba
82	Pb.

Cross sections are given for the following processes, characterized by the ENDF/B standard code MT:

MT	TYPE OF CROSS SECTION
501	Total
502	Coherent scattering
504	Incoherent scattering
516	Pair production (includes triplet)
602	Photoelectric

FILE3 was constructed by deletion of the complete Livermore library DCL-7D[13] (this deletion was made by the U.S. program DAMMET). FILE3 cannot be updated by our data-processing system in fig. 3.

FILE4: Angular Flux Results

The records of FILE4 are produced by the double-P_1 program GAMP1, cf. fig. 3 and section 5.2. Each record contains the 13 items

E, λ, ϕ_0^+, ϕ_1^+, ϕ_0^-, ϕ_1^-, i, d, N, z, IMIX1, IRADIO, IMIX2, where

E = photon energy (Mev),

λ = Compton wavelength,

$\left.\begin{matrix}\phi_0^+\\ \phi_1^+\\ \phi_0^-\\ \phi_1^-\end{matrix}\right\}$ = { Expansion coefficients in the double-P_1 approximation (eq. (98)) of the scattered flux (or the flux jump if d = 1, see below),

i = wavelength index (cf. (49)),

d = discontinuity index:
d=0 if $\lambda=\lambda_i$ is a point of continuity for ψ,
d=1 if $\lambda=\lambda_i$ is not a point of continuity for ψ,

N = number of wavelength intervals (cf. (49)),

z = height (cm) of calculation point (fig. 1), ($z \geq 0$)

IMIX1 = composition code for medium I (cf. FILE2),

IRADIO = code for radio element in medium I, being 1, 2, or 3 (cf. FILE1),

IMIX2 = composition code for medium II (cf. FILE2).

More details of these quantities and the organization of the records are given in section 5.2.

The format of a FILE4 record is:

F6.4, F7.4, 1P4E11.4, I4, I1, I4, 0PF8.1, I3, I1, I2

(1P and 0P are FORTRAN I/O scale factors).

A catalog of FILE4 per 1st September 1974 is given in Appendix XII.

5.2. The Program GAMP1

The FORTRAN program GAMP1 (Danish AEC program no. 648) carries out the double-P_1 calculations outlined in chapter 3. Its position in the data processing system is apparent from fig. 3. The description given here refers to the version as of 1st September 1974.

Structure

GAMP1 consists of a driver program (MAIN), and the subprograms GAMPA, GAMP, DATAIO, MYG, AH, EXINT2, WQUADR, AKERNL, EXPPOL, COLDEC, and COLSOL. Variable dimensions are used in order to efficiently utilize the fast memory; the array bounds are passed from the

driver program to the master subroutine GAMPA (or GAMP if medium II is vacuum), which governs the flow of the calculations, see the flow diagram in fig. 4. The other subprograms are discussed below.

Description of Subprograms

DATAIO is a subroutine that reads input data from punched cards, prints out these data, and passes them to the main program.

MYG is a subroutine calculating a set of photon cross sections for a given set of energies, a given process type, and a given material. It applies double-logarithmic interpolation on the subset of Livermore tabulations in GAMMABANK/FILE3 (section 5.1). The material is specified by its MIX code (section 5.1); hence MYG can only calculate cross sections for those materials contained in GAMMABANK/FILE2. The process type is specified by the ENDF/B code MT, see section 5.1, FILE3.

AH is a subroutine that calculates the coefficients a, b, ..., h in (39). These numbers are linear combinations of A(Y), ..., F(Y) (see (39), (40) ff., and Appendix IV), which in turn are given as infinite series:

$$A(Y) = \sum_{n=0}^{\infty} \frac{2n+1}{2} c_{no}^2 P_n(Y) , \qquad (103)$$

and similar expressions for the others. They are to be calculated for a set of discrete and equidistant Y-values in the interval $-1 \leq Y \leq 1$ (as $Y = 1 + \lambda' - \lambda$ and $\lambda' \leq \lambda \leq \lambda' + 2$). From (A13)-(A18) it appeared sufficient to calculate directly only A(Y) and E(Y) and only for $Y \geq 0$. In his paper, Gersti[7] operates with series of a nature similar to that of our series, also containing P_n. He points out that the partial sum of such series,

$$s_N = \sum_{n=0}^{N} a_n , \qquad (104)$$

converges only slowly to the limit as $N \to \infty$, but that $s - s_N$ for large N fluctuates regularly around zero. In fact, the average

$$\overline{s_N} = \frac{1}{6} \sum_{m=1}^{6} s_{N-m+1} \qquad (105)$$

has proved to approach s quite fast. In the present subroutine $\bar{s}_{200}$ is used as an approximation to s; c_{no}, c_{n1}, and $P_n(Y)$ are calculated by successive application of the appropriate recursion relations.

EXINT2 is a function subprogram calculating the second-order exponential integral

$$E_2(x) = x \int_x^{\infty} \frac{\exp(-t)}{t^2} dt \qquad (106)$$

for $x \geq 0$. The values obtained by EXINT2 were compared to Placzek's table reproduced in Goldstein pp. 358-65[9]. In no case was a deviation found of more than one in the least significant decimal place.

WQUADR is a subroutine that calculates the quadrature weights in (A19) for arbitrary values m (= $j_2 - j_1 + 1$) of the number of quadrature points. The formulas are given in Appendix V.

AKERNL is a function subprogram which calculates the variable factor of the scattering kernel (2), viz.:

$$k(\lambda', \lambda) / (\tfrac{3}{8} n_e \sigma_o) = \frac{\lambda'}{\lambda} \left(\frac{\lambda}{\lambda'} + \frac{\lambda'}{\lambda} - 2(\lambda - \lambda') + (\lambda - \lambda')^2 \right) . \qquad (107)$$

EXPPOL is a subroutine that carries out the least-squares fitting discussed in Appendix VI.

COLDEC and COLSOL are subroutines to be used in the solution of systems of linear equations with positive-definite matrices, as they occur in EXPPOL. The two routines belong to the Danish AEC Library of FORTRAN Subprograms at Risø (SF/148).

Specification of GAMP1 Input Data

GAMP1 extracts information from the first three files of the GAMMABANK tape, but in addition it reads control parameters from punched cards according to the following prescript:

GAMP1 INPUT

IDENTIFIER	FORMAT	DESCRIPTION
HEADL	13A6, A2	Headline for problem
NOTAPE	I10	|NOTAPE| must coincide with the identification no. for GAMMABANK before the updating. If NOTAPE⟨0, the tape updating is suppressed, and only lineprinter output appears.
IMIX1, IRADIO, IMIX2	3I10	IMIX1 is the material code for medium I. IRADIO denotes the radioelement in the following code: 1 for Th, 2 for U, 3 for K. IMIX2 is the material code for medium II. If this is a vacuum, set IMIX2=0.
ECUT	E10.0	Lower energy cutoff (Mev)
MLAM	I10	Number of intervals into which the unit wavelength is divided on calculating (m in fig. 2 and section 3.2); the standard value is 64.
conditioned on IMIX2 ⟩ 0 — NH	I10	Number of calculation heights in medium II.
(AZH(N), N=1, NH)	8E10.0	Calculation heights (cm).

In the present version of GAMP1 two parameters were fixed in the program itself:

NZ = 9. This is the n in Appendix VI denoting the number of fixed space mesh points in each medium.

KM1 = 2. This is the degree of the polynomials used in least-squares fit (k - 1 in (70), (71)).

It was experience from the previous GAMP1 model[6] that led to these choices.

Description of Output

Calculation results will normally be passed to the magnetic tape GAMMABANK, see section 5.2, FILE4. Each record transmitted to this file contains 13 items:

$$E,\ \lambda,\ \psi_o^+,\ \psi_1^+,\ \psi_o^-,\ \psi_1^-,\ i,\ d,\ N,\ z,\ IMIX1,\ IRADIO,\ IMIX2;$$

their formats and definitions were given in section 5.1. FILE4 is cumulative, so that records from earlier GAMP1 runs are saved.

Based on the GAMP1 input values ECUT and MLAM together with the maximum energy in the line spectrum of the actual radio element (FILE1), a set $\{\lambda_i\}$ of equidistant wavelengths is constructed. A set $\{z_n\}$ of prescribed calculation heights was specified in the GAMP1 input. The results of the GAMP1 calculations are the double-P_1 expansion coefficients $\psi_o^\pm(z_n, \lambda_i)$ and $\psi_1^\pm(z_n, \lambda_i)$, where $1 \leq i \leq N$ and $1 \leq n \leq n_{max}$ (the number of calculation heights). These double-indexed terms are calculated in the following order: first i = 1 and n = 1, 2, ..., n_{max}; then i = 2 and n = 1, 2, ..., n_{max}; and so on. However, it is more practical that the records on FILE4 are in the reverse order, i.e. all records for one height are consecutive. Hence the results must be reorganized before the transmission to tape, and this is done by means of the disk of the computer.

If we consider the variation of items in consecutive records on FILE4, then the triplet IMIX1/IRADIO/IMIX2 and N vary least rapidly and are constant within records belonging to one GAMP1 run. The next slowest variation has the height z. For each combination of the items above we have a cluster of records with fluxes at N different wavelengths $\{\lambda_i\}$. If $\lambda = \lambda_i$ is a continuity point for the flux, only one record exists with this λ and has d = 0, see description of FILE4 in section 5.1, but if $\lambda = \lambda_i$ is not a point of continuity, two records will be necessary; the first contains limits from the left, $\psi_o^+(z, \lambda-0)$, etc., and has d = 0, the second contains the jumps $\psi_o^+(z, \lambda+0) - \psi_o^+(z, \lambda-0)$ etc, and has d = 1.

The output transmitted to the tape will also appear on the lineprinter, and so will the input data.

The GAMP1 results are normalized to a radioelement content of 1 percent by weight of Th, U, or K. Together with the specific activities

4100 dis. per g Th per s,
12227 dis. per g U per s,
3.311 dis. per g K per s,

(see also Appendix XI), this fixes the source strength in photons/cm^3/s.

Check Calculations, see Appendix IX and Appendix X.

5.3. The Program GFX

The FORTRAN program GFX (Danish AEC program no. 709) calculates integral field quantities on the basis of GAMP1 results, as outlined in chapter 4. Its position in the data processing system is apparent from fig. 3. The description given here refers to the version as of 1st September 1974.

Structure

GFX consists of a main program and the subprograms SORT, EXINT2, WQUADR, MYG, MYGEA, FINT.

The main program governs the flow of calculations and contains all the input/output instructions. It reads and prints out input data from cards (see Specification of GFX input) and reads source emission data from GAMMABANK/FILE1. After this, it calculates the uncollided contribution to the number flux, the energy flux, or the absorbed dose rate, whatever is desired, using (94), (95), or (96). To obtain the scattered flux or dose contribution, GFX reads data for the scattered angular flux in the specified height from FILE4, and evaluates the integral (100), (101) or (102).

This evaluation is carried out by means of the quadrature formulas in Appendix V, with due attention to the jumps in the integrand and to fractional wavelength intervals at both limits.

Description of subprograms

SORT is a subroutine which ranges the energies in the emission spectrum in increasing magnitude, before the cross-section routine MYG is called.

EXINT2, WQUADR, and MYG are the same as in GAMP1, see section 5.1.

MYGEA evaluates the energy-absorption coefficient μ_{ea}, if a dose rate calculation is desired (cf. (85)). μ_{ea} is computed by means of the analytical expression given in Goldstein[9].

FINT is a function subprogram which evaluates the integrand of (100), (101), or (102).

Specification of GFX input

GFX extracts information from all four files of the GAMMABANK tape, but in addition it reads control parameters from punched cards according to the following prescript:

GFX INPUT

	IDENTIFIER	FORMAT	DESCRIPTION
Basic data	K	I10	Calculation type K=1: Number flux calculation K=2: Energy flux calculation K=3: Dose rate calculation
	ALPHA	A3	DIR: Contribution from uncollided radiation only SCT: Contribution from scattered radiation only TOT: Contribution from total radiation
	NINT	I10	Number of energy intervals in which flux or dose should be calculated
	(EMINI(I), EMAXI(I), I = 1, NINT)	16F5.0	Energy limits for interval nos. 1, 2,..., NINT
	IPUNCH	I10	IPUNCH = 0: Output on line-printer only IPUNCH = 1: Additional punched output ("spectrum packages")
Repetitive data	HEADL	13A6, A2	Headline for problem
	IMIX1, IRADIO, IMIX2	3I10	IMIX1 is the material code for medium I. IRADIO denotes the radio-element in the following code: 1 for Th, 2 for U, 3 for K. IMIX2 is the material code for medium II. If this is vacuum, set IMIX2 = 0
	NH	I10	Number of calculation heights in medium II
	(AZH(N), N=1, NH)	8E10.0	Calculation heights (cm)
	return to "Repetitive data" so long as all data cards have not been read.		

Description of Output

The lineprinter output from GFX explains itself. As was the case for GAMP1, the GFX results are normalized to 1 percent Th, U, or K, by weight.

Check Calculation, see Appendix X.

5.4. Editing Programs

The three auxiliary programs GBUPDATE, GBCROS, and GBPRINT (fig. 3) carry out various editing tasks related to the files in GAMMABANK.

GBUPDATE (Danish AEC program no. 710) is used for updating FILE1 and FILE2. To update FILE1, a totally new card deck (excluding the tape identification no.) is provided to replace the old file. FILE2 may be extended by the addition of new materials. Card input is prepared according to the following scheme:

GBUPDATE INPUT

IDENTIFIER	FORMAT	DESCRIPTION
NUPDT1, NUPDT2	2I10	NUPDT1 is the number of emitters in a total replacement of FILE1. NUPDT1 = 0: no replacement NUPDT2 is the number of materials which are put on FILE2 from cards. NUPDT2 = 0: no updating
NOTAPE	I10	Identification no for GAMMABANK-tape before updating
ENERGY, YIELD, ILINE, NLINE, IEMIT	F7.4, F7.2, 2I4, I6	Replacement cards to a new FILE1 (if NUPDT1 > 0)
MAT, WPCT, ICONST, NCONST, RHO, IMIX	I4, F9.4, 2I4, F12.6, I4	Updating cards to FILE2 (if NUPDT2 > 0)

The program carries out an extensive check of the updated information

GBCROS (Danish AEC program no. 711) calculates gamma cross sections (cm^{-1}) for materials in the GAMMABANK by means of the subroutine MYG (section 5.2). For each material and each type of process one or more energies may be specified, see the input scheme below:

GBCROS INPUT

	IDENTIFIER	FORMAT	DESCRIPTION
	MIX, MT, NE	3I10	MIX = material code MT = ENDF/B code for process type: 501: total 502: coherent scattering 504: incoherent scattering 516: pair production 602: photoelectric effect If total minus coherent is desired, put MT = 0 NE = 0 means that an equidistant set of energies is assumed If NE > 0 then NE = number of arbitrary input energies
conditioned on NE = 0	EMIN, EMAX, M	2E10.0, I10	Equidistant set of energies from EMIN to EMAX with spacing (EMAX-EMIN)/M
conditioned on NE > 0	E(I), I = 1, NE	8E10.0	Photon energies ranged in increasing order
	IPUNCH	I10	IPUNCH = 0: Output on lineprinter only IPUNCH = 1: Additional punched output ("spectrum packages")

return to beginning of scheme so long as all data cards have not been read.

GBPRINT (Danish AEC program no. 712) prints out the contents of the files of GAMMABANK, either as complete printouts or as catalogs.

GBPRINT INPUT

IDENTIFIER	FORMAT	DESCRIPTION
(IPRINT(N), N = 1, 4)	4I10	Array controlling lineprinter output for FILE1, ..., FILE4: IPRINT(N) = 0: No output for FILEN IPRINT(N) = 1: Catalog of FILEN IPRINT(N) = 2: Complete printout of FILEN

Appendix XII was produced by means of GBPRINT.

6. RESULTS FOR Th-U-K GAMMA-RADIATION FIELDS IN WATER

A collection of tables and graphs has been prepared with the purpose of illustrating one possible application of the data-processing system described in chapter 5. For the configuration studied, the source material (medium I) is quartz sand saturated with water (bulk density = 1.88 g/cm^3), and the source-free material (medium II) is water. We assume that the sand contains small traces of either Th, U, or K, but shall for convenience normalize all our results to a reference concentration of 1 percent radioelement. The radiation field is considered at the sand-water interface (z = 0) and at the distances z = 10, 20, 30, and 40 cm from the interface. These conditions were chosen for two reasons:

1. We know from an earlier investigation[19] that the computational method is accurate to within 10% for determination of scalar flux densities in water up to z = 50 cm.
2. The results given are relevant to the interpretation of radiometric surveys of sea-bed formations.

We point out that the sand/water configuration is less special than one might believe. First, the radiation field in medium II depends little on the composition of medium I so long as the latter contains no elements with high atomic numbers. Secondly, if the distance z is measured in units of the mean free path in medium II, the field is fairly insentitive to variations in the composition of medium II. For example, the radiation field in air at z = 300 m is very similar to that in water at z = 40 cm.

In tables 2 through 16 we present the energy distribution of the scalar number flux of uncollided as well as scattered photons produced by each

radioelement at the five reference levels in the water. As the flux is given at intervals as small as 0.01 Mev, the tables may be used for calculation of the corresponding pulse-height spectra of a gamma-ray detector with approximately constant angular counting cross section and known response function[19].

Table 17 shows the dose rate produced by the gamma-ray flux for each value of z. The dose rate was calculated as the sum of one term due to photons with E $>$ 0.1 Mev and another term with E $<$ 0.1; the latter contribution was obtained by extrapolation.

For a selected level in the water, z = 20 cm, the flux distributions are shown graphically in figs. 9, 10, and 11. It is instructive to compare the emission spectra of Th and U (figs. 7 and 8) with the flux distributions to which these radioelements give rise (figs. 10 and 11). The comparison clearly illustrates the two basic characteristics of photon transport phenomena: the attenuation of the uncollided flux components and the build-up of a scattered flux component.

Finally, we have studied the angular distribution of the photon flux in water above sand with potassium as the radioelement. Fig. 12 shows the distribution of uncollided 1.461 - Mev photons in the water at z = 10 cm and z = 40 cm, calculated from the analytical expression in chapter 2 (eq. (10)). We notice that the distribution is peaked in the upward direction $\mu = 1$, and that this peaking becomes more pronounced with increasing z. Fig. 13 shows the angular distribution of scattered photons for the same configuration, but for the photon energies 1.0 Mev, 0.3 Mev, and 0.1 Mev; these graphs were constructed from the expression for the double-P_1 approximation, eq. (98). The graphs clearly demonstrate the increasing amount of "skyshine" (photons with $\mu < 0$) when the energy decreases, and that the distributions for fixed energy tend to be more upward-peaked with increasing height in medium II. The small jumps in the transition from positive to negative μ reflect the truncation error in the double-P_1 approximation. This error is smallest when z is small, in agreement with the general experience that the accuracy of the double-P_1 method is best near the boundary[1.7]. The graphs presented in figs. 12 and 13 would be very similar to those obtained if medium II were air with z = 80 m and z = 300 m, respectively.

CONCLUSION

Starting with the double-P_1 approximation, the photon transport problem was solved for semi-infinite, plane-geometry conditions. The solution forms the basis of a data-processing system for computational evaluation of the natural radiation fields above plane geologic formations. As an application of the system, calculations were made of the contributions from thorium, uranium, and potassium to the radiation field in water superposing sand. The system appears to be very suitable as a source of information in computational studies of aerial, gamma-spectrometric survey techniques.

REFERENCES

1) B.G. Bennett and H.L. Beck, Legendre, Tschebyscheff, and Half-Range Legendre Polynomial Solutions of the Gamma Ray Transport Equation in Infinite Homogeneous and Two Media Plane Geometry. HASL-185 (1967) 68 pp.

2) H. Beck and G. de Planque, The Radiation Field in Air Due to Distributed Gamma-Ray Sources in the Ground. HASL-195 (1968) 59 pp.

3) H.L. Beck, J. De Campo, and C. Gogolak, In situ Ge (Li)and NaI(Tl) Gamma-Ray Spectrometry. HASL-258 (1972) 75 pp.

4) H.L. Beck, The Physics of Environmental Gamma Radiation Fields. In: Proceedings of the Second International Symposium on the Natural Radiation Environment, Houston, Tex., 7-11 August 1972 (in press).

5) H.L. Beck, Gamma Radiation from Radon Daughters in the Atmosphere. J. Geophys. Res. 79 (1974) 2215-2221.

6) P. Kirkegaard, Double-P_1 Calculation of Gamma-Ray Transport in Semi-Infinite Media. Risø-M-1460 (1972) 37 pp.

7) S.A. W. Gerstl, An Improved Double P_L Method Applied to Gamma Transport. Nukleonik 8 (1966) 101-108.

8) H. Goldstein and J.E. Wilkins, Jr., Calculation of the Penetration of Gamma Rays. Final Report. NYO-3075 (1954) 203 pp.

9) H. Goldstein, Fundamental Aspects of Reactor Shielding (Addison-Wesley, Reading, Mass., 1959) 416 pp.

10) P. Kirkegaard, Some Aspects of the General Least-Squares Problem for Data Fitting. Risø-M-1399 (1971) 16 pp.

11) E.T. Whittaker and G.N. Watson, A Course of Modern Analysis, 4th ed. (University Press, Cambridge, 1952) 608 pp.

12) C.-E. Fröberg, Lärobok i numerisk analys (Bonniers, Stockholm, 1962) 277 pp.

13) W.H. McMaster, N. Keer Del Grande, J.H. Mallett, J.H. Hubbell, Compilation of X-Ray Cross Sections. UCRL-50174 (Sec. 1-4)(1969-70).

14) P. Kirkegaard, Nuclear Particle Transport with Emphasis on Monte-Carlo and Shielding Calculations. Risø Report No. 136 (1966) 110 pp.

15) H. L. Beck, The Absolute Intensities of Gamma Rays from the Decay of ^{238}U and ^{232}Th. HASL-262 (1972) 14 pp.

16) C. M. Lederer, J. M. Hollander, and I. Perlman, Tables of Isotopes, 6th ed. (Wiley, New York, 1967) 594 pp.

17) E. K. Hyde, I. Perlman, and G. T. Seaborg, The Nuclear Properties of the Heavy Elements. Vol. 2 (Prentice Hall, Englewood Cliffs, N. J., 1964) 1107 pp.

18) J. A. S. Adams and P. Gasparini, Gamma-Ray Spectrometry of Rocks (Elsevier, Amsterdam, 1970) 295 pp.

19) L. Løvborg and P. Kirkegaard, Response of 3" x 3" NaI(Tl) Detectors to Terrestrial Gamma Radiation. Nucl. Instrum. Meth. (in press).

APPENDIX I
THE POLYNOMIALS $P_l^{\pm}(\omega)$

From the definition $P_l^{\pm}(\omega) = P_l(2\omega \mp 1)\, H(\pm\omega)$ $(l = 0, 1, 2, \ldots)$ and the recurrence relation for $P_l(\omega)$,

$$\omega P_l(\omega) = \frac{l+1}{2l+1} P_{l+1}(\omega) + \frac{l}{2l+1} P_{l-1}(\omega) ,$$

the following recurrence formula is obtained:

$$\pm P_l^{\pm}(\omega) = 2\omega P_l^{\pm}(\omega) - \frac{l+1}{2l+1} P_{l+1}^{\pm}(\omega) - \frac{l}{2l+1} P_{l-1}^{\pm}(\omega) \quad . \tag{A1}$$

The orthogonality relations are

$$\int_{\mp}^{+} P_l^{\pm}(\omega)\, P_m^{\pm}(\omega)\, d\omega = \frac{1}{2l+1} \delta_{lm} \tag{A2}$$

APPENDIX II
THE COEFFICIENTS $c_{nl}^{\pm}$ [7]

From the definition $c_{nl}^{\pm} = \int_{\mp}^{+} P_n(\omega)\, P_l^{\pm}(\omega)\, d\omega$, some elementary properties are deduced:

$$c_{no}^{+} + c_{no}^{-} = 2\,\delta_{no} \tag{A3}$$

$$c_{nl}^{-} = (-1)^{n+l} c_{nl}^{+} \tag{A4}$$

hence only c_{nl}^{+} need be considered (the superscript + is dropped in the following;

$$\forall\, l > n: \quad c_{nl} = 0 \tag{A5}$$

$$c_{2\nu,o} \quad \delta_{\nu o} \tag{A6}$$

$$c_{2\nu-1,o} = \frac{(-1)^{\nu-1}(2\nu)!}{2^{2\nu}(2\nu-1)(\nu!)^2} \tag{A7}$$

(cf. ref. 11 p. 306). (A6) and A7) give a convenient calculation procedure for c_{no}:

$$c_{oo} = 1, \quad c_{10} = \frac{1}{2}, \quad c_{no} = -\frac{n-2}{n+1} c_{n-2,o}, \quad n = 2,3,4, \ldots \tag{A8}$$

It may be shown that c_{n1} can be calculated from

$$c_{n1} = \frac{2}{n+2} c_{n-1,o} - c_{no} \quad . \tag{A9}$$

Finally we shall prove that

$$\sum_{n=0}^{\infty} \frac{2n+1}{2} c_{nl}^2 = \frac{1}{2l+1} \quad . \tag{A10}$$

We define a function $Y_l(\omega)$, $-1 < \omega < 1$:

$$Y_l(\omega) = \begin{cases} 0 & , \quad -1 < \omega < 0 \\ P_l^+(\omega) & . \quad 0 < \omega < 1 , \end{cases}$$

and expand it in spherical harmonics, $Y_l(\omega) = \sum_{n=0}^{\infty} a_{nl} P_n(\omega)$ with

$$a_{nl} = \frac{2n+1}{2} \int_0^1 P_l^+(\omega) P_n(\omega) \, d\omega = \frac{2n+1}{2} c_{nl} \quad .$$

But from (A2) we obtain

$$\frac{1}{2l+1} = \int_{-1}^{1} [Y_l(\omega)]^2 \, d\omega = \sum_{n=0}^{\infty} a_{nl}^2 \frac{2}{2n+1} = \sum_{n=0}^{\infty} \frac{2n+1}{2} c_{nl}^2 \quad ,$$

and thus (A10) is verified.

APPENDIX III
THE INTEGRALS V_l

The source-induced integrals $V_l(y) = \int_0^1 P_l^+(\omega) \exp\left(-\frac{y}{\omega}\right) d\omega$ can be expressed in terms of the second-order exponential integral

$$E_2(y) = y \int_y^{\infty} \frac{\exp(-t)}{t^2} \, dt \quad .$$

For $l = 0$ and 1 we find

$$V_0(y) = E_2(y) \quad , \tag{A11}$$

$$V_1(y) = \exp(-y) - (1+y) E_2(y) \quad . \tag{A12}$$

APPENDIX IV
THE COEFFICIENTS A, B, C, D, E, F

These figures were defined after eq. (37); they are functions of $\lambda - \lambda'$, or, which is the same, of the parameter $\gamma = 1 + \lambda' - \lambda$. It is easily shown that there are the following relations between them:

$$A(\gamma) + B(\gamma) = 1 \quad , \tag{A13}$$

$$C(\gamma) - D(\gamma) = 0 \quad , \tag{A14}$$

$$E(\gamma) + F(\gamma) = \frac{1}{3}\gamma - 2C(\gamma) \quad , \tag{A15}$$

$$A(\gamma) + C(\gamma) = \frac{1}{2} + \frac{1}{2}\gamma \quad . \tag{A16}$$

Once A and E are calculated, the others follow from these formulas. Further, it is only necessary to compute $A(\gamma)$ and $E(\gamma)$ for $\gamma \geq 0$ owing to the relations

$$A(-\gamma) = 1 - A(\gamma) \quad , \tag{A17}$$

$$E(-\gamma) = 1 + \frac{2}{3}\gamma - 2A(\gamma) + E(\gamma) \quad . \tag{A18}$$

For $\gamma = 1$ we find $A(1) = \sum_{n=0}^{\infty} \frac{2n+1}{2} c_{no}^{+2}$ and $E(1) = \sum_{n=0}^{\infty} \frac{2n+1}{2} c_{n1}^{+2}$;

(A10) gives immediately $A(1) = 1$ and $E(1) = \frac{1}{3}$, whereafter (A13-16) give $B(1) = 0$, $C(1) = 0$, $D(1) = 0$, and $F(1) = 0$.

APPENDIX V
NUMERICAL QUADRATURE

Eq. (43) contains integrals which in (48) were replaced by sums

$$\int_{\lambda_1}^{\lambda_2} F(\lambda)\, d\lambda \approx \sum_{j=j_1}^{j_2} w_j F(\lambda_j)\, \Delta\lambda \quad ; \qquad \text{(A19)}$$

we shall in particular be concerned with the quadrature weights w_j (ξ_{ij} in (48)). The integrand may have discontinuities in the interval considered; such points will be taken as boundaries between different quadrature ranges for evaluation of the sum, which breaks into parts representing intervals of continuity (for a discontinuity point, w_j will be the sum of two terms). In (A19) we may hereafter suppose that $F(\lambda)$ is continuous, and we shall state the applied quadrature rules with the associated weights w_j. The formula chosen depends on the number of intervals $n = j_2 - j_1$, as specified below.

n	Quadrature rule	Quadrature weights
1	Trapezoidal	$w_{j_1} = w_{j_2} = \frac{1}{2}$
3	Cote's 3rd order[12]	$w_{j_1} = w_{j_2} = \frac{3}{8}$, $w_{j_1+1} = w_{j_2-1} = \frac{9}{8}$
even	Simpson	$w_{j_1} = w_{j_2} = \frac{1}{3}$, $w_{j_1+1} = w_{j_1+3} = \ldots = w_{j_2-1} = \frac{4}{3}$, $w_{j_1+2} = w_{j_1+4} = \ldots = w_{j_2-2} = \frac{2}{3}$
odd, $\rangle 3$	Cote's 3 rd order for the short-wavelength part, Simpson for the remaining	Combination of the two types above

APPENDIX VI
LEAST - SQUARES FIT

We shall consider the determination of the coefficients in the expressions (70) and (71) for each function

$$h(z) = \begin{cases} h_m^{I\pm}(z) \\ h_m^{II\pm}(z) \end{cases} . \qquad \text{(A20)}$$

In each medium a fixed set $\{z_i\}$ of discrete z-values ($i = 1, \ldots, n$) is selected in advance; we have chosen this set such that

$$\exp(-c|z_i|) = 1 - (i-1)/n \quad . \qquad \text{(A21)}$$

The transformation parameter c is taken to be equal to the γ-ray cross section for the medium at the shortest wavelength in the calculation range (this choice was promoted by considerations of numerical stability).

Each h(z) of (A20) is well-defined (although it might have resulted from fitting procedures at shorter wavelengths), so the values $h(z_i)$ can be calculated. The constant terms in (70) and (71) could be found analytically. Hence the general problem we face is to find a set of parameters $\{\alpha_1, \ldots, \alpha_k, \beta\}$ that makes the function

$$\left.\begin{aligned} f(x) &= \sum_{j=1}^{k} \alpha_j \varphi_j(x;\beta) \\ \text{with} \quad \varphi_j(x;\beta) &\equiv \exp(\beta x)\, x^{j-1} \end{aligned}\right\} \qquad \text{(A22)}$$

at $\{x_1, \ldots, x_n\}$ take on values $\{f_1, \ldots, f_n\}$ that are as close as possible to prescribed ordinates $\{y_1, \ldots, y_n\}$. A least squares fit is obtained by requiring that

$$\Phi = \sum_{i=1}^{n} w_i (y_i - f_i)^2 \qquad \text{(A23)}$$

must be minimum. w_i are the weights of the data points (in our case, the choice $w_i = i$ (cf. (A21)) was made; this emphasizes a good fit at great heights in medium II). We use the semi-linear method described in ref. 10. In this method, Marquardt iterations are performed in the non-linear space, which in our case is the one-dimensional β-space. The linear space is k-dimensional (cf. (70) and (71)) with points $\underline{\alpha} = (\alpha_1, \ldots, \alpha_k)^T$. The controlling equation $(\underline{A} + \lambda \underline{D}^2)\, \underline{\delta\beta} = \underline{g}$ [10] for Marquardt iterations specializes to

$$\delta\beta = \frac{g}{a(1+\lambda)} \qquad \text{(A24)}$$

with $a = \sum_i w_i \left(\frac{\partial f_i}{\partial \beta}\right)^2$ and $g = \sum_i w_i (y_i - f_i) \frac{\partial f_i}{\partial \beta}$. Given a β (guessed or iterated), the linear part of the problem will be to find the $\underline{\alpha}$-vector that minimizes Φ. This $\underline{\alpha}$ is a solution to the k th order linear system

$$\underline{\underline{C}}\,\underline{\alpha} = \underline{\gamma} \qquad \text{(A25)}$$

with

$$C_{j_1 j_2} = \sum_i w_i \varphi_{i j_1} \varphi_{i j_2} = \sum_i w_i \exp(\beta x_i)\, x_i^{j_1 - 1} \exp(\beta x_i)\, x_i^{j_2 - 1}$$

and

$$\gamma_j = \sum_i w_i y_i \varphi_{ij} = \sum_i w_i y_i \exp(\beta x_i) x_i^{j-1} \qquad (\varphi_{ij} \equiv \varphi(x_i;\beta)).$$

The derivative $\frac{\partial f_i}{\partial \beta}$ to be used to form (A24) has the value

$$\frac{\partial f_i}{\partial \beta} = \sum_{j=1}^{k} \left[\frac{\partial \alpha_j}{\partial \beta}\varphi_{ij} + \alpha_j \frac{\partial \varphi_{ij}}{\partial \beta}\right] = \sum_j \left[\frac{\partial \alpha_j}{\partial \beta}\exp(\beta x_i) x_i^{j-1} + \alpha_j x_i \exp(\beta x_i) x_i^{j-1}\right]$$

$$= x_i f_i + \exp(\beta x_i) \sum_j \frac{\partial \alpha_j}{\partial \beta} x_i^{j-1},$$

where $\underline{d} = \left(\frac{\partial \alpha_1}{\partial \beta}, \ldots, \frac{\partial \alpha_k}{\partial \beta}\right)^T$ satisfies the linear system

$$\underline{\underline{C}}\,\underline{d} = \underline{t} \quad \text{with} \quad t_j = \sum_i w_i \left[(y_i - f_i)\frac{\partial \varphi_{ij}}{\partial \beta} - \varphi_{ij} \sum_{j_1=1}^{k} \alpha_{j_1} \frac{\partial \varphi_{ij_1}}{\partial \beta}\right]$$

$$= \sum_i w_i (y_i - 2f_i) \exp(\beta x_i)\, x_i^j .$$

In the fitting procedure it was necessary to put some limitations on the variation of β. First, the sign of β is fixed by the requirement that the exponential must decay when moving away from the interface; further, we prevent β from approaching zero or infinity by stating a lower and an upper limitation for β, i.e. $\beta_{min} < |\beta| < \beta_{max}$.

APPENDIX VII
INDETERMINATE $\varkappa$-EXPRESSIONS

If one of the decay constants $\alpha_m^{I\pm}$ or $\alpha_m^{II\pm}$, resulting from the least-squares fit and entering the expressions (70) and (71), happens to be equal to $\varkappa_I A_m^{\pm}$ or $\varkappa_{II} A_m^{\pm}$, respectively, then the $\varkappa$-expressions (74) (or the analogous expressions for medium II) are indeterminate. In this case the solution (72) (or 73)) must be replaced by

$$\left.\begin{aligned} \chi_m^{I\pm}(z) = -\frac{h_{m0}^{I\pm}}{\mu_I \Lambda_m^{\pm}} + C_m^{I\pm} \exp(\mu_I \Lambda_m^{\pm} z) + z \exp(\alpha_m^{I\pm} z) \sum_{j=1}^{k} \varkappa_{mj}^{I\pm} z^{j-1} \\ (z < 0) \end{aligned}\right\} \qquad \text{(A26)}$$

with $\varkappa_{mj}^{I\pm} = h_{mj}^{I\pm} / j \quad (j = 1, \ldots, k)$

(or the analogous expression for medium II). The only differences between (A26) and (72) are that a factor z has entered into the last term in (A26) and that the $\varkappa_{mj}^{I\pm}$ have different meanings. If this modification is necessary, we must also replace the corresponding $\varkappa_{m1}$ in the boundary conditions (80) and (81) by zero.

Numerical considerations lead to use of the modified procedure also when a denominator in (74) should be close to zero.

APPENDIX VIII
VACUUM IN MEDIUM II [6)]

In this particular case the angular photon flux is constant everywhere in medium II, and we need only consider the transport equation in medium I ($z < 0$). All the equations for this zone derived for non-vacuum medium II are still valid up to eq. (72), where we must replace the boundary conditions by

$$|\chi_m^{I+}(-\infty)| < \infty \qquad \text{(A27)}$$

and

$$\chi_m^{I-}(0) = 0 \qquad \text{(A28)}$$

(A28) reflects the fact that we have no down-streaming photons at the interface. These conditions determine $C_m^{I\pm}$ in (72) to be:

$$C_m^{I+} = 0 \qquad \text{(A29)}$$

and

$$C_m^{I-} = - \chi_{m1}^{I-} + \frac{h_{m0}^{I-}}{\mu_I \Lambda_m^-} \quad . \qquad \text{(A30)}$$

APPENDIX IX
ANALYTICAL CHECK OF GAMP1

An analytical check of the double-P_1 expansion coefficients calculated by GAMP1 is possible, if we consider photons from a single-line source in medium I that have suffered only glancing collisions. The energy flux of these photons satisfies (7), which in this particular case reduces to:

$$\omega \frac{\partial}{\partial z} \psi(z,\omega) + \mu(z)\, \psi(z,\omega) = C\, n_e(z)\, u_0(z,\omega) \quad . \qquad \text{(A31)}$$

The argument $\lambda = \lambda_0 = f_0/E_0$ (the source wavelength) has been dropped in (A31). The constant C has the value

$$C = \frac{\lambda_0 r_0^2 Q}{2 \mu_I} \quad , \qquad \text{(A32)}$$

where r_0 is the classical electron radius (see (2) and ff.), Q is the source strength (photons/cm^3/s), and μ_I is the cross section for medium I at the source energy E_0. $n_e(z)$ is the density of electrons. As only positive values of ω are relevant in (A31), we have (cf. (10)):

$$u_0(z,\omega) = \begin{cases} 1 & \text{for} \quad z \le 0 \\ \exp\left(-\frac{\mu_{II}}{\omega} z\right) & \text{for} \quad z \ge 0 \end{cases} \qquad \text{(A33)}$$

(μ_{II} is the cross section for medium II at E_0). It is now easy to establish the complete solution of (A31) for $z < 0$ (medium I) as well as for $z > 0$ (medium II):

$$\psi(z,\omega) = \frac{C n_e^I}{\mu_I} + A_I(\omega) \exp\left(-\frac{\mu_I}{\omega} z\right), \quad z<0 \qquad \text{(A34)}$$

$$\psi(z,\omega) = \frac{C n_e^{II}}{\omega} z \exp\left(-\frac{\mu_{II}}{\omega} z\right) + A_{II}(\omega) \exp\left(-\frac{\mu_{II}}{\omega} z\right), \quad z>0 \qquad \text{(A35)}$$

(n_e^I and n_e^{II} are the electron concentrations in the media; $A_I(\omega)$ and $A_{II}(\omega)$ are integration constants). The usual boundary conditions imply that $A_I(\omega) = 0$ and $A_{II}(\omega) = C n_e^I / \mu_I$, i.e. the glancing-scattered energy flux in medium II has the analytical expression:

$$\psi(z,\omega) = C \left(\frac{n_e^{II}}{\omega} z + \frac{n_e^I}{\mu_I}\right) \exp\left(-\frac{\mu_{II}}{\omega} z\right) . \qquad \text{(A36)}$$

$(\omega > 0,\ z > 0)$

This flux can be represented exactly by an infinite expansion in half-range spherical harmonics:

$$\psi(z,\omega) = \sum_{l=0}^{\infty} (2l+1)\, \psi_l^+(z)\, P_l^+(\omega) \qquad \text{(A37)}$$

with expansion coefficients

$$\psi_l^+(z) = C \int_0^1 \left(\frac{n_e^{II}}{\omega} z + \frac{n_e^I}{\mu_I}\right) \exp\left(-\frac{\mu_{II}}{\omega} z\right) P_l(2\omega - 1)\, d\omega . \qquad \text{(A38)}$$

In particular we find for $l = 0$ and $l = 1$ that:

$$\psi_0^+(z) = C \left[n_e^{II} z\, E_1(\mu_{II} z) + \frac{n_e^I}{\mu_I} E_2(\mu_{II} z)\right] \qquad \text{(A39)}$$

and

$$\psi_1^+(z) = C \left[-n_e^{II} z\, E_1(\mu_{II} z) + \left(2 n_e^{II} z - \frac{n_e^I}{\mu_I}\right) E_2(\mu_{II} z) + \frac{2 n_e^I}{\mu_I} E_3(\mu_{II} z)\right] ; \qquad \text{(A40)}$$

$E_n(x)$ stands for the nth-order exponential integral (cf. Appendix III):

$$E_n(x) = \left\{ \int_0^1 \omega^{n-2} \exp(-x/\omega)\, d\omega \right\} = x^{n-1} \left\{ \int_x^\infty \exp(-t)/t^n \, dt \right\} \quad \text{(A41)}$$

Now, a comparison can be made between the analytical expressions (A39, A40) for the expansion coefficients Ψ_0^+ and Ψ_1^+, and the corresponding values calculated by GAMP1. The latter are approximate both because of the truncation of the double-P_l equations (20) beyond the first-order terms and because of the least-squares fitting in the variable z. This comparison was made for water above sand with 1% K, and the result is shown in fig. 5 for the range of heights $0 < z < 40$ cm.

APPENDIX X
MONTE CARLO CHECK OF GAMP1/GFX

An independent check of the programs and files in our data processing system (fig. 3) was made by calculation of the absorbed dose rate in water above sand by GFX as well as by the Monte Carlo code MC4[14]. The latter is primarily intended to solve shielding problems with multi-layer slabs of finite thicknesses. When applying it to the present problem, we assumed a 35 cm sand layer with uniform and monoenergetic K-sources and above this 100 cm water. Dose rates from MC4 throughout the range $0 < z < 60$ cm are given in fig. 6 as a histogram plot, and the corresponding GFX results as a curve drawn through five calculated ordinates. The effect of the finite extension of the media in MC4 will be small in the range considered. The computational principles underlying GAMP1/GFX and MC4 are of course completely different, but also the data sources differ: GAMP1/GFX uses point cross sections derived from the Livermore Library[13], whereas MC4 uses group-averaged cross sections based on an earlier compilation. Further, the sampling technique for picking deflection angles and energy losses in MC4 is the approximate device of Carlson[14]. Taking all this into consideration, the agreement between the two models is satisfactory.

APPENDIX XI
PHOTON EMISSION DATA

The photon energies and the photon yields entering GAMMABANK/FILE1, and the specific activities used in the programs GAMP1 and GFX, were taken from references[15-18]. Reference[15] is an up-to-date tabulation of emission lines from ^{232}Th and ^{238}U in secular equilibrium with their respective daughters. Since the photon emission spectrum of ^{235}U + daughters is not reported in reference[15], this spectrum was evaluated independently from the decay schemes (^{235}U through ^{207}Pb) given in reference[16]. The specific activities of ^{232}Th, ^{238}U and ^{235}U in natural thorium and uranium were chosen in accordance with the "best values" recommended in reference[17].

Data on the 1.461-Mev photon emission from ^{40}K were derived from reference[18]. The specific gamma activity of potassium was evaluated from table IX in reference[18], which summarizes 19 determinations carried out in the years 1950-1966. Only the 12 determinations for which an experimental error is stated are included. From a statistically weighted average of these we arrived at a figure of 3.31 ± 0.04 photons $\cdot$ s^{-1} / g K.

A survey of the photon emission data adopted in this work is given in Table 1. It follows from the table that one gram of natural thorium and uranium results in the emission of 17370 and 33280 photons $\cdot$ s^{-1} $\cdot$ g^{-1} respectively. The emission spectra of thorium and uranium are shown in figs. 7 and 8. The average photon energies of the two radioelements equal 0.591 and 0.617 Mev respectively.

Appendix XII: Contents of GAMMABANK

PRINTOUT OF GAMMABANK/FILE1

	48													
2.6147	35.90	1	94	1232	0.2881	0.40	65	94	1232	1.0010	0.60	35	75	2238
1.8863	0.10	2	94	1232	0.2809	0.30	66	94	1232	0.9642	0.40	36	75	2238
1.8060	0.20	3	94	1232	0.2772	2.40	67	94	1232	0.9341	3.10	37	75	2238
1.6857	0.10	4	94	1232	0.2702	3.80	68	94	1232	0.8391	0.60	38	75	2238
1.6665	0.30	5	94	1232	0.2520	0.30	69	94	1232	0.8212	0.20	39	75	2238
1.6313	3.40	6	94	1232	0.2410	4.00	70	94	1232	0.8062	1.20	40	75	2238
1.6208	1.80	7	94	1232	0.2386	45.00	71	94	1232	0.7861	1.10	41	75	2238
1.6056	0.20	8	94	1232	0.2335	0.10	72	94	1232	0.7684	4.80	42	75	2238
1.5881	4.60	9	94	1232	0.2161	0.40	73	94	1232	0.7664	0.20	43	75	2238
1.5805	0.90	10	94	1232	0.2095	4.10	74	94	1232	0.7530	0.10	44	75	2238
1.5735	0.10	11	94	1232	0.2043	0.10	75	94	1232	0.7428	0.10	45	75	2238
1.5570	0.20	12	94	1232	0.1997	0.30	76	94	1232	0.7199	0.40	46	75	2238
1.5131	0.30	13	94	1232	0.1914	0.20	77	94	1232	0.7031	0.50	47	75	2238
1.4988	2.10	14	94	1232	0.1846	0.10	78	94	1232	0.6656	1.50	48	75	2238
1.4592	1.20	15	94	1232	0.1767	0.20	79	94	1232	0.6094	43.00	49	75	2238
1.2874	0.10	16	94	1232	0.1665	0.20	80	94	1232	0.5803	0.30	50	75	2238
1.2467	0.70	17	94	1232	0.1541	0.80	81	94	1232	0.5338	0.20	51	75	2238
1.1536	0.20	18	94	1232	0.1316	0.20	82	94	1232	0.5110	0.10	52	75	2238
1.1105	0.30	19	94	1232	0.1291	2.50	83	94	1232	0.4872	0.40	53	75	2238
1.0957	0.10	20	94	1232	0.1152	0.50	84	94	1232	0.4805	0.30	54	75	2238
1.0939	0.20	21	94	1232	0.0996	1.30	85	94	1232	0.4700	0.10	55	75	2238
1.0791	0.50	22	94	1232	0.0956	6.30	86	94	1232	0.4621	0.20	56	75	2238
1.0651	0.20	23	94	1232	0.0858	44.00	87	94	1232	0.4550	0.30	57	75	2238
1.0402	0.10	24	94	1232	0.0845	1.20	88	94	1232	0.4265	0.10	58	75	2238
1.0332	0.20	25	94	1232	0.0789	34.00	89	94	1232	0.4059	0.20	59	75	2238
0.9880	0.20	26	94	1232	0.0767	2.30	90	94	1232	0.3879	0.70	60	75	2238
0.9667	23.00	27	94	1232	0.0578	0.50	91	94	1232	0.3520	35.00	61	75	2238
0.9585	0.40	28	94	1232	0.0399	1.10	92	94	1232	0.3142	0.10	62	75	2238
0.9530	0.10	29	94	1232	0.0124	40.40	93	94	1232	0.2952	17.90	63	75	2238
0.9111	29.00	30	94	1232	0.0106	22.20	94	94	1232	0.2748	0.50	64	75	2238
0.9041	1.00	31	94	1232	2.4480	1.50	1	75	2238	0.2588	0.60	65	75	2238
0.8934	0.40	32	94	1232	2.2937	0.30	2	75	2238	0.2580	0.10	66	75	2238
0.8601	4.70	33	94	1232	2.2045	4.70	3	75	2238	0.2419	7.00	67	75	2238
0.8403	1.00	34	94	1232	2.1189	1.10	4	75	2238	0.1861	3.40	68	75	2238
0.8329	2.80	35	94	1232	2.1104	0.10	5	75	2238	0.0930	4.00	69	75	2238
0.7949	4.90	36	94	1232	1.8968	0.20	6	75	2238	0.0825	23.80	70	75	2238
0.7854	1.00	37	94	1232	1.8910	0.10	7	75	2238	0.0630	3.50	71	75	2238
0.7819	0.70	38	94	1232	1.8736	0.20	8	75	2238	0.0532	2.20	72	75	2238
0.7719	1.70	39	94	1232	1.8477	2.10	9	75	2238	0.0465	4.00	73	75	2238
0.7633	0.70	40	94	1232	1.8386	0.40	10	75	2238	0.0290	6.50	74	75	2238
0.7551	1.10	41	94	1232	1.7647	14.70	11	75	2238	0.0113	26.10	75	75	2238
0.7272	7.00	42	94	1232	1.7299	2.80	12	75	2238	0.8318	4.00	1	22	2235
0.7268	0.90	43	94	1232	1.6842	0.20	13	75	2238	0.4010	5.00	2	22	2235
0.7013	0.20	44	94	1232	1.6615	1.10	14	75	2238	0.3510	14.00	3	22	2235
0.5831	30.00	45	94	1232	1.5996	0.40	15	75	2238	0.3380	2.80	4	22	2235
0.5716	0.30	46	94	1232	1.5949	0.30	16	75	2238	0.3297	2.70	5	22	2235
0.5624	1.00	47	94	1232	1.5835	0.70	17	75	2238	0.2720	9.00	6	22	2235
0.5463	0.20	48	94	1232	1.5434	0.30	18	75	2238	0.2696	10.00	7	22	2235
0.5214	0.20	49	94	1232	1.5388	0.50	19	75	2238	0.2564	5.20	8	22	2235
0.5107	9.00	50	94	1232	1.5095	2.10	20	75	2238	0.2361	10.00	9	22	2235
0.5091	0.60	51	94	1232	1.4080	2.40	21	75	2238	0.2040	5.00	10	22	2235
0.5036	0.20	52	94	1232	1.4017	1.40	22	75	2238	0.1850	54.00	11	22	2235
0.4783	0.30	53	94	1232	1.3854	0.90	23	75	2238	0.1630	5.00	12	22	2235
0.4630	4.70	54	94	1232	1.3778	4.60	24	75	2238	0.1541	5.50	13	22	2235
0.4528	0.40	55	94	1232	1.3038	0.10	25	75	2238	0.1442	4.10	14	22	2235
0.4407	0.10	56	94	1232	1.2811	1.50	26	75	2238	0.1430	11.00	15	22	2235
0.4095	2.10	57	94	1232	1.2382	5.60	27	75	2238	0.1100	2.50	16	22	2235
0.3603	0.50	58	94	1232	1.2077	0.50	28	75	2238	0.1000	3.70	17	22	2235
0.3385	12.30	59	94	1232	1.1553	1.80	29	75	2238	0.0940	4.60	18	22	2235
0.3325	0.50	60	94	1232	1.1338	0.20	30	75	2238	0.0842	7.00	19	22	2235
0.3286	0.20	61	94	1232	1.1204	14.50	31	75	2238	0.0797	2.70	20	22	2235
0.3280	3.30	62	94	1232	1.1040	0.20	32	75	2238	0.0500	7.50	21	22	2235
0.3217	0.30	63	94	1232	1.0701	0.30	33	75	2238	0.0256	12.00	22	22	2235
0.3006	3.40	64	94	1232	1.0529	0.40	34	75	2238	1.4610	11.00	1	1	3040

continued overleaf

PRINTOUT OF GAMMABANK/FILE2

1	2.7500	1	3	1.000000	29
0	61.9090	2	3	1.000000	29
14	35.2610	3	3	1.000000	29
7	79.0000	1	2	0.001204	3
0	21.0000	2	2	0.001204	3
1	1.1110	1	6	1.600000	70
6	1.2200	2	6	1.600000	70
0	55.0140	3	6	1.600000	70
13	7.1440	4	6	1.600000	70
14	31.5560	5	6	1.600000	70
26	3.1470	6	6	1.600000	70
1	11.1900	1	2	1.000000	10
0	88.8100	2	2	1.000000	10
0	53.2500	1	2	2.640000	11
14	46.7500	2	2	2.640000	11
11	15.3370	1	2	3.670000	20
53	84.6630	2	2	3.670000	20
0	27.4200	1	3	4.480000	22
16	13.7400	2	3	4.480000	22
56	58.8400	3	3	4.480000	22
1	0.6000	1	0	2.000000	30
0	50.3000	2	0	2.000000	30
11	0.6000	3	0	2.000000	30
13	2.7000	4	0	2.000000	30
14	33.9000	5	0	2.000000	30
19	1.0000	6	0	2.000000	30
20	10.2000	7	0	2.000000	30
26	0.7000	8	0	2.000000	30
1	0.6000	1	0	2.000000	31
0	47.0000	2	0	2.000000	31
11	0.6000	3	0	2.000000	31
13	7.6000	4	0	2.000000	31
14	25.7000	5	0	2.000000	31
19	6.9000	6	0	2.000000	31
20	18.9000	7	0	2.000000	31
26	0.7000	8	0	2.000000	31
7	79.0000	1	2	0.001273	1
0	21.0000	2	2	0.001273	1
1	0.6930	1	12	2.670000	40
0	48.6020	2	12	2.670000	40
11	2.5020	3	12	2.670000	40
12	0.5310	4	12	2.670000	40
13	7.6580	5	12	2.670000	40
14	32.8090	6	12	2.670000	40
15	0.0830	7	12	2.670000	40
19	3.4120	8	12	2.670000	40
20	1.4220	9	12	2.670000	40
22	0.2340	10	12	2.670000	40
25	0.0930	11	12	2.670000	40
26	2.4020	12	12	2.670000	40

CATALOG OF GAMMABANK/FILE4

MEDIUM I	RADIOELEM.	MEDIUM II	HEIGHT	GROUPS	RECORDS
29	3	10	0.0	306	300
29	3	10	10.0	306	300
29	3	10	20.0	306	300
29	3	10	30.0	306	300
29	3	10	40.0	306	300
29	1	10	0.0	316	420
29	1	10	10.0	316	420
29	1	10	20.0	316	420
29	1	10	30.0	316	420
29	1	10	40.0	316	420
29	2	10	0.0	315	420
29	2	10	10.0	315	420
29	2	10	20.0	315	420
29	2	10	30.0	315	420
29	2	10	40.0	315	420
70	3	3	0.0	306	300
70	3	3	100.0	306	300
70	3	3	3000.0	306	300
70	3	3	10000.0	306	300
70	3	3	30000.0	306	300

Table 1

Photon emission data adopted in this work

Radioelement	γ-emitter(s)	No. of emission lines	Total photon yield (%)	Spec. activity (dis.s^{-1}/g radioelement
Thorium	^{232}Th+daughters	94	423.6	4100
Uranium	^{238}U +daughters	75	263.6	12227
	^{235}U +daughters	22	187.3	562
Potassium	^{40}K	1	11	30.1

Tables 2 - 16

Scalar number flux in the energy intervals 0.10 - 0.11, 0.11 - 0.12, ..., 2.99 - 3.00 MeV at different levels z in water above sand with a reference content of 1 percent Th, U, or K. The flux is due to uncollided as well as scattered photons. The unit is photons cm^{-2} s^{-1}.

Table 2

Th, z = 0 cm

MEV	0.00-0.01	0.01-0.02	0.02-0.03	0.03-0.04	0.04-0.05	0.05-0.06	0.06-0.07	0.07-0.08	0.08-0.09	0.09-0.10
0.10	1.829E 02	1.614E 02	1.503E 02	1.377E 02	1.118E 02	9.935E 01	8.800E 01	8.116E 01	7.500E 01	7.053E 01
0.20	7.321E 01	6.986E 01	5.603E 01	1.287E 02	4.649E 01	3.692E 01	3.377E 01	4.220E 01	2.997E 01	2.699E 01
0.30	3.151E 01	2.870E 01	2.694E 01	4.609E 01	1.961E 01	1.784E 01	1.711E 01	1.651E 01	1.508E 01	1.540E 01
0.40	1.932E 01	1.431E 01	1.303E 01	1.351E 01	1.337E 01	1.369E 01	2.270E 01	1.249E 01	1.150E 01	1.132E 01
0.50	1.270E 01	3.090E 01	1.038E 01	9.733E 00	1.006E 01	9.394E 00	1.100E 01	9.517E 00	8.040E 01	6.749E 00
0.60	6.635E 00	6.538E 00	6.445E 00	6.357E 00	6.273E 00	6.194E 00	6.118E 00	6.045E 00	5.976E 00	5.911E 00
0.70	6.373E 00	5.778E 00	2.710E 01	5.454E 00	5.201E 00	8.132E 00	6.978E 00	9.012E 00	9.535E 00	1.020E 01
0.80	6.445E 00	6.412E 00	6.350E 00	1.220E 01	7.062E 00	3.902E 00	1.762E 01	3.048E 00	3.024E 00	6.966E 00
0.90	6.719E 00	9.084E 01	2.604E 00	2.457E 00	2.435E 00	3.945E 00	7.350E 01	2.012E 00	2.000E 00	1.443E 00
1.00	1.431E 00	1.420E 00	1.409E 00	2.035E 00	1.690E 00	1.367E 00	2.008E 00	2.960E 00	1.314E 00	2.291E 00
1.10	1.292E 00	2.200E 00	1.250E 00	1.250E 00	1.240E 00	1.903E 00	1.220E 00	1.213E 00	1.205E 00	1.199E 00
1.20	1.193E 00	1.188E 00	1.179E 00	1.159E 00	3.604E 00	1.140E 00	1.134E 00	1.128E 00	1.070E 00	1.114E 00
1.30	1.109E 00	1.104E 00	1.098E 00	1.093E 00	1.089E 00	1.085E 00	1.080E 00	1.075E 00	1.071E 00	1.066E 00
1.40	1.063E 00	1.059E 00	1.055E 00	1.052E 00	1.047E 00	5.565E 00	1.009E 00	1.006E 00	1.003E 00	9.997E 00
1.50	9.964E-01	2.155E 00	9.313E-01	9.271E-01	9.256E-01	1.710E 00	9.220E-01	1.315E 00	2.270E 01	7.795E-01
1.60	1.038E 00	6.372E-01	7.803E 00	1.433E 01	6.311E-01	6.290E-01	1.004E 00	6.213E-01	1.023E 00	6.121E-01
1.70	6.105E-01	6.088E-01	6.071E-01	6.053E-01	6.036E-01	6.015E-01	5.990E-01	5.939E-01	5.927E-01	5.914E-01
1.80	1.040E 00	5.887E-01	5.872E-01	5.857E-01	5.841E-01	5.825E-01	5.808E-01	5.770E-01	1.011E 00	5.736E-01
1.90	5.746E-01	5.736E-01	5.725E-01	5.713E-01	5.701E-01	5.688E-01	5.675E-01	5.661E-01	5.650E-01	5.645E-01
2.00	5.639E-01	5.632E-01	5.624E-01	5.616E-01	5.607E-01	5.598E-01	5.588E-01	5.578E-01	5.567E-01	5.556E-01
2.10	5.544E-01	5.539E-01	5.536E-01	5.532E-01	5.528E-01	5.523E-01	5.518E-01	5.512E-01	5.505E-01	5.498E-01
2.20	5.491E-01	5.483E-01	5.475E-01	5.466E-01	5.456E-01	5.449E-01	5.449E-01	5.448E-01	5.447E-01	5.445E-01
2.30	5.443E-01	5.440E-01	5.437E-01	5.433E-01	5.428E-01	5.424E-01	5.418E-01	5.412E-01	5.406E-01	5.400E-01
2.40	5.393E-01	5.385E-01	5.382E-01	5.381E-01	5.383E-01	5.384E-01	5.385E-01	5.389E-01	5.389E-01	5.384E-01
2.50	5.383E-01	5.381E-01	5.379E-01	5.378E-01	5.373E-01	5.370E-01	5.366E-01	5.362E-01	5.357E-01	5.352E-01
2.60	5.347E-01	1.850E 02								

Table 3

Th, z = 10 cm

MEV	0.00-0.01	0.01-0.02	0.02-0.03	0.03-0.04	0.04-0.05	0.05-0.06	0.06-0.07	0.07-0.08	0.08-0.09	0.09-0.10
0.10	1.012E 02	8.004E 01	7.404E 01	6.387E 01	5.501E 01	4.906E 01	4.372E 01	3.960E 01	3.605E 01	3.313E 01
0.20	3.131E 01	2.904E 01	2.706E 01	3.135E 01	2.061E 01	1.840E 01	1.715E 01	1.710E 01	1.495E 01	1.394E 01
0.30	1.370E 01	1.234E 01	1.206E 01	1.407E 01	1.018E 01	9.641E 00	9.200E 00	8.843E 00	8.503E 00	8.219E 00
0.40	8.526E 00	7.614E 00	7.338E 00	7.138E 00	6.950E 00	6.867E 00	7.994E 00	6.290E 00	6.040E 00	5.870E 00
0.50	5.954E 00	6.639E 00	5.388E 00	5.097E 00	5.074E 00	4.877E 00	5.157E 00	4.695E 00	1.639E 01	3.782E 00
0.60	3.652E 00	3.588E 00	3.526E 00	3.468E 00	3.412E 00	3.358E 00	3.307E 00	3.257E 00	3.210E 00	3.165E 00
0.70	3.220E 00	3.075E 00	7.284E 00	2.909E 00	2.787E 00	3.336E 00	3.081E 00	3.367E 00	3.523E 00	5.204E 00
0.80	2.390E 00	2.366E 00	2.333E 00	3.959E 00	2.849E 00	2.185E 00	5.030E 00	2.088E 00	2.048E 00	2.879E 00
0.90	2.652E 00	2.127E 01	1.866E 00	1.893E 00	1.878E 00	1.713E 00	1.761E 01	1.173E 00	1.052E 00	8.995E-01
1.00	8.912E-01	8.837E-01	8.763E-01	1.019E 00	9.328E-01	8.449E-01	9.996E-01	1.223E 00	8.102E-01	1.056E 00
1.10	8.042E-01	1.035E 00	7.884E-01	7.787E-01	7.722E-01	9.348E-01	7.597E-01	7.546E-01	7.495E-01	7.449E-01
1.20	7.405E-01	7.361E-01	7.316E-01	7.200E-01	1.357E 00	7.078E-01	7.037E-01	6.996E-01	7.897E-01	6.905E-01
1.30	6.866E-01	6.833E-01	6.796E-01	6.760E-01	6.728E-01	6.689E-01	6.667E-01	6.635E-01	6.602E-01	6.572E-01
1.40	6.547E-01	6.521E-01	6.495E-01	6.467E-01	8.439E-01	1.928E 00	6.218E-01	6.198E-01	6.177E-01	3.967E 00
1.50	6.132E-01	9.473E-01	5.700E-01	5.703E-01	5.736E-01	8.034E-01	5.714E-01	6.870E-01	7.042E 00	6.869E-01
1.60	6.501E-01	6.106E-01	2.574E 00	6.523E 00	6.066E-01	6.049E-01	7.744E-01	6.000E-01	5.809E-01	5.944E-01
1.70	5.933E-01	5.921E-01	5.909E-01	5.897E-01	5.884E-01	5.871E-01	5.859E-01	5.823E-01	5.814E-01	5.805E-01
1.80	6.675E-01	5.788E-01	5.776E-01	5.765E-01	5.754E-01	5.743E-01	5.729E-01	5.710E-01	5.103E-01	5.690E-01
1.90	5.691E-01	5.683E-01	5.674E-01	5.666E-01	5.656E-01	5.650E-01	5.641E-01	5.633E-01	5.625E-01	5.621E-01
2.00	5.617E-01	5.612E-01	5.607E-01	5.602E-01	5.596E-01	5.590E-01	5.583E-01	5.577E-01	5.570E-01	5.562E-01
2.10	5.555E-01	5.551E-01	5.549E-01	5.546E-01	5.543E-01	5.540E-01	5.536E-01	5.532E-01	5.528E-01	5.523E-01
2.20	5.518E-01	5.513E-01	5.507E-01	5.502E-01	5.496E-01	5.490E-01	5.491E-01	5.491E-01	5.490E-01	5.489E-01
2.30	5.488E-01	5.488E-01	5.484E-01	5.482E-01	5.479E-01	5.477E-01	5.473E-01	5.470E-01	5.466E-01	5.462E-01
2.40	5.458E-01	5.453E-01	5.452E-01	5.454E-01	5.458E-01	5.461E-01	5.464E-01	5.467E-01	5.469E-01	5.471E-01
2.50	5.473E-01	5.474E-01	5.475E-01	5.475E-01	5.475E-01	5.475E-01	5.474E-01	5.474E-01	5.472E-01	5.471E-01
2.60	5.469E-01	6.873E 01								

Table 4

Th, z = 20 cm

MEV	0.00-0.01	0.01-0.02	0.02-0.03	0.03-0.04	0.04-0.05	0.05-0.06	0.06-0.07	0.07-0.08	0.08-0.09	0.09-0.10
0.10	5.335E 01	4.492E 01	3.845E 01	3.295E 01	2.865E 01	2.523E 01	2.250E 01	2.033E 01	1.847E 01	1.692E 01
0.20	1.574E 01	1.432E 01	1.325E 01	1.361E 01	1.073E 01	9.839E 00	9.154E 00	8.762E 00	8.001E 00	7.511E 00
0.30	7.211E 00	6.687E 00	6.541E 00	6.660E 00	5.589E 00	5.322E 00	5.095E 00	4.904E 00	4.705E 00	4.547E 00
0.40	4.523E 00	4.219E 00	4.066E 00	3.954E 00	3.838E 00	3.751E 00	3.968E 00	3.465E 00	3.356E 00	3.274E 00
0.50	3.228E 00	3.868E 00	2.940E 00	2.853E 00	2.816E 00	2.727E 00	2.772E 00	2.589E 00	5.747E 00	2.155E 00
0.60	2.114E 00	2.076E 00	2.039E 00	2.003E 00	1.969E 00	1.937E 00	1.905E 00	1.875E 00	1.847E 00	1.819E 00
0.70	1.822E 00	1.765E 00	3.934E 00	1.672E 00	1.610E 00	1.769E 00	1.677E 00	1.814E 00	1.787E 00	2.318E 00
0.80	1.389E 00	1.374E 00	1.352E 00	1.873E 00	1.499E 00	1.231E 00	2.201E 00	1.207E 00	1.195E 00	1.266E 00
0.90	1.383E 00	7.734E 00	8.863E-01	8.482E-01	8.390E-01	9.493E-01	6.504E 00	7.233E-01	6.384E-01	5.818E-01
1.00	5.761E-01	5.710E-01	5.659E-01	6.147E-01	5.808E-01	5.487E-01	6.010E-01	6.795E-01	5.289E-01	6.136E-01
1.10	5.195E-01	6.018E-01	5.071E-01	5.033E-01	4.989E-01	5.581E-01	4.906E-01	4.871E-01	4.836E-01	4.803E-01
1.20	4.772E-01	4.741E-01	4.709E-01	4.639E-01	7.090E-01	4.561E-01	4.532E-01	4.503E-01	4.843E-01	4.442E-01
1.30	4.417E-01	4.392E-01	4.367E-01	4.342E-01	4.321E-01	4.299E-01	4.277E-01	4.255E-01	4.232E-01	4.211E-01
1.40	4.193E-01	4.175E-01	4.150E-01	4.130E-01	4.116E-01	9.359E-01	3.985E-01	3.970E-01	3.954E-01	1.361E 00
1.50	3.922E-01	5.305E-01	3.706E-01	3.687E-01	3.677E-01	4.637E-01	3.655E-01	4.136E-01	3.105E 00	3.167E-01
1.60	3.737E-01	2.714E-01	1.194E 00	2.030E 00	2.685E-01	2.675E-01	4.263E-01	2.643E-01	3.156E-01	2.608E-01
1.70	2.600E-01	2.592E-01	2.583E-01	2.575E-01	2.566E-01	2.557E-01	2.546E-01	2.527E-01	2.521E-01	2.514E-01
1.80	3.695E-01	2.501E-01	2.494E-01	2.487E-01	2.480E-01	2.472E-01	2.463E-01	2.450E-01	3.075E-01	2.441E-01
1.90	2.436E-01	2.431E-01	2.426E-01	2.420E-01	2.414E-01	2.408E-01	2.402E-01	2.395E-01	2.390E-01	2.387E-01
2.00	2.384E-01	2.380E-01	2.376E-01	2.372E-01	2.368E-01	2.363E-01	2.359E-01	2.354E-01	2.349E-01	2.343E-01
2.10	2.338E-01	2.335E-01	2.333E-01	2.331E-01	2.328E-01	2.325E-01	2.322E-01	2.319E-01	2.316E-01	2.312E-01
2.20	2.308E-01	2.304E-01	2.300E-01	2.296E-01	2.292E-01	2.288E-01	2.287E-01	2.285E-01	2.283E-01	2.281E-01
2.30	2.279E-01	2.277E-01	2.274E-01	2.272E-01	2.269E-01	2.266E-01	2.262E-01	2.259E-01	2.255E-01	2.252E-01
2.40	2.248E-01	2.244E-01	2.242E-01	2.240E-01	2.239E-01	2.238E-01	2.237E-01	2.236E-01	2.235E-01	2.233E-01
2.50	2.231E-01	2.229E-01	2.227E-01	2.225E-01	2.223E-01	2.220E-01	2.217E-01	2.214E-01	2.212E-01	2.208E-01
2.60	2.205E-01	3.428E 01								

Table 5

Th, z = 30 cm

MEV	0.00-0.01	0.01-0.02	0.02-0.03	0.03-0.04	0.04-0.05	0.05-0.06	0.06-0.07	0.07-0.08	0.08-0.09	0.09-0.10
0.10	2.795E 01	2.350E 01	2.008E 01	1.724E 01	1.499E 01	1.321E 01	1.179E 01	1.065E 01	9.670E 00	8.862E 00
0.20	8.194E 00	7.509E 00	6.955E 00	6.729E 00	5.794E 00	5.354E 00	4.991E 00	4.713E 00	4.374E 00	4.119E 00
0.30	3.918E 00	3.681E 00	3.545E 00	3.477E 00	3.113E 00	2.974E 00	2.848E 00	2.742E 00	2.631E 00	2.542E 00
0.40	2.486E 00	2.382E 00	2.278E 00	2.213E 00	2.145E 00	2.088E 00	2.114E 00	1.937E 00	1.882E 00	1.834E 00
0.50	1.792E 00	1.952E 00	1.656E 00	1.610E 00	1.581E 00	1.535E 00	1.531E 00	1.455E 00	2.402E 00	1.281E 00
0.60	1.238E 00	1.213E 00	1.190E 00	1.169E 00	1.148E 00	1.128E 00	1.108E 00	1.089E 00	1.071E 00	1.053E 00
0.70	1.046E 00	1.019E 00	1.450E 00	9.694E-01	9.365E-01	9.847E-01	9.464E-01	9.868E-01	9.712E-01	1.150E 00
0.80	8.130E-01	8.026E-01	7.895E-01	9.724E-01	8.322E-01	7.239E-01	1.077E 00	7.063E-01	6.981E-01	7.206E-01
0.90	7.638E-01	3.158E 00	5.443E-01	5.236E-01	5.175E-01	5.577E-01	2.698E 00	4.565E-01	4.057E-01	3.821E-01
1.00	3.784E-01	3.749E-01	3.715E-01	3.894E-01	3.744E-01	3.604E-01	3.800E-01	4.098E-01	3.479E-01	3.810E-01
1.10	3.417E-01	3.735E-01	3.340E-01	3.314E-01	3.286E-01	3.519E-01	3.231E-01	3.208E-01	3.184E-01	3.162E-01
1.20	3.141E-01	3.120E-01	3.099E-01	3.056E-01	4.086E-01	3.006E-01	2.987E-01	2.968E-01	3.108E-01	2.927E-01
1.30	2.910E-01	2.893E-01	2.876E-01	2.859E-01	2.845E-01	2.830E-01	2.814E-01	2.799E-01	2.783E-01	2.769E-01
1.40	2.756E-01	2.743E-01	2.730E-01	2.717E-01	2.703E-01	5.038E-01	2.622E-01	2.612E-01	2.601E-01	6.962E-01
1.50	2.578E-01	3.201E-01	2.467E-01	2.435E-01	2.428E-01	2.866E-01	2.414E-01	2.632E-01	1.504E 00	2.120E-01
1.60	2.323E-01	1.847E-01	6.129E-01	1.002E 00	1.827E-01	1.820E-01	2.562E-01	1.799E-01	2.038E-01	1.778E-01
1.70	1.770E-01	1.764E-01	1.759E-01	1.753E-01	1.746E-01	1.740E-01	1.731E-01	1.720E-01	1.715E-01	1.711E-01
1.80	2.277E-01	1.701E-01	1.696E-01	1.690E-01	1.685E-01	1.680E-01	1.673E-01	1.664E-01	1.967E-01	1.657E-01
1.90	1.653E-01	1.649E-01	1.645E-01	1.640E-01	1.636E-01	1.631E-01	1.626E-01	1.621E-01	1.617E-01	1.615E-01
2.00	1.612E-01	1.609E-01	1.605E-01	1.602E-01	1.598E-01	1.595E-01	1.591E-01	1.587E-01	1.583E-01	1.579E-01
2.10	1.575E-01	1.572E-01	1.570E-01	1.568E-01	1.565E-01	1.563E-01	1.560E-01	1.557E-01	1.555E-01	1.552E-01
2.20	1.548E-01	1.545E-01	1.542E-01	1.538E-01	1.535E-01	1.532E-01	1.530E-01	1.529E-01	1.527E-01	1.525E-01
2.30	1.523E-01	1.521E-01	1.519E-01	1.517E-01	1.515E-01	1.512E-01	1.509E-01	1.507E-01	1.504E-01	1.501E-01
2.40	1.498E-01	1.495E-01	1.493E-01	1.491E-01	1.490E-01	1.489E-01	1.488E-01	1.486E-01	1.485E-01	1.483E-01
2.50	1.481E-01	1.480E-01	1.478E-01	1.476E-01	1.474E-01	1.471E-01	1.469E-01	1.467E-01	1.464E-01	1.462E-01
2.60	1.459E-01	1.839E 01								

Table 6

Th, z = 40 cm

MEV	0.00-0.01	0.01-0.02	0.02-0.03	0.03-0.04	0.04-0.05	0.05-0.06	0.06-0.07	0.07-0.08	0.08-0.09	0.09-0.10
0.10	1.462E 01	1.226E 01	1.037E 01	8.923E 00	7.761E 00	6.841E 00	6.104E 00	5.492E 00	4.974E 00	4.540E 00
0.20	4.165E 00	3.830E 00	3.536E 00	3.363E 00	3.090E 00	2.863E 00	2.670E 00	2.515E 00	2.352E 00	2.216E 00
0.30	2.103E 00	1.985E 00	1.890E 00	1.839E 00	1.711E 00	1.636E 00	1.565E 00	1.506E 00	1.444E 00	1.394E 00
0.40	1.351E 00	1.290E 00	1.247E 00	1.211E 00	1.171E 00	1.137E 00	1.130E 00	1.059E 00	1.028E 00	9.994E-01
0.50	9.770E-01	1.015E 00	9.193E-01	8.844E-01	8.646E-01	8.388E-01	8.272E-01	8.048E-01	1.110E 00	7.241E-01
0.60	7.090E-01	6.966E-01	6.807E-01	6.673E-01	6.544E-01	6.418E-01	6.296E-01	6.177E-01	6.062E-01	5.950E-01
0.70	5.878E-01	5.730E-01	7.268E-01	5.484E-01	5.313E-01	5.452E-01	5.274E-01	5.397E-01	5.316E-01	5.940E-01
0.80	4.640E-01	4.574E-01	4.497E-01	5.170E-01	4.614E-01	4.152E-01	5.493E-01	4.030E-01	3.975E-01	4.043E-01
0.90	4.230E-01	1.375E 00	3.271E-01	3.158E-01	3.118E-01	3.287E-01	1.198E 00	2.864E-01	2.589E-01	2.483E-01
1.00	2.458E-01	2.435E-01	2.413E-01	2.479E-01	2.408E-01	2.342E-01	2.418E-01	2.535E-01	2.266E-01	2.400E-01
1.10	2.226E-01	2.353E-01	2.179E-01	2.162E-01	2.143E-01	2.238E-01	2.130E-01	2.092E-01	2.070E-01	2.082E-01
1.20	2.048E-01	2.034E-01	2.020E-01	1.990E-01	2.447E-01	1.962E-01	1.949E-01	1.936E-01	1.993E-01	1.909E-01
1.30	1.897E-01	1.885E-01	1.873E-01	1.862E-01	1.851E-01	1.840E-01	1.829E-01	1.818E-01	1.807E-01	1.797E-01
1.40	1.788E-01	1.779E-01	1.770E-01	1.761E-01	1.752E-01	2.840E-01	1.702E-01	1.695E-01	1.687E-01	3.748E-01
1.50	1.672E-01	1.965E-01	1.595E-01	1.589E-01	1.587E-01	1.797E-01	1.581E-01	1.687E-01	7.666E-01	1.410E-01
1.60	1.478E-01	1.247E-01	3.323E-01	5.219E-01	1.232E-01	1.227E-01	1.584E-01	1.213E-01	1.227E-01	1.198E-01
1.70	1.194E-01	1.190E-01	1.185E-01	1.181E-01	1.176E-01	1.172E-01	1.166E-01	1.158E-01	1.155E-01	1.151E-01
1.80	1.434E-01	1.144E-01	1.140E-01	1.136E-01	1.133E-01	1.129E-01	1.124E-01	1.118E-01	1.471E-01	1.112E-01
1.90	1.109E-01	1.106E-01	1.103E-01	1.100E-01	1.096E-01	1.093E-01	1.090E-01	1.086E-01	1.083E-01	1.081E-01
2.00	1.079E-01	1.076E-01	1.074E-01	1.071E-01	1.069E-01	1.066E-01	1.063E-01	1.061E-01	1.058E-01	1.055E-01
2.10	1.052E-01	1.050E-01	1.048E-01	1.047E-01	1.045E-01	1.043E-01	1.042E-01	1.040E-01	1.038E-01	1.035E-01
2.20	1.033E-01	1.031E-01	1.029E-01	1.028E-01	1.026E-01	1.022E-01	1.021E-01	1.020E-01	1.019E-01	1.018E-01
2.30	1.017E-01	1.015E-01	1.014E-01	1.013E-01	1.011E-01	1.009E-01	1.008E-01	1.006E-01	1.004E-01	1.002E-01
2.40	1.001E-01	9.986E-02	9.974E-02	9.963E-02	9.959E-02	9.954E-02	9.944E-02	9.941E-02	9.934E-02	9.925E-02
2.50	9.918E-02	9.906E-02	9.896E-02	9.885E-02	9.873E-02	9.860E-02	9.847E-02	9.833E-02	9.819E-02	9.804E-02
2.60	9.789E-02	1.025E 01								

Table 7

U, z = 0 cm

MEV	0.00-0.01	0.01-0.02	0.02-0.03	0.03-0.04	0.04-0.05	0.05-0.06	0.06-0.07	0.07-0.08	0.08-0.09	0.09-0.10
0.10	4.111E 02	3.505E 02	3.150E 02	2.818E 02	2.581E 02	2.314E 02	2.037E 02	1.817E 02	1.705E 02	1.574E 02
0.20	1.407E 02	1.306E 02	1.228E 02	1.162E 02	1.380E 02	9.865E 01	8.993E 01	8.672E 01	7.724E 01	1.701E 02
0.30	6.211E 01	5.987E 01	5.748E 01	5.512E 01	5.243E 01	2.500E 02	3.587E 01	3.462E 01	3.763E 01	3.200E 01
0.40	3.354E 01	2.990E 01	2.966E 01	2.822E 01	2.746E 01	2.871E 01	2.803E 01	2.908E 01	2.906E 01	2.916E 01
0.50	2.371E 01	2.391E 01	2.281E 01	2.380E 01	2.202E 01	2.167E 01	2.135E 01	2.105E 01	2.089E 01	2.063E 01
0.60	3.407E 02	1.418E 01	1.153E 01	1.138E 01	1.111E 01	1.103E 01	2.251E 01	1.067E 01	1.033E 01	1.027E 01
0.70	1.401E 01	1.308E 01	9.697E 00	9.575E 00	1.027E 01	1.017E 01	5.708E 01	8.584E 00	1.752E 01	8.449E 00
0.80	1.815E 01	7.788E 00	9.347E 00	1.425E 01	7.422E 00	7.358E 00	7.279E 00	7.439E 00	7.184E 00	7.167E 00
0.90	7.677E 00	7.532E 00	6.788E 00	3.467E 01	6.598E 00	6.445E 00	1.000E 01	6.338E 00	6.279E 00	6.206E 00
1.00	1.185E 01	6.131E 00	6.097E 00	6.065E 00	6.003E 00	9.810E 00	5.978E 00	5.809E 00	5.859E 00	5.844E 00
1.10	7.747E 00	6.449E 00	1.488E 02	6.247E 00	6.222E 00	2.222E 01	5.948E 00	5. 02E 00	5.785E 00	5.784E 00
1.20	9.003E 00	5.678E 00	5.866E 00	6.231E 01	5.350E 00	5.367E 00	5.447E 00	5.285E 00	1.307E 01	5.167E 00
1.30	6.183E 00	5.102E 00	5.069E 00	5.081E 00	5.072E 00	5.087E 00	5.086E 00	5.377E 01	1.247E 01	5.061E 00
1.40	6.657E 01	2.284E 00	6.258E 00	2.252E 00	2.245E 00	2.249E 00	2.222E 00	2.222E 00	2.222E 00	2.222E 00
1.50	2.883E 01	2.212E 00	2.207E 00	2.846E 00	5.483E 00	1.978E 00	1.975E 00	1.971E 00	1.965E 01	1.589E 01
1.60	1.972E 00	1.859E 00	1.855E 00	1.854E 00	1.852E 00	1.850E 00	1.515E 01	1.844E 00	6.265E 00	1.553E 00
1.70	1.560E 00	1.562E 00	3.623E 01	1.564E 00	1.564E 00	1.564E 00	1.859E 02	1.564E 00	7.048E-01	5.943E-01
1.80	5.948E-01	5.937E-01	5.933E-01	5.707E 00	6.751E 01	5.913E-01	5.908E-01	3.172E 00	6.822E-01	6.300E 00
1.90	6.028E-01	6.025E-01	6.021E-01	6.018E-01	6.011E-01	6.005E-01	3.744E-01	3.992E-01	3.985E-01	3.978E-01
2.00	3.978E-01	3.977E-01	3.977E-01	3.976E-01	3.975E-01	3.973E-01	3.971E-01	3.969E-01	3.966E-01	3.964E-01
2.10	3.958E-01	1.891E 01	3.949E-01	3.284E-01	3.947E-01	3.294E-01	3.301E-01	3.305E-01	3.309E-01	3.313E-01
2.20	6.838E 01	3.318E-01	3.324E-01	3.322E-01	3.343E-01	3.344E-01	3.342E-01	2.594E-01	7.144E-02	6.973E 00
2.30	7.145E-02	7.145E-02	7.145E-02	7.145E-02	7.144E-02	7.144E-02	7.141E-02	7.138E-02	7.133E-02	7.127E-02
2.40	7.123E-02	7.117E-02	7.110E-02	7.103E-02	6.730E 01					

Table 8

U, z = 10 cm

MEV	0.00-0.01	0.01-0.02	0.02-0.03	0.03-0.04	0.04-0.05	0.05-0.06	0.06-0.07	0.07-0.08	0.08-0.09	0.09-0.10
0.10	2.276E 02	1.749E 02	1.650E 02	1.444E 02	1.265E 02	1.117E 02	9.913E 01	8.904E 01	8.057E 01	7.342E 01
0.20	6.729E 01	6.235E 01	5.810E 01	5.406E 01	5.249E 01	4.573E 01	4.236E 01	3.988E 01	3.693E 01	4.550E 01
0.30	3.081E 01	2.934E 01	2.793E 01	2.658E 01	2.537E 01	4.724E 01	1.939E 01	1.869E 01	1.853E 01	1.724E 01
0.40	1.698E 01	1.605E 01	1.504E 01	1.505E 01	1.459E 01	1.446E 01	1.404E 01	1.387E 01	1.370E 01	1.403E 01
0.50	1.234E 01	1.215E 01	1.177E 01	1.173E 01	1.128E 01	1.103E 01	1.081E 01	1.060E 01	1.075E 01	1.018E 01
0.60	6.635E 01	7.610E 00	6.521E 00	6.408E 00	6.299E 00	6.196E 00	6.172E 00	5.894E 00	5.803E 00	5.716E 00
0.70	6.377E 00	6.141E 00	5.917E 00	5.739E 00	5.425E 00	5.356E 00	1.345E 01	4.812E 00	6.561E 00	4.564E 00
0.80	9.604E 00	4.390E 00	4.697E 00	5.664E 00	4.191E 00	4.148E 00	4.108E 00	4.067E 00	4.030E 00	3.992E 00
0.90	3.958E 00	3.926E 00	3.802E 00	9.991E 00	3.853E 00	3.804E 00	4.412E 00	3.544E 00	3.517E 00	3.493E 00
1.00	4.777E 00	3.413E 00	3.390E 00	3.368E 00	3.331E 00	4.227E 00	3.286E 00	3.965E 00	3.238E 00	3.229E 00
1.10	3.703E 00	2.754E 00	3.811E 01	2.922E 00	2.811E 00	6.903E 00	2.286E 00	2.274E 00	2.263E 00	2.240E 00
1.20	3.564E 00	2.211E 00	2.203E 00	1.748E 01	1.952E 00	1.908E 00	1.900E 00	1.892E 00	6.123E 00	1.882E 00
1.30	2.088E 00	1.788E 00	1.781E 00	1.774E 00	1.768E 00	1.764E 00	1.761E 00	1.576E 01	4.508E 00	1.748E 00
1.40	1.314E 01	1.328E 00	1.324E 00	1.319E 00	1.315E 00	1.310E 00	1.306E 00	1.303E 00	1.301E 00	1.298E 00
1.50	8.301E 00	1.292E 00	1.289E 00	2.881E 00	2.186E 00	1.161E 00	1.158E 00	1.156E 00	3.605E 00	3.625E 00
1.60	1.128E 00	1.090E 00	1.089E 00	1.088E 00	1.088E 00	1.088E 00	5.129E 00	1.083E 00	1.615E 00	9.193E-01
1.70	9.211E-01	9.227E-01	1.164E 01	9.252E-01	9.261E-01	9.268E-01	5.833E 01	9.277E-01	4.284E-01	3.024E-01
1.80	3.024E-01	3.022E-01	3.021E-01	1.988E 00	8.942E 00	3.012E-01	3.008E-01	1.189E 00	2.965E-01	1.506E 00
1.90	2.495E-01	2.493E-01	2.490E-01	2.487E-01	2.483E-01	2.480E-01	2.476E-01	2.471E-01	2.467E-01	2.462E-01
2.00	2.461E-01	2.462E-01	2.462E-01	2.462E-01	2.462E-01	2.461E-01	2.460E-01	2.459E-01	2.457E-01	2.455E-01
2.10	2.453E-01	5.446E 00	2.414E-01	2.039E-01	2.045E-01	2.051E-01	2.057E-01	2.062E-01	2.066E-01	2.070E-01
2.20	2.300E 01	2.078E-01	2.081E-01	2.084E-01	2.086E-01	2.088E-01	2.090E-01	1.834E-01	4.504E-02	1.550E 00
2.30	4.514E-02	4.518E-02	4.521E-02	4.524E-02	4.526E-02	4.528E-02	4.529E-02	4.530E-02	4.530E-02	4.529E-02
2.40	4.529E-02	4.527E-02	4.526E-02	4.524E-02	8.070E 00					

Table 9

U, z = 20 cm

MEV	0.00-0.01	0.01-0.02	0.02-0.03	0.03-0.04	0.04-0.05	0.05-0.06	0.06-0.07	0.07-0.08	0.08-0.09	0.09-0.10
0.10	1.193E 02	1.002E 02	8.545E 01	7.369E 01	6.434E 01	5.667E 01	5.032E 01	4.524E 01	4.156E 01	3.726E 01
0.20	3.423E 01	3.173E 01	2.954E 01	2.740E 01	2.565E 01	2.325E 01	2.163E 01	2.028E 01	1.896E 01	1.990E 01
0.30	1.614E 01	1.535E 01	1.462E 01	1.392E 01	1.330E 01	1.722E 01	1.069E 01	1.031E 01	1.004E 01	9.520E 00
0.40	9.267E 00	8.867E 00	8.504E 00	8.313E 00	8.056E 00	7.894E 00	7.662E 00	7.404E 00	7.346E 00	6.986E 00
0.50	6.801E 00	6.657E 00	6.475E 00	6.386E 00	6.184E 00	6.054E 00	5.930E 00	5.811E 00	5.794E 00	5.582E 00
0.60	2.165E 01	6.335E 00	3.837E 00	3.769E 00	3.704E 00	3.641E 00	4.189E 00	3.474E 00	3.419E 00	3.365E 00
0.70	3.538E 00	3.440E 00	3.189E 00	3.141E 00	3.145E 00	3.102E 00	5.652E 00	2.844E 00	3.378E 00	2.711E 00
0.80	3.355E 00	2.608E 00	2.693E 00	2.990E 00	2.497E 00	2.462E 00	2.436E 00	2.410E 00	2.386E 00	2.361E 00
0.90	2.338E 00	2.316E 00	2.298E 00	4.360E 00	2.104E 00	2.135E 00	2.409E 00	2.097E 00	2.079E 00	2.063E 00
1.00	2.511E 00	2.016E 00	2.001E 00	1.986E 00	1.964E 00	2.282E 00	1.936E 00	2.177E 00	1.904E 00	1.893E 00
1.10	2.062E 00	1.835E 00	1.672E 01	1.843E 00	1.449E 00	3.124E 00	1.379E 00	1.372E 00	1.364E 00	1.350E 00
1.20	1.848E 00	1.330E 00	1.324E 00	7.227E 00	1.174E 00	1.160E 00	1.154E 00	1.149E 00	2.863E 00	1.078E 00
1.30	1.207E 00	1.088E 00	1.084E 00	1.079E 00	1.074E 00	1.070E 00	1.066E 00	6.697E 00	2.169E 00	1.058E 00
1.40	5.807E 00	8.191E-01	8.162E-01	8.132E-01	8.100E-01	8.068E-01	8.039E-01	8.015E-01	7.993E-01	7.970E-01
1.50	3.708E 00	7.921E-01	7.895E-01	1.439E 00	1.145E 00	7.144E-01	7.125E-01	7.106E-01	1.748E 00	1.757E 00
1.60	8.924E-01	6.700E-01	6.689E-01	6.678E-01	6.663E-01	6.648E-01	2.405E 00	6.617E-01	9.756E-01	5.648E-01
1.70	5.648E-01	5.648E-01	5.245E 00	5.643E-01	5.640E-01	5.635E-01	2.580E 01	5.623E-01	2.671E-01	2.242E-01
1.80	2.289E-01	2.286E-01	2.283E-01	9.531E-01	4.060E 00	2.270E-01	2.266E-01	5.978E-01	1.880E-01	7.260E-01
1.90	1.598E-01	1.596E-01	1.593E-01	1.590E-01	1.587E-01	1.584E-01	1.581E-01	1.578E-01	1.574E-01	1.571E-01
2.00	1.568E-01	1.568E-01	1.567E-01	1.565E-01	1.564E-01	1.562E-01	1.560E-01	1.558E-01	1.556E-01	1.554E-01
2.10	1.552E-01	2.772E 00	1.526E-01	1.295E-01	1.297E-01	1.299E-01	1.301E-01	1.302E-01	1.304E-01	1.305E-01
2.20	1.092E 01	1.306E-01	1.307E-01	1.307E-01	1.307E-01	1.307E-01	1.307E-01	1.023E-01	2.885E-02	7.528E-01
2.30	2.882E-02	2.880E-02	2.878E-02	2.876E-02	2.873E-02	2.870E-02	2.867E-02	2.863E-02	2.860E-02	2.856E-02
2.40	2.852E-02	2.848E-02	2.843E-02	2.839E-02	3.950E 00					

Table 11

U, z = 40 cm

MEV	0.00-0.01	0.01-0.02	0.02-0.03	0.03-0.04	0.04-0.05	0.05-0.06	0.06-0.07	0.07-0.08	0.08-0.09	0.09-0.10
0.10	3.153E 01	2.642E 01	2.240E 01	1.918E 01	1.660E 01	1.454E 01	1.279E 01	1.170E 01	1.060E 01	9.670E 00
0.20	8.098E 00	8.234E 00	7.695E 00	7.062E 00	6.559E 00	6.054E 00	5.632E 00	5.261E 00	4.918E 00	4.579E 00
0.30	4.375E 00	4.165E 00	3.927E 00	3.716E 00	3.531E 00	3.362E 00	3.208E 00	3.069E 00	2.938E 00	2.815E 00
0.40	2.706E 00	2.602E 00	2.497E 00	2.401DE 00	2.303E 00	2.211E 00	2.127E 00	2.050E 00	1.978E 00	2.068E 00
0.50	2.013E 00	1.935E 00	1.850L 00	1.801L 00	1.753E 00	1.706L 00	1.661L 00	1.626E 00	1.572E 00	
0.60	3.314E 00	1.409E 00	1.310E 00	1.261E 00	1.234E 00	1.288E 00	1.188E 00	1.167E 00	1.147E 00	
0.70	1.193E 00	1.121E 00	1.068E 00	1.057L 00	1.041E 00	1.36VE 00	9.839E-01	1.044E 00	9.441E-01	
0.80	1.024E 00	9.119E-01	9.163E-01	9.089E-01	8.716E-01	8.607E-01	8.502E-01	8.400E-01	8.300E-01	8.202E-01
0.93	8.117E-01	8.041E-01	7.953IE-01	1.098E 00	7.581E-01	7.477E-01	7.851E-01	7.316E-01	7.426E-01	7.137E-01
1.00	7.048E-01	6.995E-01	6.929E-01	6.866E-01	6.708E-01	7.271E-01	6.637E-01	7.028E-01	6.555E-01	6.549E-01
1.10	6.402E-01	5.838E-01	2.851E 00	5.640E-01	5.276E-01	8.209E-01	5.050E-01	5.015E-01	4.908E-01	4.827E-01
1.20	5.025E-01	4.884E-01	4.845E-01	1.592E 00	4.378E-01	4.326E-01	4.103E-01	4.278E-01	7.446E-01	4.103E-01
1.30	4.300E-01	4.054E-01	4.030E-01	4.005E-01	3.984E-01	3.975E-01	3.965E-01	1.539E 00	0.196E 00	3.843E-01
1.40	1.298E 00	3.191E-01	3.136E-01	3.120E-01	3.104E-01	3.088E-01	3.073E-01	3.058E-01	3.053E-01	3.042E-01
1.50	9.429E-01	3.021E-01	3.010E-01	4.341E-01	3.088E-01	2.741E-01	2.732E-01	4.723E-01	5.018E-01	5.048E-01
1.60	4.052E-01	2.571E-01	4.567E-01	2.561E-01	2.556E-01	2.550E-01	6.534E-01	2.538E-01	4.429E-01	4.183E-01
1.70	4.187E-01	2.14E-01	1.31VE 00	2.195E-01	2.197E-01	2.198E-01	6.22JE 00	2.199E-01	1.048E-01	9.427E-02
1.80	9.420E-02	9.010E-02	9.398E-02	2.708E-01	1.032E 00	9.336E-02	9.340E-02	1.850E-01	7.048E-02	2.063E-01
1.90	6.750E-02	6.735E-02	6.292E-02	6.705E-02	4.689E-02	6.672E-02	6.635E-02	6.637E-02	6.018E-02	6.000E-02
2.00	6.591E-02	6.508E-02	6.584E-02	6.578E-02	6.572E-02	6.505E-02	6.556E-02	6.550E-02	6.941E-02	6.531E-02
2.10	6.521E-02	7.601E-01	6.415E-02	5.466E-02	5.481E-02	5.493E-02	5.504E-02	5.514E-02	5.523E-02	5.531E-02
2.20	2.V87L 00	5.545E-02	5.595E-02	5.559E-02	5.562E-02	5.564E-02	4.361E-02	1.240E-02	2.138E-01	
2.30	1.240E-02	1.245E-02	1.284E-02	1.242E-02	1.241E-02	1.239E-02	1.238E-02	1.238E-02	1.238E-02	
2.40	1.232E-02	1.231E-02	1.225E-02	1.227E-02	1.192E 00					

Table 10

U, z = 30 cm

MEV	0.00-0.01	0.01-0.02	0.02-0.03	0.03-0.04	0.04-0.05	0.05-0.06	0.06-0.07	0.07-0.08	0.08-0.09	0.09-0.10
0.10	6.162E 01	9.163E 01	4.39BE 01	3.782E 01	3.295E 01	2.990E 01	2.584E 01	2.324E 01	2.120E 01	1.V40E 01
0.20	1.766E 01	1.637E 01	1.525E 01	1.412E 01	1.3VVE 01	1.2VVE 01	1.12IE 01	1.050E 01	V.834E 00	V.712E 00
0.30	7.111E 00	7.214E 00	7.233E 00	6.VV4E 00	7.707E 00	5.V13E 00	5.718E 00	5.316E 00	5.42JE 00	
0.40	5.10VE 00	4.914E 00	4.701E 00	4.605E 00	4.401E 00	4.350E 00	4.225E 00	4.089E 00	4.013E 00	3.849E 00
0.50	3.754E 00	3.662E 00	3.563E 00	3.49VE 00	3.392E 00	3.312E 00	3.235E 00	3.161E 00	3.11VE 00	3.016E 00
0.60	2.141E 00	2.49ZE 00	2.267E 00	2.226E 00	2.18ZE 00	2.14VE 00	2.315E 00	2.055E 00	2.021E 00	1.V68E 00
0.70	2.032E 00	1.945E 00	1.864E 00	1.885E 00	1.844E 00	1.817E 00	2.705E 00	1.692E 00	1.668E 00	1.618E 00
0.80	1.846E 00	1.559E 00	1.5ZVE 00	1.689E 00	1.672E 00	1.655E 00	1.638E 00	1.623E 00	1.607E 00	
0.90	1.393E 00	1.379E 00	1.365E 00	2.134E 00	1.279E 00	1.377E 00	1.252E 00	1.241E 00	1.230E 00	
1.00	1.401E 00	1.201E 00	1.191E 00	1.181E 00	1.167E 00	1.159E 00	1.241E 00	1.129E 00	1.124E 00	
1.10	1.192E 00	9.867E-01	9.659E-01	8.834E-01	1.560E 00	8.643E-01	8.352E-01	8.328E-01	8.242E-01	
1.20	1.030E 00	8.126E-01	8.040E-01	7.243E-01	7.135E-01	7.011E-01	1.413E 00	1.140E 00	6.887E-01	
1.30	7.423E-01	6.707E-01	6.647E-01	6.601E-01	6.581E-01	6.555E-01	1.130E 00	1.140E 00	6.087E-01	
1.40	2.632E 00	5.127E-01	5.104E-01	5.081E-01	5.057E-01	5.032E-01	5.010E-01	4.997E-01	4.977E-01	4.960E-01
1.50	1.815E 00	4.V45E-01	4.900E-01	7.786E-01	4.652E-01	4.627E-01	4.438E-01	4.423E-01	V.188E-01	V.249E-01
1.60	4.006E-01	4.170E-01	4.181E-01	4.152E-01	4.142E-01	4.132E-01	1.222E 00	4.109E-01	5.372E-01	3.321E-01
1.70	3.525E-01	3.525E-01	2.9ZZE 00	3.526E-01	3.526E-01	3.524E-01	1.240E 01	3.520E-01	1.709E-01	1.477E-01
1.80	V.V4VE-01	1.V7VE-01	4.978E-01	2.002E 00	1.464E-01	1.459E-01	3.246E-01	1.214E-01	3.084E-01	
1.90	1.V43E-01	1.V41E-01	1.V34E-01	1.V34E-01	1.031E-01	1.V24E-01	1.V26E-01	1.V42E-01	1.V20E-01	
2.00	1.V18E-01	1.V18E-01	1.017E-01	1.016E-01	1.015E-01	1.013E-01	1.V10E-01	1.00VE-01	1.00VE-01	
2.10	1.003E-01	1.421E 00	V.805E-02	8.411E-02	8.425E-02	8.437E-02	8.457E-02	8.465E-02	8.47ZE-02	
2.20	2.V87E 00	8.482E-02	8.485E-02	8.487E-02	8.488E-02	8.489E-02	8.488E-02	8.487E-02	1.899E-02	3.V31E-01
2.30	1.V9IE-02	1.V89E-02	1.8V7E-02	1.883E-02	1.882E-02	1.880E-02	1.878E-02	1.878E-02	1.878E-02	1.888E-02
2.40	1.865E-02	1.862E-02	1.858E-02	1.855E-02	2.082E 00					

Table 12

K_z z = 0 cm

MEV	0.00-0.01	0.01-0.02	0.02-0.03	0.03-0.04	0.04-0.05	0.05-0.06	0.06-0.07	0.07-0.08	0.08-0.09	0.09-0.10
0.10	5.341E-02	4.048E-02	4.391E-02	3.860E-02	3.443E-02	3.065E-02	2.762E-02	2.512E-02	2.312E-02	2.134E-02
0.20	2.008E-02	1.976E-02	2.027E-02	1.831E-02	1.665E-02	1.524E-02	1.404E-02	1.299E-02	1.206E-02	1.126E-02
0.30	1.059E-02	9.970E-03	9.400E-03	8.858E-03	8.431E-03	8.046E-03	7.699E-03	7.333E-03	7.017E-03	6.731E-03
0.40	6.466E-03	6.229E-03	6.007E-03	5.801E-03	5.604E-03	5.435E-03	5.258E-03	5.107E-03	4.956E-03	4.810E-03
0.50	4.689E-03	4.569E-03	4.450E-03	4.349E-03	4.246E-03	4.153E-03	4.064E-03	3.977E-03	3.895E-03	3.818E-03
0.60	3.745E-03	3.676E-03	3.611E-03	3.549E-03	3.489E-03	3.432E-03	3.378E-03	3.326E-03	3.277E-03	3.229E-03
0.70	3.183E-03	3.140E-03	3.098E-03	3.058E-03	3.020E-03	2.984E-03	2.947E-03	2.913E-03	2.880E-03	2.849E-03
0.80	2.818E-03	2.787E-03	2.757E-03	2.728E-03	2.711E-03	2.688E-03	2.663E-03	2.644E-03	2.618E-03	2.597E-03
0.90	2.577E-03	2.557E-03	2.538E-03	2.520E-03	2.503E-03	2.486E-03	2.468E-03	2.452E-03	2.437E-03	2.423E-03
1.00	2.409E-03	2.394E-03	2.380E-03	2.369E-03	2.357E-03	2.346E-03	2.335E-03	2.324E-03	2.313E-03	2.304E-03
1.10	2.294E-03	2.284E-03	2.276E-03	2.267E-03	2.258E-03	2.249E-03	2.241E-03	2.235E-03	2.228E-03	2.220E-03
1.20	2.214E-03	2.208E-03	2.201E-03	2.194E-03	2.188E-03	2.183E-03	2.178E-03	2.173E-03	2.167E-03	2.163E-03
1.30	2.159E-03	2.155E-03	2.150E-03	2.145E-03	2.141E-03	2.139E-03	2.134E-03	2.132E-03	2.128E-03	2.124E-03
1.40	2.122E-03	2.120E-03	2.118E-03	2.115E-03	2.112E-03	2.109E-03	2.107E-01			

Table 13

K_z z = 10 cm

MEV	0.00-0.01	0.01-0.02	0.02-0.03	0.03-0.04	0.04-0.05	0.05-0.06	0.06-0.07	0.07-0.08	0.08-0.09	0.09-0.10
0.10	3.067E-02	3.152E-02	2.760E-02	2.415E-02	2.123E-02	1.883E-02	1.688E-04	1.529E-02	1.397E-02	1.287E-02
0.20	1.196E-02	1.119E-02	1.049E-02	1.004E-02	9.239E-03	8.549E-03	7.938E-03	7.401E-03	6.926E-03	6.507E-03
0.30	6.142E-03	5.812E-03	5.506E-03	9.222E-03	4.981E-03	4.753E-03	4.546E-03	4.353E-03	4.172E-03	4.006E-03
0.40	3.857E-03	3.717E-03	3.587E-03	3.466E-03	3.350E-03	3.247E-03	3.144E-03	3.053E-03	2.968E-03	2.879E-03
0.50	2.804E-03	2.728E-03	2.656E-03	2.593E-03	2.531E-03	2.472E-03	2.406E-03	2.362E-03	2.306E-03	2.256E-03
0.60	2.210E-03	2.175E-03	2.134E-03	2.095E-03	2.059E-03	2.022E-03	1.990E-03	1.956E-03	1.923E-03	1.893E-03
0.70	1.863E-03	1.835E-03	1.808E-03	1.782E-03	1.758E-03	1.734E-03	1.711E-03	1.688E-03	1.667E-03	1.647E-03
0.80	1.628E-03	1.609E-03	1.591E-03	1.575E-03	1.557E-03	1.541E-03	1.526E-03	1.510E-03	1.496E-03	1.482E-03
0.90	1.468E-03	1.455E-03	1.442E-03	1.430E-03	1.418E-03	1.406E-03	1.395E-03	1.384E-03	1.374E-03	1.364E-03
1.00	1.354E-03	1.344E-03	1.336E-03	1.327E-03	1.318E-03	1.311E-03	1.303E-03	1.295E-03	1.288E-03	1.281E-03
1.10	1.274E-03	1.267E-03	1.261E-03	1.255E-03	1.249E-03	1.243E-03	1.238E-03	1.233E-03	1.227E-03	1.222E-03
1.20	1.218E-03	1.213E-03	1.209E-03	1.204E-03	1.200E-03	1.196E-03	1.193E-03	1.189E-03	1.185E-03	1.182E-03
1.30	1.179E-03	1.176E-03	1.173E-03	1.170E-03	1.166E-03	1.164E-03	1.162E-03	1.159E-03	1.156E-03	1.153E-03
1.40	1.152E-03	1.151E-03	1.150E-03	1.149E-03	1.148E-03	1.146E-03	0.794E-04			

Table 14

K, z = 20 cm

MEV	0.00-0.01	0.01-0.02	0.02-0.03	0.03-0.04	0.04-0.05	0.05-0.06	0.06-0.07	0.07-0.08	0.08-0.09	0.09-0.10
0.10	2.253E-02	1.918E-02	1.660E-02	1.461E-02	1.301E-02	1.175E-02	9.979E-03	9.026E-03	8.238E-03	7.578E-03
0.20	7.031E-03	6.651E-03	6.326E-03	5.792E-03	5.335E-03	4.942E-03	4.600E-03	4.297E-03	4.031E-03	3.794E-03
0.30	3.588E-03	3.402E-03	3.231E-03	3.069E-03	2.933E-03	2.805E-03	2.677E-03	2.576E-03	2.473E-03	2.378E-03
0.40	2.292E-03	2.212E-03	2.137E-03	2.067E-03	2.000E-03	1.940E-03	1.880E-03	1.828E-03	1.774E-03	1.726E-03
0.50	1.682E-03	1.638E-03	1.597E-03	1.559E-03	1.522E-03	1.487E-03	1.447E-03	1.423E-03	1.393E-03	1.365E-03
0.60	1.338E-03	1.312E-03	1.288E-03	1.265E-03	1.242E-03	1.221E-03	1.200E-03	1.180E-03	1.160E-03	1.141E-03
0.70	1.124E-03	1.106E-03	1.090E-03	1.073E-03	1.058E-03	1.043E-03	1.029E-03	1.015E-03	1.001E-03	9.884E-04
0.80	9.760E-04	9.642E-04	9.528E-04	9.417E-04	9.311E-04	9.207E-04	9.107E-04	9.009E-04	8.917E-04	8.829E-04
0.90	8.738E-04	8.650E-04	8.570E-04	8.493E-04	8.419E-04	8.349E-04	8.284E-04	8.198E-04	8.133E-04	8.069E-04
1.00	8.005E-04	7.947E-04	7.893E-04	7.838E-04	7.784E-04	7.736E-04	7.686E-04	7.636E-04	7.591E-04	7.547E-04
1.10	7.503E-04	7.459E-04	7.421E-04	7.382E-04	7.341E-04	7.301E-04	7.267E-04	7.231E-04	7.194E-04	7.157E-04
1.20	7.126E-04	7.093E-04	7.059E-04	7.024E-04	6.991E-04	6.963E-04	6.933E-04	6.902E-04	6.870E-04	6.843E-04
1.30	6.816E-04	6.788E-04	6.760E-04	6.730E-04	6.702E-04	6.677E-04	6.650E-04	6.622E-04	6.594E-04	6.565E-04
1.40	6.538E-04	6.510E-04	6.482E-04	6.453E-04	6.423E-04	6.393E-04	6.600E-04			

Table 15

K, z = 30 cm

MEV	0.00-0.01	0.01-0.02	0.02-0.03	0.03-0.04	0.04-0.05	0.05-0.06	0.06-0.07	0.07-0.08	0.08-0.09	0.09-0.10
0.10	1.340E-02	1.136E-02	9.775E-03	8.451E-03	7.378E-03	6.521E-03	5.835E-03	5.279E-03	4.819E-03	4.433E-03
0.20	4.113E-03	3.872E-03	3.649E-03	3.345E-03	3.085E-03	2.861E-03	2.666E-03	2.494E-03	2.343E-03	2.208E-03
0.30	2.092E-03	1.986E-03	1.889E-03	1.797E-03	1.720E-03	1.647E-03	1.574E-03	1.517E-03	1.458E-03	1.404E-03
0.40	1.354E-03	1.309E-03	1.266E-03	1.226E-03	1.187E-03	1.153E-03	1.118E-03	1.088E-03	1.057E-03	1.029E-03
0.50	1.004E-03	9.781E-04	9.546E-04	9.323E-04	9.111E-04	8.909E-04	8.675E-04	8.532E-04	8.355E-04	8.187E-04
0.60	8.028E-04	7.877E-04	7.732E-04	7.593E-04	7.459E-04	7.328E-04	7.203E-04	7.081E-04	6.965E-04	6.852E-04
0.70	6.743E-04	6.638E-04	6.537E-04	6.440E-04	6.346E-04	6.256E-04	6.166E-04	6.081E-04	5.998E-04	5.919E-04
0.80	5.844E-04	5.771E-04	5.702E-04	5.636E-04	5.569E-04	5.506E-04	5.445E-04	5.385E-04	5.328E-04	5.272E-04
0.90	5.219E-04	5.167E-04	5.116E-04	5.068E-04	5.020E-04	4.974E-04	4.930E-04	4.886E-04	4.844E-04	4.804E-04
1.00	4.764E-04	4.727E-04	4.692E-04	4.656E-04	4.621E-04	4.589E-04	4.555E-04	4.522E-04	4.491E-04	4.461E-04
1.10	4.430E-04	4.400E-04	4.372E-04	4.344E-04	4.316E-04	4.288E-04	4.262E-04	4.238E-04	4.210E-04	4.183E-04
1.20	4.160E-04	4.136E-04	4.112E-04	4.087E-04	4.064E-04	4.043E-04	4.022E-04	4.000E-04	3.978E-04	3.959E-04
1.30	3.941E-04	3.923E-04	3.904E-04	3.885E-04	3.867E-04	3.852E-04	3.837E-04	3.820E-04	3.804E-04	3.787E-04
1.40	3.772E-04	3.759E-04	3.745E-04	3.730E-04	3.715E-04	3.700E-04	1.615E-04			

Table 16

K, z = 40 cm

MEV	0.00-0.01	0.01-0.02	0.02-0.03	0.03-0.04	0.04-0.05	0.05-0.06	0.06-0.07	0.07-0.08	0.08-0.09	0.09-0.10
0.10	8.016E-03	6.710E-03	5.713E-03	4.910E-03	4.281E-03	3.784E-03	3.389E-03	3.067E-03	2.798E-03	2.572E-03
0.20	2.384E-03	2.227E-03	2.065E-03	1.895E-03	1.751E-03	1.627E-03	1.519E-03	1.423E-03	1.339E-03	1.265E-03
0.30	1.200E-03	1.141E-03	1.087E-03	1.035E-03	9.921E-04	9.513E-04	9.103E-04	8.780E-04	8.447E-04	8.144E-04
0.40	7.864E-04	7.605E-04	7.363E-04	7.136E-04	6.915E-04	6.721E-04	6.526E-04	6.352E-04	6.175E-04	6.014E-04
0.50	5.871E-04	5.721E-04	5.586E-04	5.456E-04	5.333E-04	5.216E-04	5.079E-04	4.996E-04	4.892E-04	4.793E-04
0.60	4.700E-04	4.611E-04	4.526E-04	4.444E-04	4.364E-04	4.288E-04	4.214E-04	4.143E-04	4.074E-04	4.007E-04
0.70	3.943E-04	3.881E-04	3.822E-04	3.764E-04	3.708E-04	3.654E-04	3.602E-04	3.551E-04	3.502E-04	3.456E-04
0.80	3.411E-04	3.360E-04	3.327E-04	3.286E-04	3.248E-04	3.210E-04	3.174E-04	3.138E-04	3.104E-04	3.070E-04
0.90	3.038E-04	3.007E-04	2.976E-04	2.947E-04	2.918E-04	2.889E-04	2.862E-04	2.835E-04	2.809E-04	2.784E-04
1.00	2.759E-04	2.736E-04	2.713E-04	2.691E-04	2.669E-04	2.649E-04	2.628E-04	2.607E-04	2.587E-04	2.568E-04
1.10	2.549E-04	2.530E-04	2.514E-04	2.496E-04	2.479E-04	2.462E-04	2.446E-04	2.431E-04	2.415E-04	2.399E-04
1.20	2.384E-04	2.372E-04	2.358E-04	2.344E-04	2.331E-04	2.320E-04	2.308E-04	2.296E-04	2.284E-04	2.274E-04
1.30	2.265E-04	2.255E-04	2.245E-04	2.234E-04	2.225E-04	2.216E-04	2.210E-04	2.202E-04	2.194E-04	2.189E-04
1.40	2.179E-04	2.174E-04	2.166E-04	2.162E-04	2.156E-04	2.149E-04	7.579E-05			

Table 17

Dose rates in water at the distance z from the source material (sand)

z (cm)	Dose rate (MeV · g^{-1} · s^{-1}) per % radioelement		
	Th	U	K
0	52.47	107.8	0.02587
10	22.34	44.24	0.01128
20	11.78	22.49	0.00602
30	6.56	11.97	0.00334
40	3.71	6.40	0.00187

1 MeV · g^{-1} · s^{-1} = 57.676 μrad/h

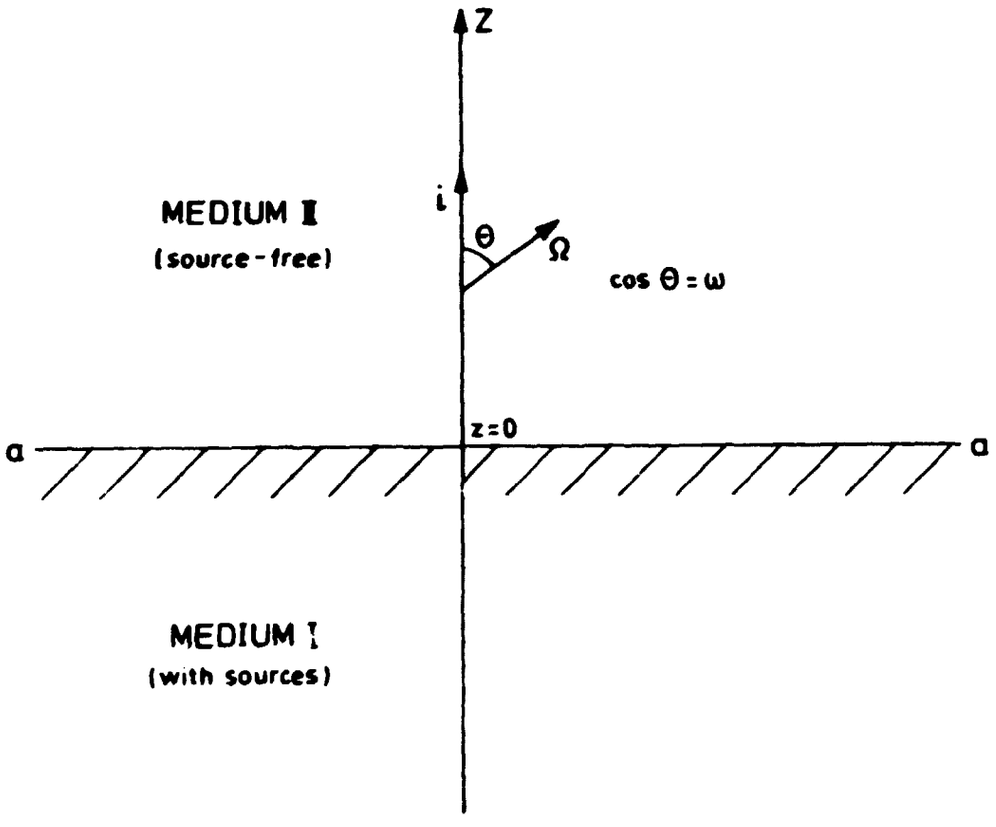

Fig. 1. Geometry for the Two-media Problem.

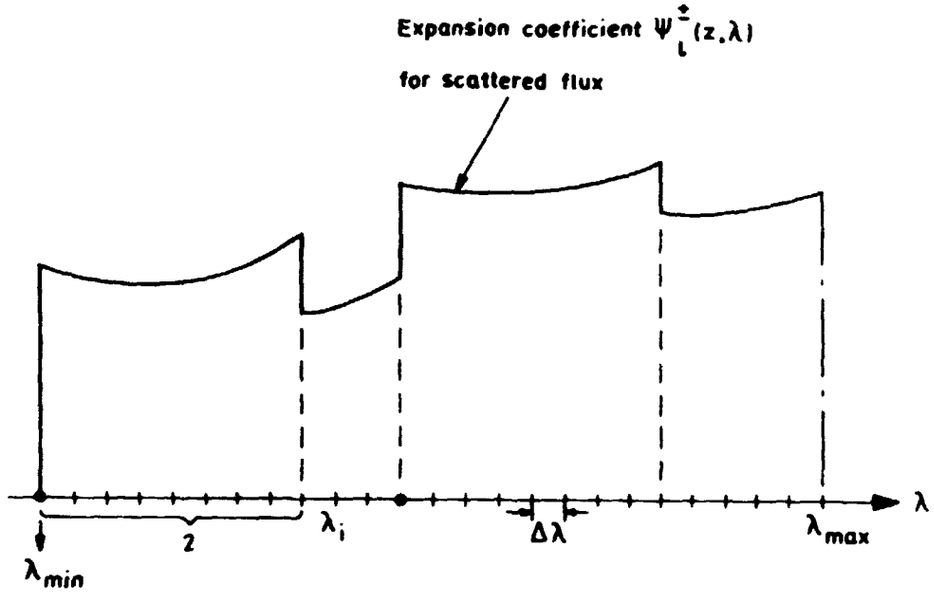

• : position of source lines (adjusted)

$\lambda_{min} = f_0/E_{max}$, $\lambda_{max} \simeq f_0/E_{cut}$.

$N = (\lambda_{max} - \lambda_{min})/\Delta\lambda$, $m = 1/\Delta\lambda$.

In this example N=24 and m=4

Fig. 2. Wavelength Scale and a Qualitative Solution for a Scattered Flux Component.

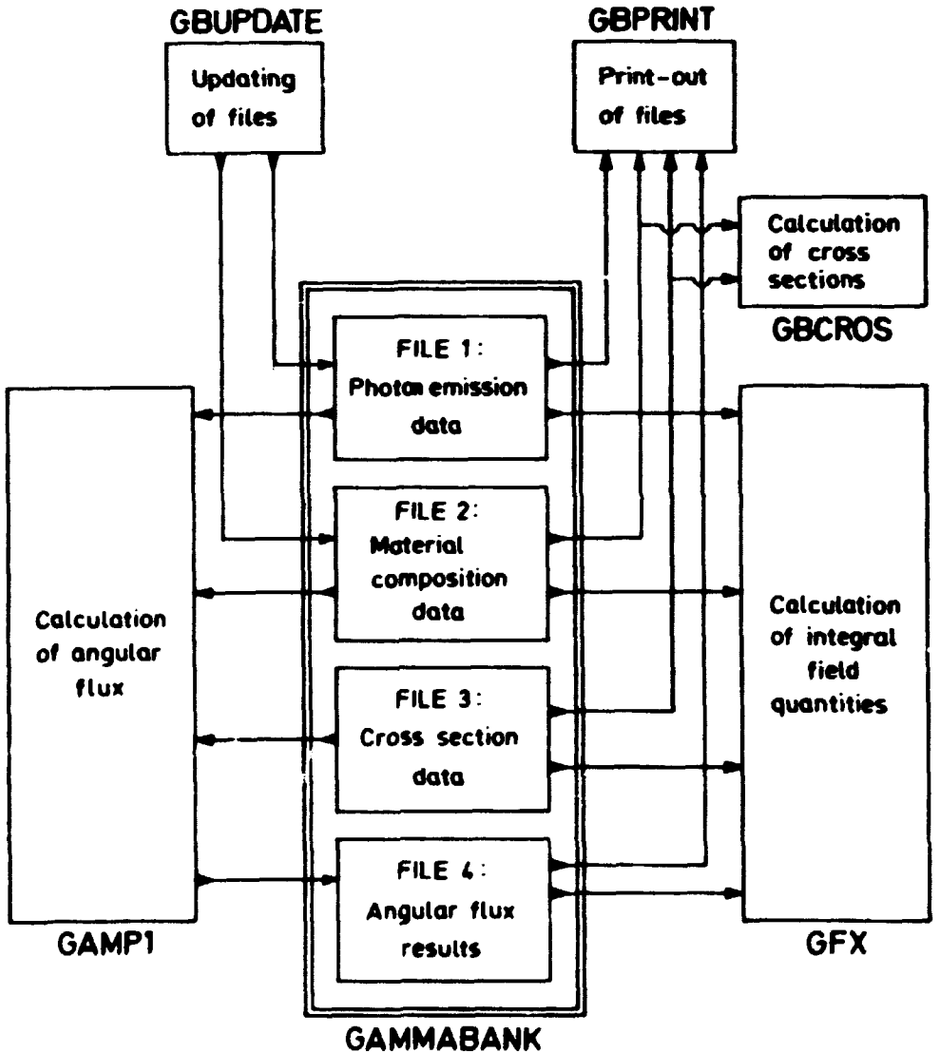

Fig. 3. Flow Diagram for Complete Data Processing System.

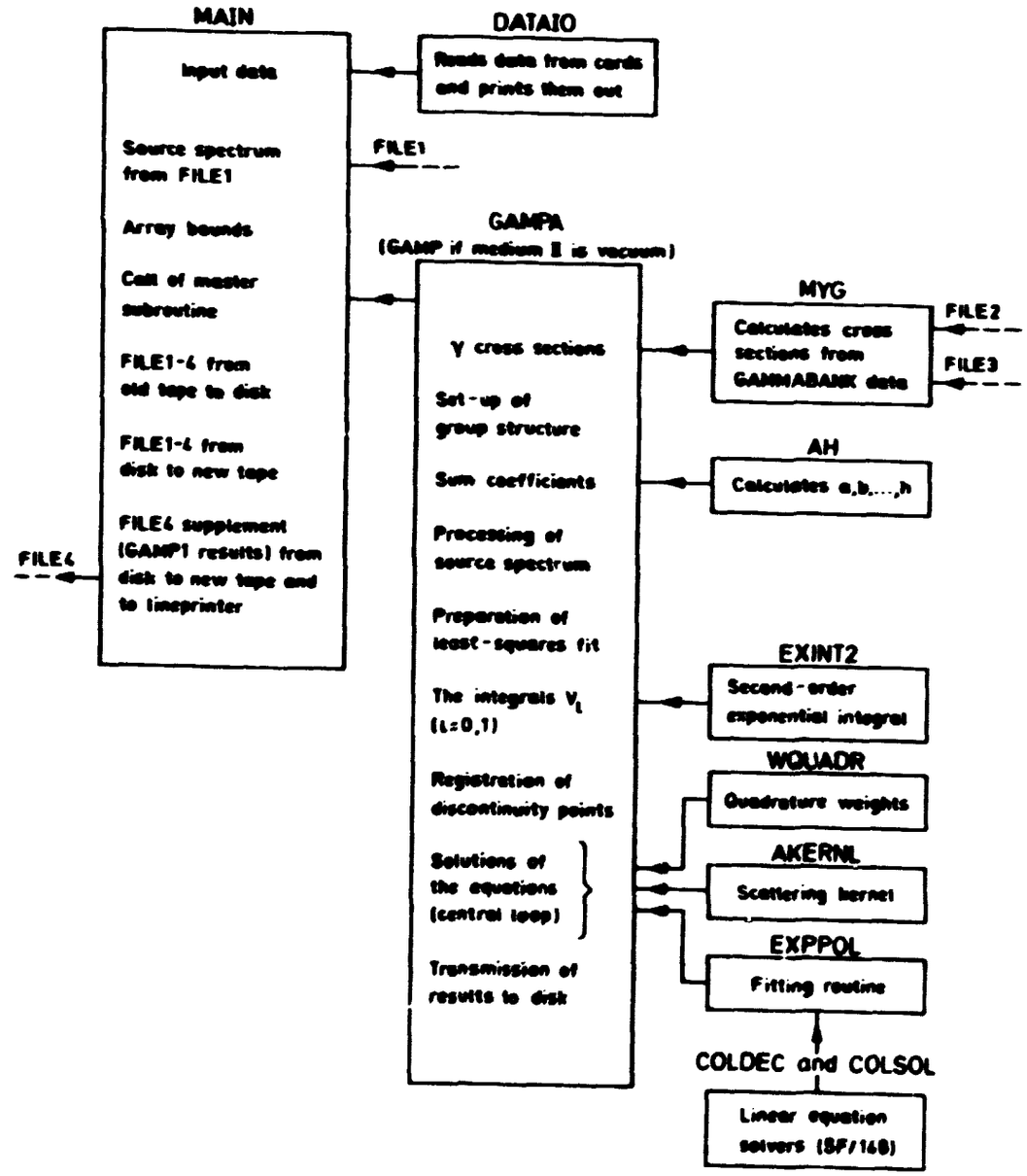

Fig. 4. Flow Diagram for GAMP1/SEP74.

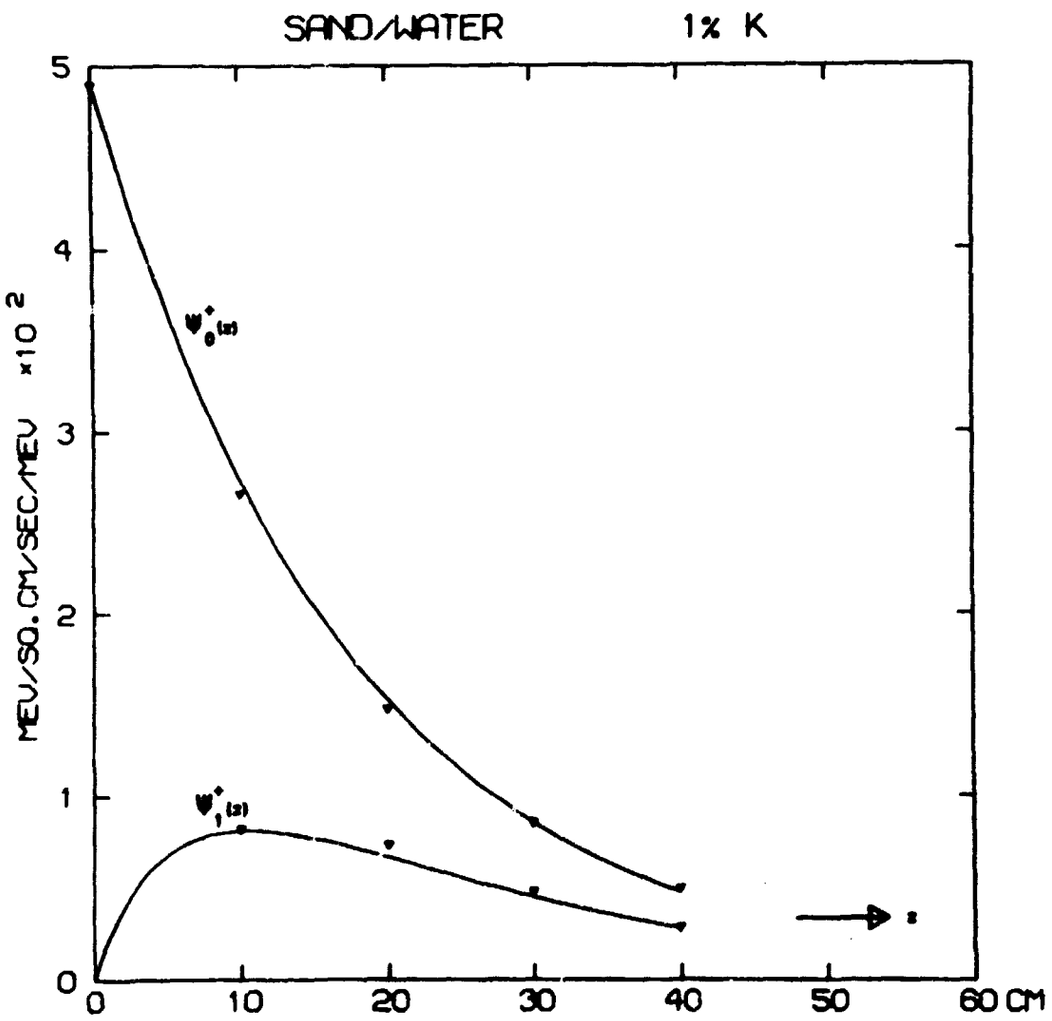

Fig. 5. Expansion Coefficients for Scattered Flux at Source Wavelength.

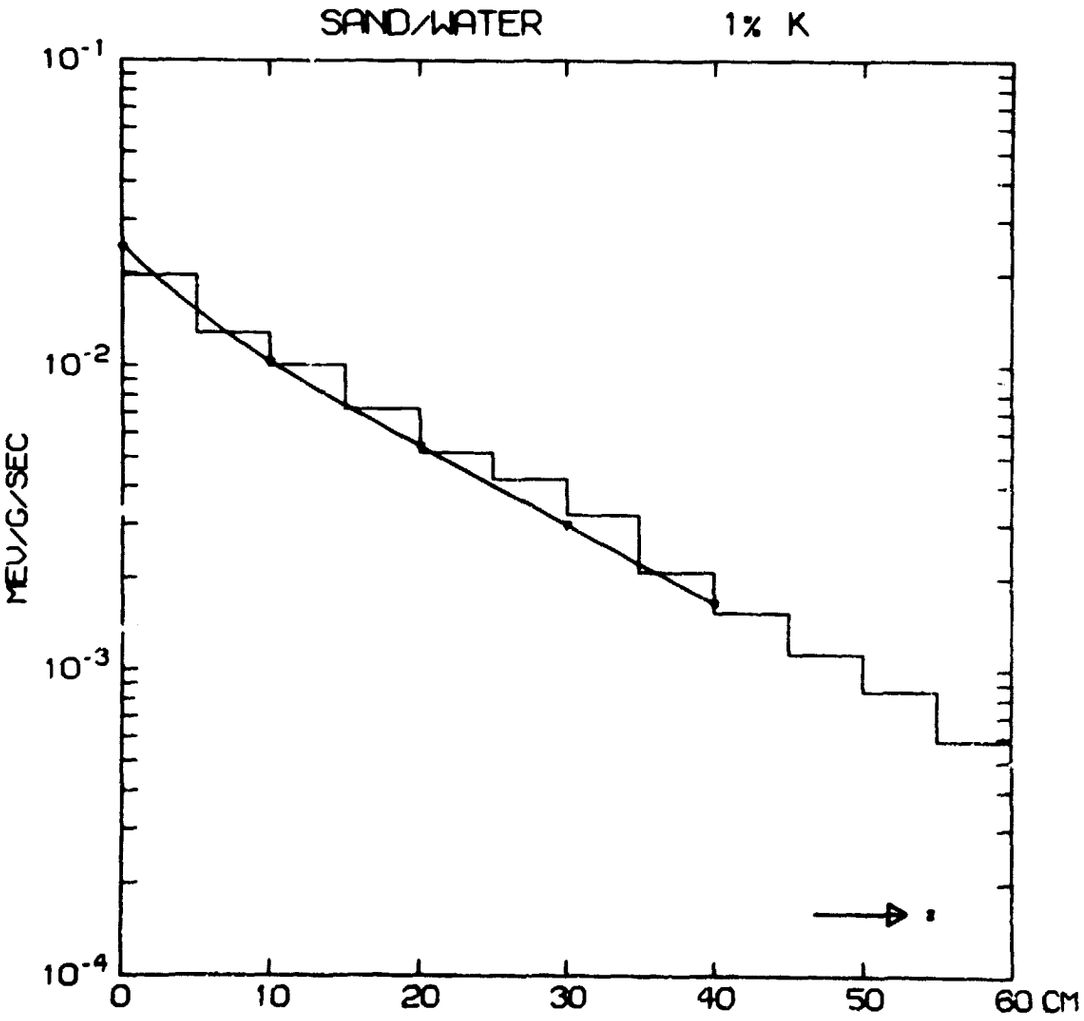

Fig. 6. Absorbed Dose Rate in Water above Sand.

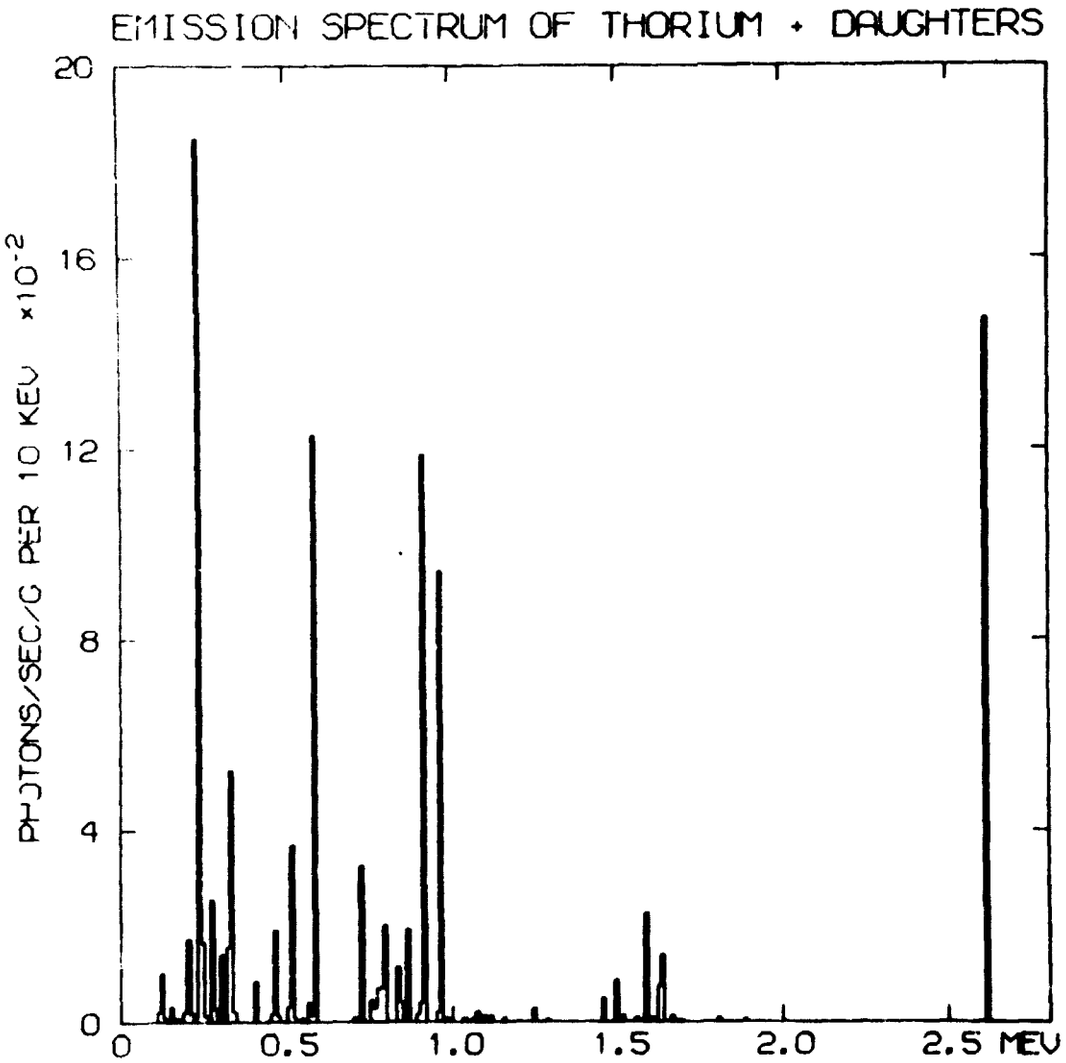

Fig. 7. Photon Emission Spectrum of ^{232}Th in Secular Equilibrium.

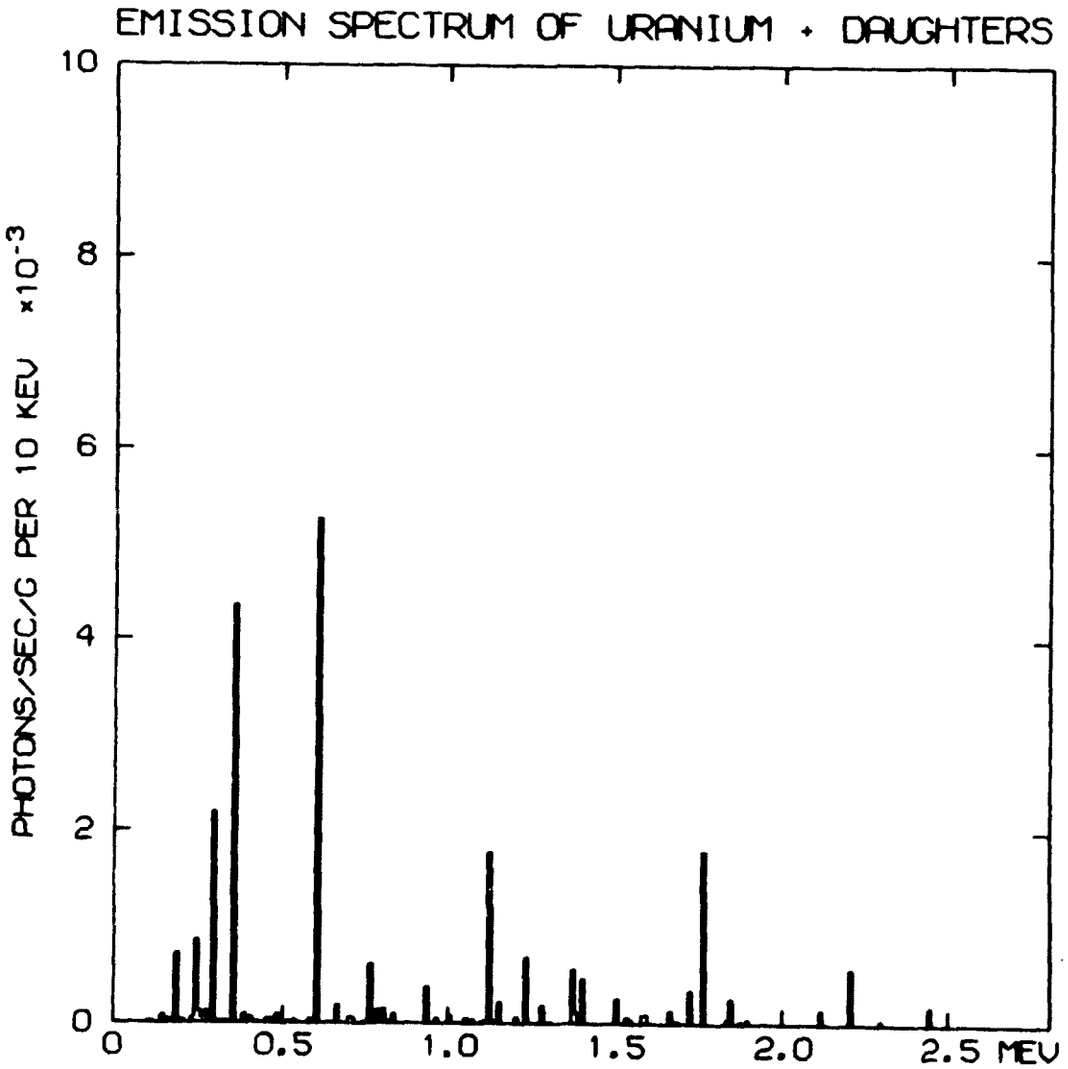

Fig. 8. Photon Emission Spectrum of ^{238}U + ^{235}U in Secular Equilibrium.

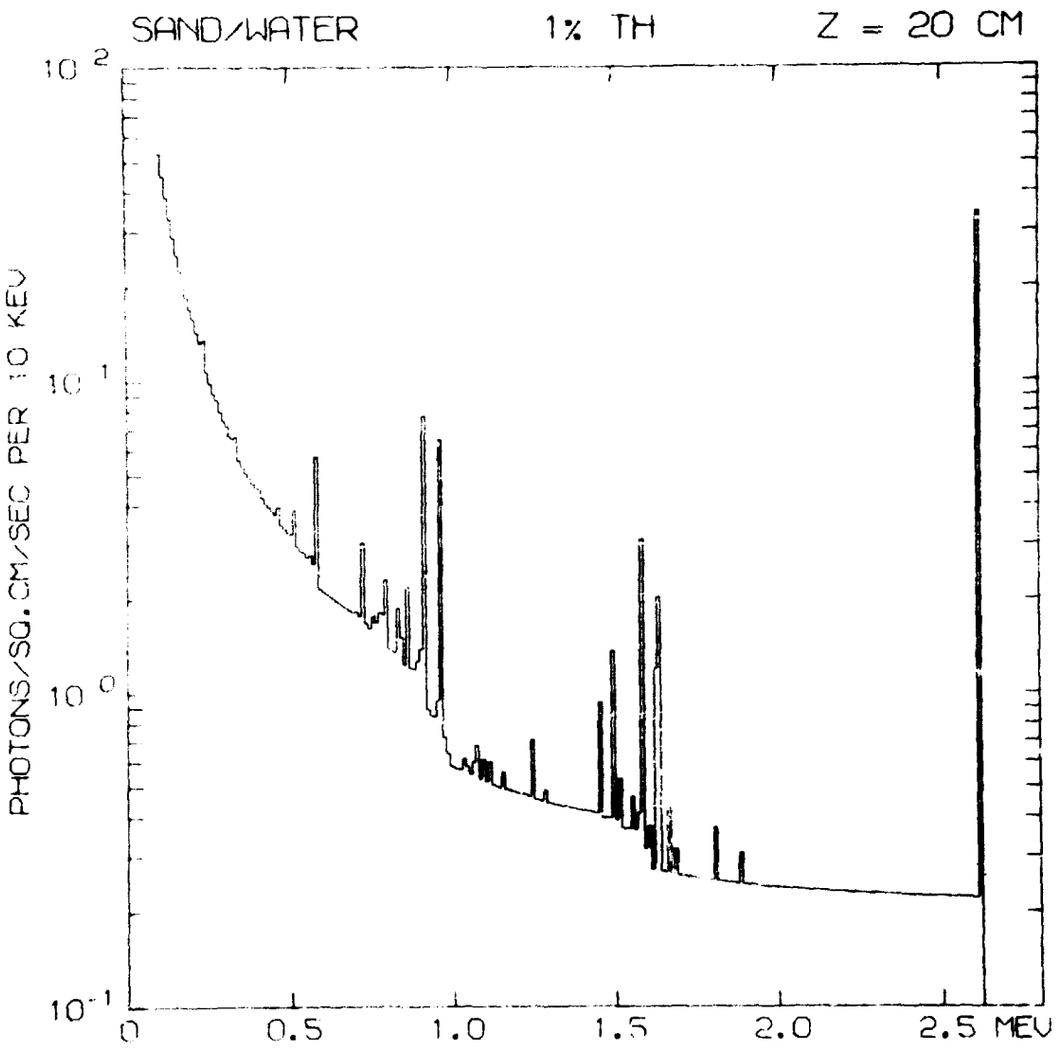

Fig. 9. Energy Distribution of the Scalar Photon Flux in Water Produced by Th in Sand.

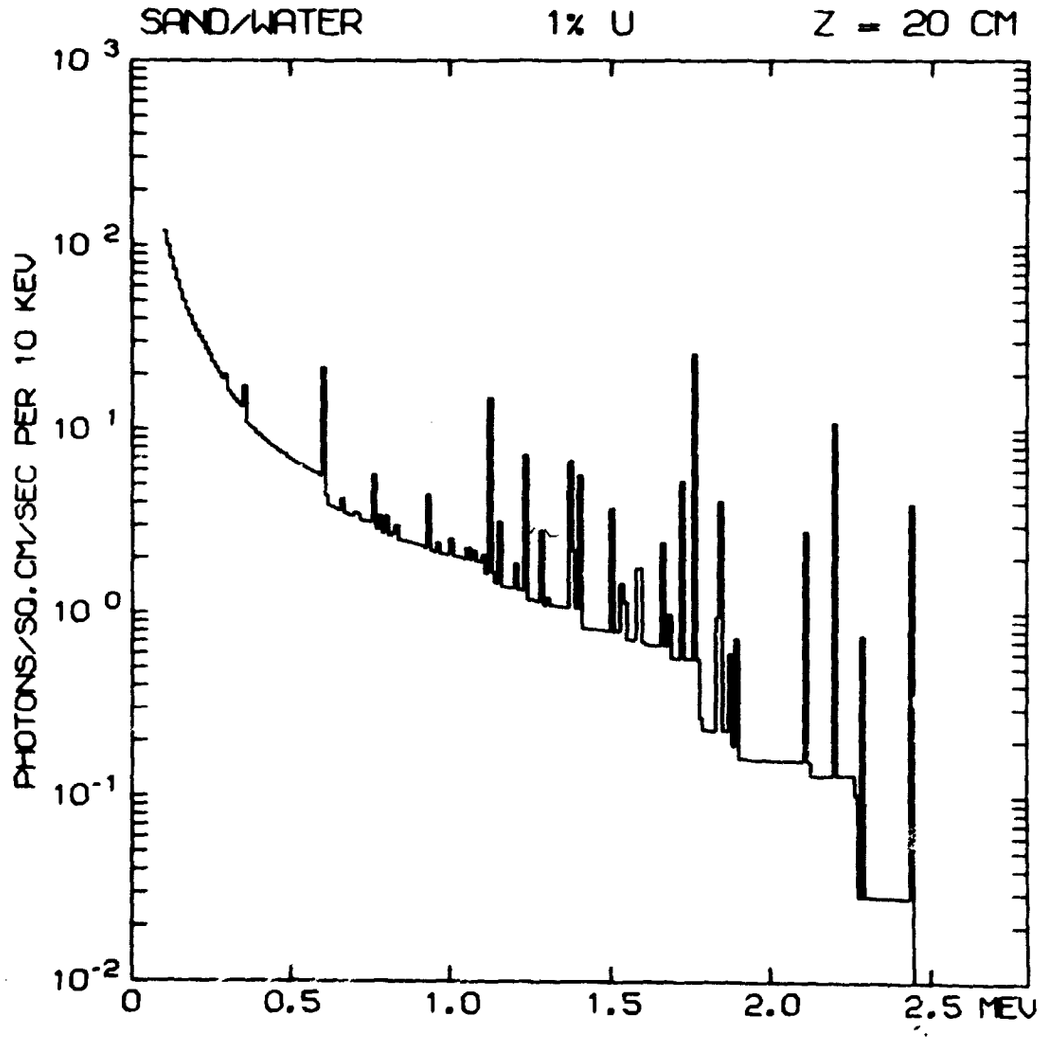

Fig. 10. Energy Distribution of the Scalar Photon Flux in Water Produced by U in Sand.

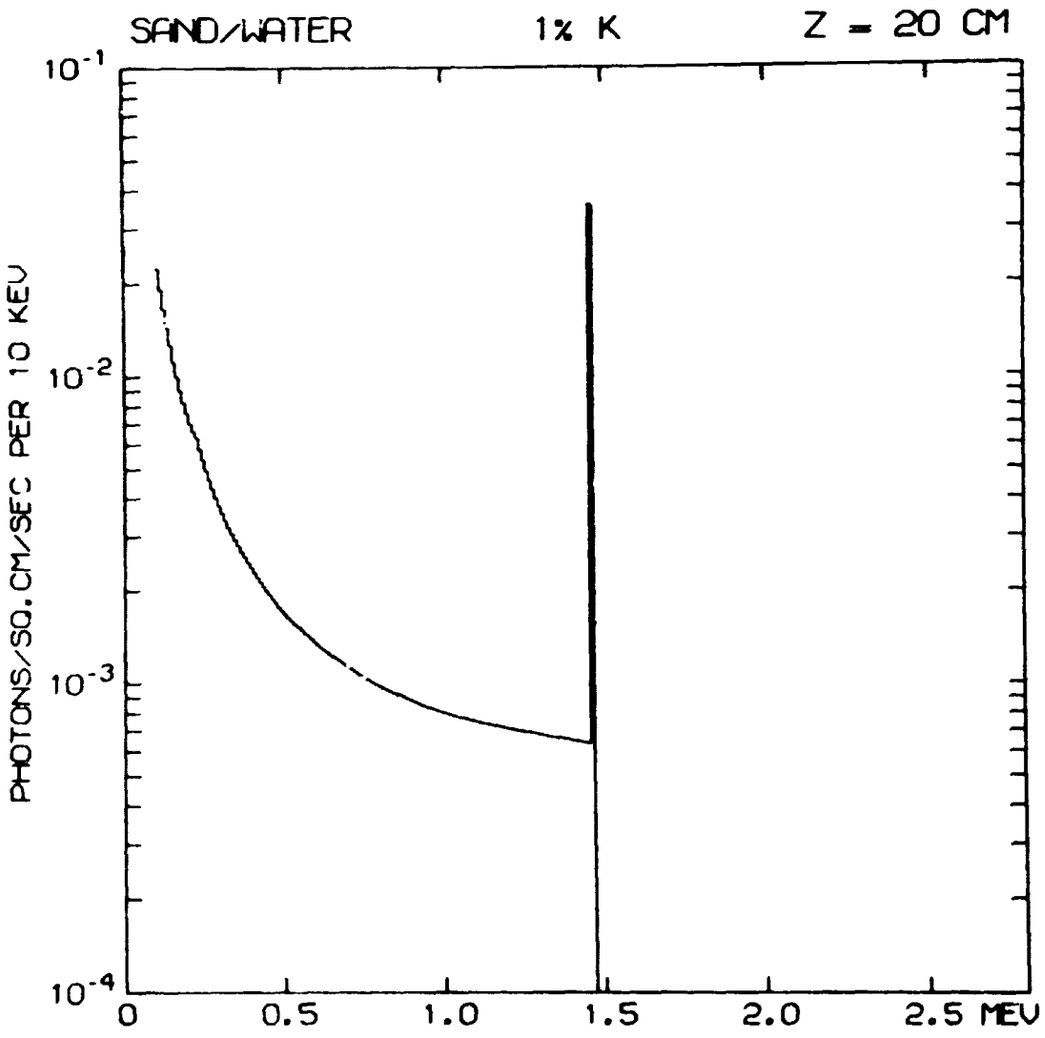

Fig. 11. Energy Distribution of the Scalar Photon Flux in Water Produced by K in Sand.

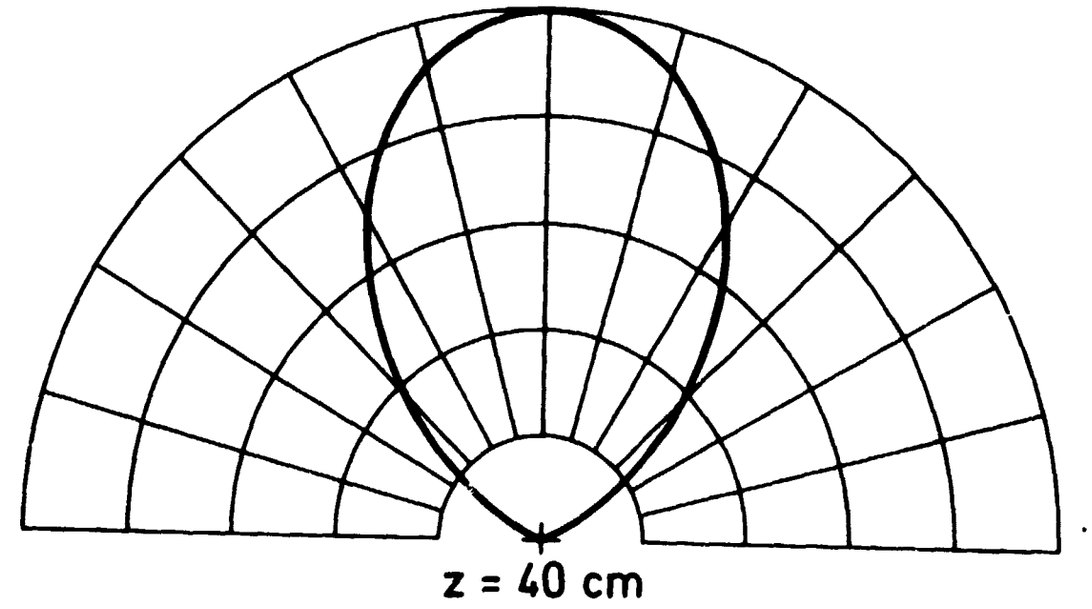

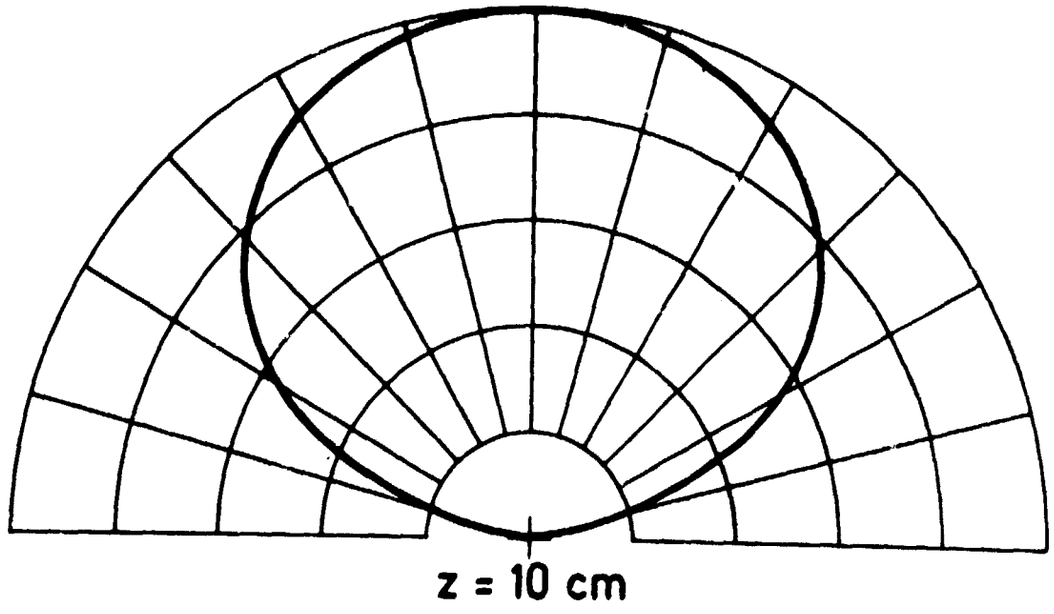

Fig. 12. Anguiar distributions (relative flux per steradian) of uncollided 1.46 M·V photons in water. $\theta = 0^{\circ}$ corresponds to top orientation.

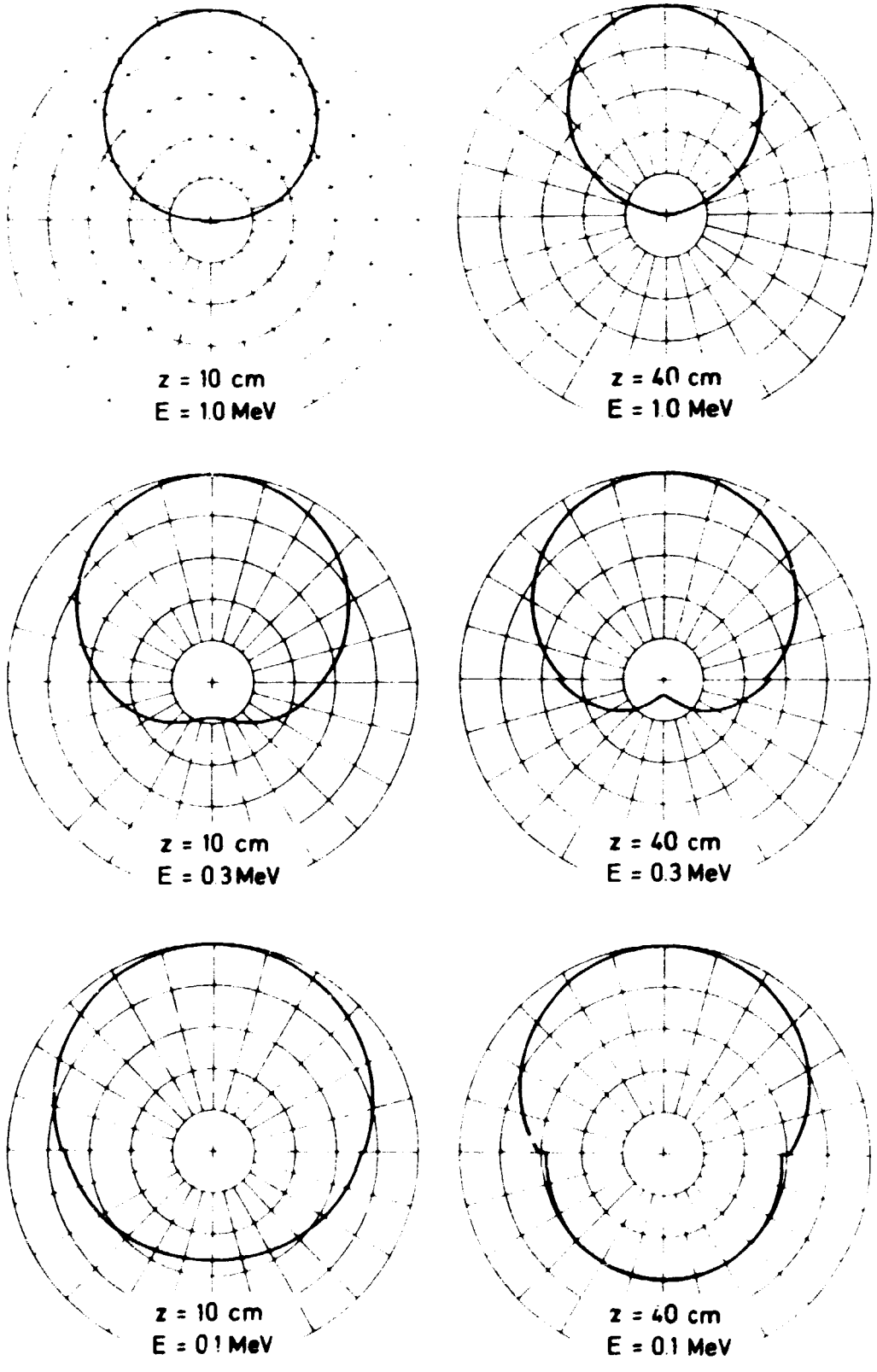

Fig. 13. Angular Distributions (relative flux per steradian) of scattered photons in water at selected heights and energies, calculated by the double-P_1 approximation. The source is ^{40}K in the underlying sand. $\theta = 0^{\circ}$ corresponds to top orientation.